Eindhoven University of Technology

MASTER

Scalar control of voltage fed induction machines

van der Hooft, E.L.

Award date:
1994

Link to publication

Disclaimer
This document contains a student thesis (bachelor's or master's), as authored by a student at Eindhoven University of Technology. Student theses are made available in the TU/e repository upon obtaining the required degree. The grade received is not published on the document as presented in the repository. The required complexity or quality of research of student theses may vary by program, and the required minimum study period may vary in duration.

General rights
Copyright and moral rights for the publications made accessible in the public portal are retained by the authors and/or other copyright owners and it is a condition of accessing publications that users recognise and abide by the legal requirements associated with these rights.

- Users may download and print one copy of any publication from the public portal for the purpose of private study or research.
- You may not further distribute the material or use it for any profit-making activity or commercial gain

7246

Faculteit der Elektrotechniek

Vakgroep Elektromechanica en Vermogenselektronica

Afstudeerverslag

SCALAR CONTROL OF VOLTAGE FED INDUCTION MACHINES

EMV 94-20 E.L. van der Hooft

Hoogleraar: Prof. dr. ir. A.J.A. Vandenput

Mentor: Dr. ir. J.L. Duarte

Auteur: E.L. van der Hooft

Eindhoven, December 1994

De Faculteit der Elektrotechiek van de Technische Universiteit Eindhoven aanvaardt geen verantwoordelijkheid voor de inhoud van stage- en afstudeerverslagen

ABSTRACT

The major part of all controlled ac drives belongs to the scalar-controlled category. Scalar-controlled drives generally have a simple configuration, are of low cost, have satisfactory stationary properties but moderate dynamic properties. Different scalar speed-control methods are discussed for a typical drive system.

A conventional way of speed control makes use of speed-measurement and slip correction. Constant flux is achieved by using a (non-linear) v/f-characteristic. Simulations show that the control method leads to satisfying results. However, in most (industrial) applications direct speed-measurement is undesirable.

A non-linear control approach, based on the steady-state equations of the field-oriented voltage fed induction machine, is derived. This control method combines the v/f principle with slip compensation, by using only current measurement in the dc-link of the voltage source converter. Usually measurement of the dc-link current is already available for protecting purposes, so no additional hardware is needed. Besides, there is no direct feedback from the induction machine to the control system. Simulations show that there is no steady-state speed deviation and the flux remains almost constant. However, in the low-speed region (<15% of rated speed), machine dynamics are badly damped if the control parameters are kept constant. Due to the non-linear character of the control method, a microprocessor-based system is necessary for implementation.

Linearising the non-linear control method results in a simple control structure, which is suited to be implemented by analogue hardware. Unfortunately, linearisation is unfavourable for the performance. Simulations show not only stationary deviations, but considerable flux deviations as well.

The non-linear control method was implemented in a digital signal processing system and tested with an induction machine (2.2 kW) fed by a pulse width modulated voltage source converter (5 kVA, IGBT's). Although the simulation results are not in fully agreement with experimental results in the low-speed region, the main working principle of the control method is proven to be valid in the high-speed region.

SAMENVATTING

Van de geregelde aandrijvingen zijn de zogenaamde scalaire regelingen het meest voorkomend. Kenmerkend voor dit type regeling is de eenvoudige structuur, de lage kostprijs, de goede stationaire maar matige dynamische eigenschappen. Voor een practisch aandrijfsysteem worden verschillende scalaire snelheidsregelingen beschouwd.

Een klassieke manier van snelheidsregeling maakt gebruik van een snelheidsmeting (tachometer) met een slipregeling. Een constante flux wordt gehandhaafd met behulp van een (niet-lineaire) v/f-karakteristiek. Met simulaties wordt aangetoond dat de regeling goed voldoet. Echter, de noodzakelijke snelheidsmeting is voor veel (industriële) toepassingen bezwaarlijk.

Vanuit de stationaire vergelijkingen van de veldgeoriënteerde spanningsgestuurde asynchrone machine is een niet-lineaire scalaire regeling afgeleid. De regeling combineert het v/f-principe met een slipcompensatie die uitsluitend gebruik maakt van een stroommeting in de tussenkring van de spanningsbron converter. Deze stroommeting is om beveiligingsredenen al vaak aanwezig, zodat er in principe geen extra sensoren vereist zijn. Bovendien is er geen terugkoppeling vanaf de asynchrone motor naar het regelsysteem. Met simulaties wordt aangetoond dat de niet-lineaire regeling geen stationaire fout heeft en dat er een nagenoeg constante flux wordt gehandhaafd. Echter voor lagere snelheden (<15% van de nominale snelheid) wordt de machinedynamica slecht gedempt als de regelparameters constant worden gehouden. Vanwege het niet-lineaire karakter van de regeling, is voor het implementeren een microprocessor systeem nodig.

Door de niet-lineaire regeling te lineariseren ontstaat een regeling met een veel eenvoudigere structuur, die met analoge schakelingen gerealiseerd kan worden. Het lineariseren gaat helaas ten koste van de kwaliteit. Simulaties tonen aan dat er zowel stationaire fouten als behoorlijke fluxafwijkingen kunnen ontstaan.

De niet-lineaire regelstructuur is geïmplementeerd in een digitaal signaalprocessor systeem en getest met een asynchrone machine (2,2 kW), die gevoed werd door een pulsbreedte gemodelleerde spanningbroninverter (5 kVA, IGBT's). Hoewel de simulatieresultaten bij lage toerentallen niet geheel overeenstemmen met de gemeten resultaten, is het werkingsprincipe van de regeling wel aangetoond bij hoge toerentallen.

LIST OF SYMBOLS

Parameters

c_{dc}	Dc-link capacitance
I_f	Bias (slip frequency)
I_u	Bias (voltage boost)
K_f	Gain (slip frequency)
K_u	Gain (voltage boost)
K_{vf}	Gain (voltage/frequency)
l_l	Air-gap inductance
l_m	Main inductance (two inductor model)
l_σ	Leakage inductance (two inductor model)
$l_{\sigma k}$	Absolute leakage inductance of cage
$l_{\sigma s}$	Absolute leakage inductance of stator
N_p	Pulse number
M_i	Modulation index
r_k	Cage resistance
r_k'	Cage resistance (two inductor model)
r_s	Stator resistance
T_{rise}	Rise time
T_{set}	Settling time
κ_p	Proportional gain (controller)
κ_{el}	Electrical gain
σ	Relative leakage factor
σ_k	Relative leakage inductance of cage with respect to air-gap inductance
σ_s	Relative leakage inductance of stator with respect to air-gap inductance
θ	Momentum of inertia
τ_{el}	Electrical time constant
τ_i	Integration time constant
τ_k	Cage time constant
τ_s	Stator time constant

Variables

E_{kin}	Kinetic energy
i_{dc}	Dc-link current
i_k^b	Cage current component in the cage-flux direction
i_k^w	Cage current component perpendicular to the cage-flux direction
i_{rec}	Output current of rectifier
i_s	Amplitude of the fundamental component of the stator current
i_{sa}, i_{sb}, i_{sc}	Three phase stator currents
i_s^b	Flux generating component of the stator current
i_s^w	Torque generating component of the stator current
m_{el}	Electric torque
m_{load}	Load torque
p_{mech}	Mechanical power

p_s	Motor input power
S	Slip
u_a, u_b, u_c	Three phase grid voltages
u_{ab}, u_{bc}, u_{ca}	Three phase grid line voltages
u_{aN}, u_{bN}, u_{cN}	Three phase stator voltages with respect to the inverter reference
$u_{sab}, u_{sbc}, u_{sca}$	Three phase stator line voltages
u_{dc}	Dc-link voltage
u_{grid}	Amplitude of three phase grid voltage
u_{rec}	Output voltage of rectifier
u_s	Amplitude of the fundamental component of the stator voltage
u_{tri}	Triangular modulation voltage
u_{sa}, u_{sb}, u_{sc}	Three phase stator voltages with respect to the star point of the motor
u_s^b	Stator voltage component in the cage-flux direction
u_s^w	Stator voltage component perpendicular to the cage-flux direction

Greek variables

$\dot{\alpha}_{grid}$	Frequency of three phase grid
α_s^r	Stator voltage angle with respect to the rotor axis
$\dot{\alpha}_s^r$	Slip frequency of stator voltage
α_s^s	Stator voltage angle with respect to the stator axis
$\dot{\alpha}_s^s$	Stator voltage frequency
α_s^ψ	Stator voltage angle with respect to the cage-flux axis
$\dot{\alpha}_s^\psi$	Stator voltage frequency with respect to the cage-flux axis
ϕ	Angle between stator voltage vector and stator current vector
φ^r	Cage-flux angle with respect to the rotor axis
$\dot{\varphi}^r$	Angular frequency of cage-flux with respect to the rotor
φ^s	Cage-flux angle with respect to the stator axis
$\dot{\varphi}^s$	Angular frequency of cage-flux with respect to the stator
ρ^s	Angle between rotor and stator axis
$\dot{\rho}^s$	Mechanical angular frequency
ψ_k	Cage-flux
Ω_1	Stationary frequency variable dependent of $\dot{\alpha}_s^s$ and $\dot{\alpha}_s^r$
Ω_2	Stationary frequency variable dependent of $\dot{\alpha}_s^s$ and $\dot{\alpha}_s^r$
$\omega_{cut\ off}$	Cut-off frequency of a filter

Space vectors

$\vec{i}_k^a$	Cage current vector in arbitrary coordinates, $a \in \{r,s,\psi\}$
$\vec{i}_k^r$	Cage current vector in rotor coordinates
$\vec{i}_k^\psi$	Cage current vector in cage-flux coordinates
$\vec{i}_s^a$	Stator current vector in arbitrary coordinates, $a \in \{r,s,\psi\}$
$\vec{i}_s^s$	Stator current vector in stator coordinates
$\vec{i}_s^\psi$	Stator current vector in cage-flux coordinates

$\vec{i}_{\mu l}^{\,a}$	Magnetising current vector in arbitrary coordinates, a $\in\{r,s,\psi\}$
$\vec{u}_s^{\,s}$	Stator voltage vector in stator coordinates
$\vec{u}_s^{\,\psi}$	Stator voltage vector in cage-flux coordinates
$\vec{\psi}_k^{\,a}$	Cage-flux vector in arbitrary coordinates, a $\in\{r,s,\psi\}$
$\vec{\psi}_k^{\,r}$	Cage-flux vector in rotor coordinates
$\vec{\psi}_k^{\,\psi}$	Cage-flux vector in cage-flux coordinates
$\vec{\psi}_l^{\,a}$	Air-gap flux vector in arbitrary coordinates, a $\in\{r,s,\psi\}$
$\vec{\psi}_l^{\,s}$	Air-gap flux vector in stator coordinates
$\vec{\psi}_s^{\,s}$	Stator flux vector in stator coordinates
$\vec{0}$	Zero vector

Subscripts: X is an arbitrary variable

x_{grid}	Referring to the three phase symmetrical grid
x_k	Referring to the cage
x_l	Referring to the air-gap
x_{max}	Maximum value
x_{rec}	Referring to rectifier
x_s	Referring to the stator
$[x]_0$	Steady-state value
$[x]_N$	Rated value
$x_{(1)}$	Fundamental component
x_σ	As a result of leakage

Superscripts: X is an arbitrary variable

x^r	In relation to the rotor axis
x^{s1}	In the direction of the stator-axis
x^{s2}	In the direction perpendicular to the stator-axis
x^a	In relation to an arbitrary axis
x^b	In the direction of the cage-flux
x^s	In relation to the stator axis
x^w	In the direction perpendicular to the cage-flux
x^ψ	In relation to the cage-flux axis
x^*	Desired value

Operators: X is an arbitrary variable

$\frac{d}{dt}x$	Derivative with respect to time
$\frac{\partial}{\partial t}x$	Partial derivative with respect to time
$\frac{\partial}{\partial x}x\Big\|_p$	Linearizing around point p
$\overline{x}$	Mean value
$\dot{x}$	Derivative with respect to time
$\hat{x}$	Maximum value

$R(\frac{\pi}{2})x$	Vector rotation over $(\frac{\pi}{2})$ radians counter clockwise
$\|x\|$	Absolute value
$\langle x \rangle$	Physical quantity (with dimension)
$[\langle x \rangle]_{ref}$	Reference quantity with dimension
$[\vec{x}]^T$	Transposed vector

Abbreviations

DSP	Digital signal processor
IGBT	Insulated gate bipolar transistor
PAM	Pulse amplitude modulation
PI	Proportional-integrating
PO	Percentage overshoot
pu	Per unit
PUS	Per unit system
PWM	Pulse-width modulation
SC	Scalar control
SO	Symmetric optimum
UA_σ	Voltage fed induction machine, including cage leakage inductance
v/f	voltage/frequency
VR	Vector rotation
VSC	Voltage source converter

CONTENTS

1. INDUCTION MACHINE CONTROL

1.1. OVERVIEW

Electric machines have been the workhorses in industry for many years. Until a few years ago, dc machines dominated in drive systems, because control principles and converter equipment are relatively simple. The ac machine was favoured only for constant speed drives because the equipment, required to use them in variable speed drives, was complex and expensive. Although, the advantages of an ac-machine, especially the cage-type induction machine, with respect to a dc machine are considerable:

- rugged and reliable
- high power to weight ratio
- less expensive
- hardly periodic maintenance
- sparkles
- capability to overload

Many of these advantages are due to the lack of commutator and brushes. Recent advancements in high power electronics and microcomputers have made it possible to implement sophisticated control tasks at reasonable costs. Therefore, the induction machine drives play nowadays a prominent role in electrical drive systems.
Principally, electrical drives can be divided in two groups: *non-controlled drives* and *controlled drives.*
Most drive applications in industry are non-controlled drives for constant speed operation. They are either 'on' or 'off', such as pumps, fans, blowers, etc. The majority of all induction machines operates directly connected to a three-phase power grid. In such applications, the torque at standstill should be high enough (double cage, deep bar rotor) to accelerate and reach the steady-state speed within acceptable time. The speed deviation, due to the slip speed if the machine is loaded, is taken for granted.
Besides non-controlled drives (fixed speed drives), the number of controlled drives (variable speed drives), is increasing in industry. Many drive systems need speed control, such as cranes, roller mills, vehicles, ships, etc. Controlled drives can be divided in two categories: *scalar controlled drives* and *vector controlled drives.*
Over 90% of all controlled ac drives belongs to the scalar controlled category [Stef, '92]. Scalar controlled drives only use the *magnitude* of quantities and are often used in multi-motor applications (general purpose). The converter is configured as an adjustable voltage source, with feedback loops intended primarily for converter operation and protection rather than motor control. Scalar controlled drives generally have a simple configuration, are of low cost, have satisfied stationary properties but moderate dynamic properties.
Less than 10% of the controlled ac drives are vector controlled drives. Vector controlled drives use both the *magnitude* and the *angle* of quantities. Vector controlled drives always operate in single motor configurations. They are intended for a specific

application (spindle, winder, robots, etc.) and normally use a current regulator (converter). There are two categories of vector control: *field oriented control* [Blaschke and Hasse, 1971] and *direct torque control.*

Field oriented control is a technique that provides a method of decoupling the two components of the stator current (field coordinates): one producing the flux and the other producing the torque. Therefore, it provides independent control of torque and flux, which is similar to a separately excited dc machine. The stator currents are controlled in such a way that the flux and the torque components of the current remain decoupled during dynamic and stationary conditions. There are two categories of field oriented control: *direct field oriented control* and *indirect field oriented control.* Direct field oriented drives make use of the measured or directly estimated value of the flux vector. Flux measurement is problematic because it is not directly measurable in a standard machine. Standard machines contain no flux-sensing windings (or Hall-probes) nor a rotor position sensor. Therefore, an on-line simulation model is normally used to estimate the flux from measured currents and voltages. In indirect field oriented control, the flux vector is calculated by an on-line simulation model. However, this model depends heavily on the model parameters and needs a shaft position or speed measurement. In both cases of field oriented control, reliable on-line parameter estimation is problematic (mainly around standstill and low speeds).

The other method of vector control, *direct torque control,* is based on the switching character of the invertor and makes use of the stator flux and the electric torque of the machine. There are different methods of direct torque control. Two important methods are: *Direct Self Control* (DSC, [Depenbrock 1985]) and the *Improved Field Acceleration Method* (IFAM, [Takahashi, 1986]).

Figure 1.1 gives an overview of the classification of electric drives.

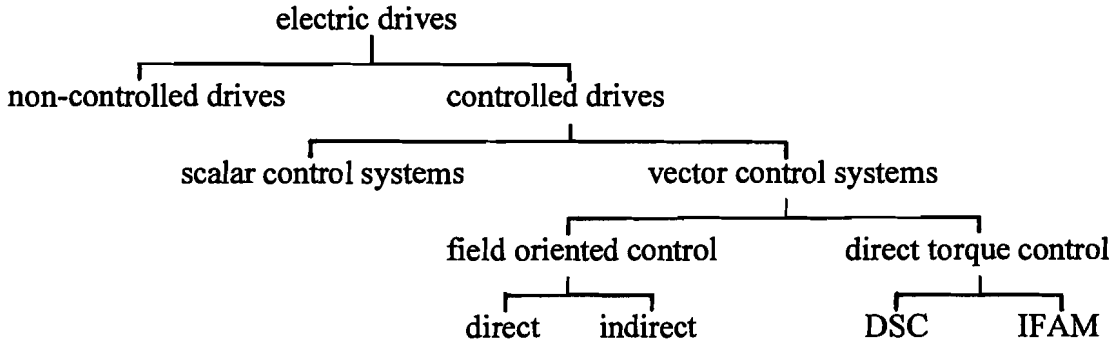

Figure: 1-1: Overview of electrical drives

1.2. SCALAR CONTROL

Scalar control is the term used to embrace general drive systems that are not vector controlled. A scalar variable is one represented by its magnitude alone. Scalar control uses a steady-state model of the induction motor, neglecting the dynamics, which results in a considerably simpler structure. It is this use of scalar quantities which gives these control systems their basic characteristic of satisfactory steady-state behaviour, but poorly controlled transient response.
In drives requiring only steady-state control (of torque), an induction motor offers advantages in cost and robustness. It is, therefore, recommended that the controller matches the induction motor in terms of cost and in the avoidance of shaft mounted transducers. The simplest way of scalar control is *variable voltage operation*, although this gives poor efficiency due to high slip power loss (paragraph 3.1).
Scalar control of a drive system is usually arranged to yield maximum torque per ampere stator current, independent of the frequency, by maintaining a constant flux. Approximately constant flux is achieved by adjusting the magnitude of the stator voltage such that the voltage to frequency ratio is maintained constant. This is the cornerstone of all *v/f controlled systems* (paragraph 3.4). However, an open loop constant v/f ratio (with fixed low speed voltage boost) has poor static accuracy and dynamic properties. Closed loop constant v/f controlled systems results in a constant cage-flux in any situation, however flux-sensors are expensive and impractical. Recently, new control structures have been developed [Vuck '91][Vuck '92], which are derived of field oriented control (paragraph 3.6 and 3.7). The structures make use of the dc-link current measurement of a voltage source converter, without measurement of other quantities.

1.3. OUTLINE

In chapter 2 a description of the electrical drive system is given. The system is divided in three main parts: the control system, the converter and the electric machine. Both the *voltage source converter* and the *voltage fed induction machine* are discussed and mathematically described in this chapter.
The control methods are discussed in chapter 3. The first paragraphs of chapter 3 explain why it is favourable to vary both the voltage and frequency of the stator (constant v/f control). Three scalar control methods are described in detail: a conventional method, *constant v/f speed control with slip regulation*, and two new scalar control methods, *a non-linear and a linearised control method* which use the dc-link current of the voltage source converter.
Simulation results of these control methods, are presented in chapter 4. Not only the quasi-stationary and dynamic behaviour of the different control methods are simulated, but the parameter sensitivity as well.
In chapter 5 the non-linear control method that uses the dc-link current is implemented. A 2.2 kW induction machine fed by a PWM-inverter is controlled by a digital signal processing system. The practical results are compared with the simulated results.
Finally, conclusions are made concerning the discussed scalar control methods.

2. ELECTRICAL DRIVE SYSTEM

In this chapter an overview of the total electrical drive system is given. The drive system is divided in three main parts: the electrical machine, the converter and the control system. Both the electrical machine and the converter are discussed in separated paragraphs.
The induction machine in this chapter is described in field coordinates. This description forms a base for the scalar control methods as discussed in chapter 3. Also for later use in chapter 4, an induction machine model is derived. The voltage source converter is assumed to be ideal in this thesis.

2.1. SYSTEM DESCRIPTION

In general an electrical drive system consists of three main parts: the electrical machine, the power converter and the control system. In this thesis, the following configuration is used:

- a voltage fed induction machine with single-cage rotor (UA)
- a voltage source converter (VSC)
- a scalar control method (SC).

The composition of the configuration is based on practice. It is a typical combination for general purpose applications (like pumps, fans and blowers). The block scheme of figure 2.1, gives a survey.

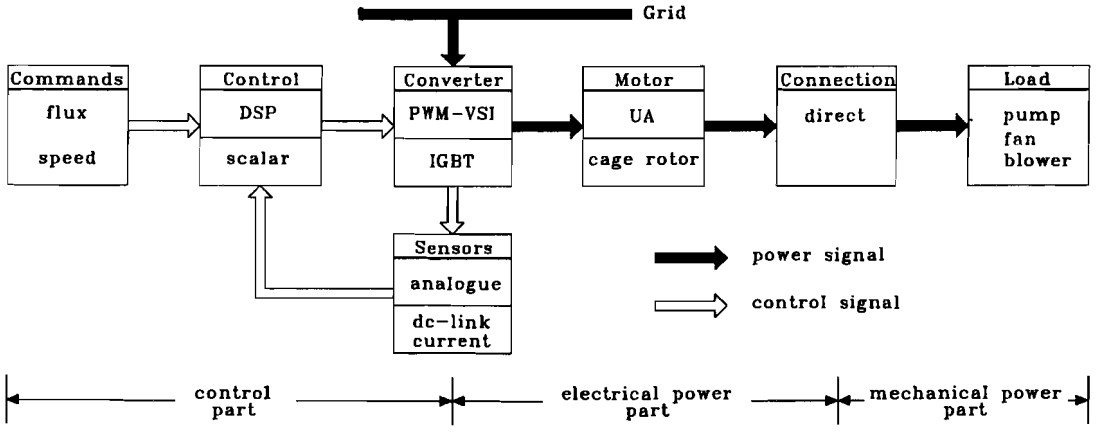

Figure 2-1: Block scheme of the electrical drive system

The converter is the link between the control part and the electrical power part, therefore it is connected to the supplying three phase grid, the control system and the motor. A scalar control program imposes two control signals: the amplitude and the frequency of the fundamental stator voltage. With these reference signals the voltage source inverter generates three stator voltages, 120 degrees shifted with respect to each other. They are block shaped, have constant amplitude and the width of the pulses are dependent of the

reference signals. The induction motor is directly connected to the load. In the control algorithms analysed in this thesis, there is no machine feedback to the control system. The only feedback signal is the dc-link current of the converter. In practice it is often present for converter protecting purposes. Both the flux and speed of the motor are adjustable desired values. For high efficiency of the drive system, the desired flux value is fixed and set to the rated value.

2.2. VOLTAGE SOURCE CONVERTER

2.2.1. GENERAL DESCRIPTION

As seen in figure 2.1, the voltage source converter is the link between the control and the power part of the drive system. Normally, it consists of three parts:

- a rectifier
- a filter
- an inverter.

The voltage source converter is characterised by a stiff dc-voltage between the rectifier and the inverter. A schematic diagram of the power converter is given in figure 2.2.

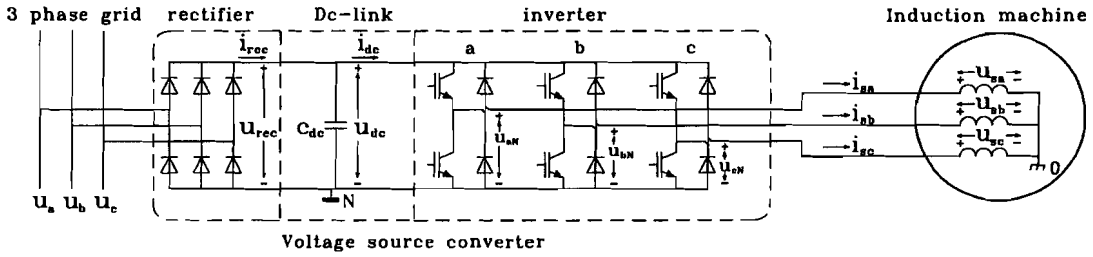

Figure 2-2: Schematic diagram of the voltage source power converter

The three phase diode bridge rectifier is connected to the symmetrical three phase grid (380/220V, 50 Hz)

$$\begin{aligned} u_a &= u_{grid} \cdot \cos\left(\dot{\alpha}_{grid} t\right) \\ u_b &= u_{grid} \cdot \cos\left(\dot{\alpha}_{grid} t - \tfrac{2}{3}\pi\right) \\ u_c &= u_{grid} \cdot \cos\left(\dot{\alpha}_{grid} t + \tfrac{2}{3}\pi\right). \end{aligned} \tag{2-1}$$

Ideally, the full bridge rectifier can be seen as a 'logical or-gate' which permits to pass, in absolute sense, the highest line voltage (ideal means: constant dc-link current, ideal rectifying diodes and zero grid impedance). This is shown in figure 2-2.
The capacitance, c_{dc}, reduces the voltage ripple on the dc-link voltage, u_{dc}. The mean value of u_{dc} is equal to

$$\bar{u}_{dc} = \frac{6}{2\pi} \int_{\frac{\pi}{3}}^{\frac{2\pi}{3}} u_{bc}\, dt = \frac{3}{\pi} \int_{\frac{\pi}{3}}^{\frac{2\pi}{3}} u_{grid}\sqrt{3}\, \sin\left(\dot{\alpha}_{grid} t\right) d\left(\dot{\alpha}_{grid} t\right) = \frac{3\sqrt{3}}{\pi} u_{grid}. \tag{2-2}$$

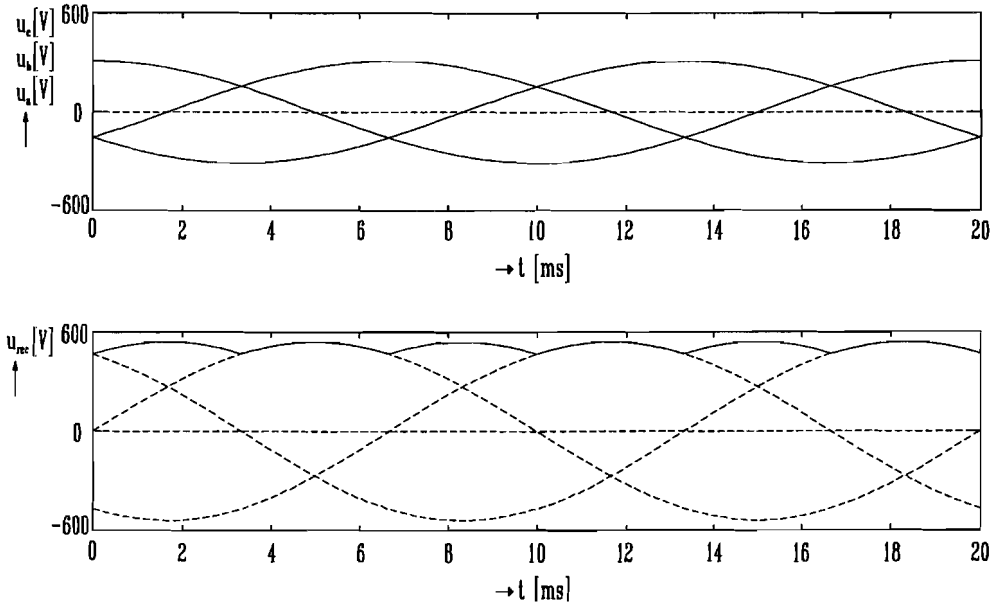

Figure 2-3: Grid line voltages and ideal rectifier output voltage

For a three phase grid of figure 2-3 (380/220 V, 50 Hz), this means a dc-link voltage value of about 515 V. In this thesis a constant dc-link voltage, $\bar{u}_{dc}$, is assumed.
As depicted in figure 2-2, the voltage source inverter has three phase legs, each leg consists of a pair of power semiconductor switching devices (IGBT's). Ideally, a phase leg can be considered as a 2-level switch that can switch between two levels: the positive- and the negative dc-link terminals (figure 2-4).

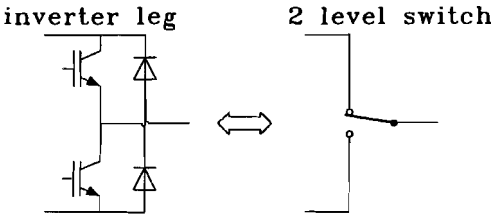

Figure 2-4: Electric equivalent of an inverter leg

Through different switching patterns of the 2-level switches, it is possible to vary both the amplitude and frequency of the output voltages. Because of the inductive character of the asynchronous machine and the possibility to deliver reactive power (freewheel diodes), the voltage source converter is a suitable (voltage) supply. Therefore, the three terminals of the 3-phase induction machine are directly connected to the centre of the accompanying inverter leg.

2.2.2. PULSE-WIDTH MODULATION

The conversion of a constant dc-link voltage to a voltage whose amplitude and frequency are controllable is achieved, for instance, with a *sinusoidal pulse-width modulation* technique (PWM).
Pulse-width modulation approaches sinusoidal stator currents in the induction machine.
In the case of sinusoidal PWM, the control signals of the 2-level switches (IGBT's) are obtained by comparing a sinusoidal reference signal (added with 12% of third harmonic component), u_{ref}, with a carrier signal, u_{tri}, which is triangular in shape (figure 2-5).

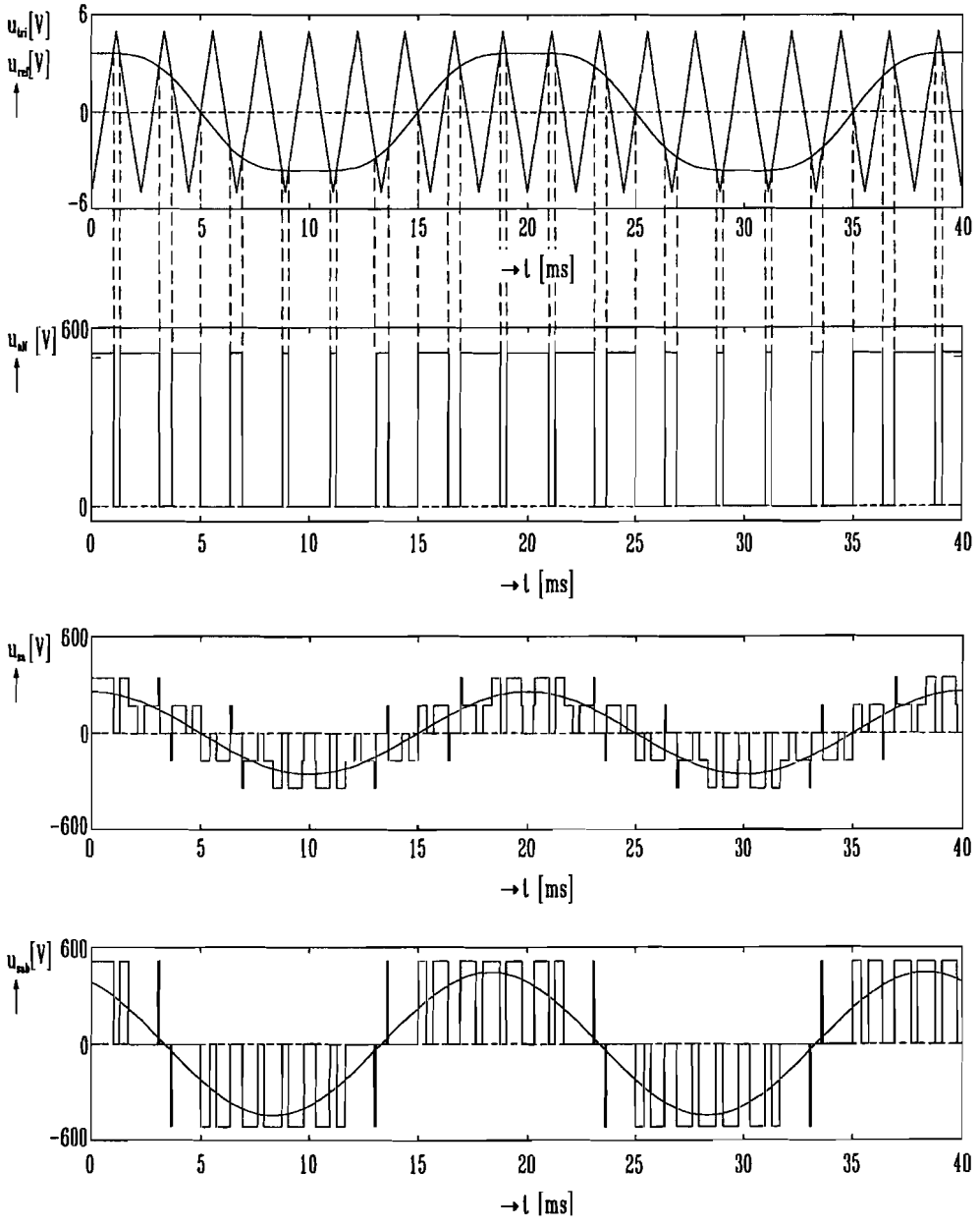

Figure 2-5: Pulse-width modulation

The frequency of the triangular carrier, $\dot{\alpha}_{tri}$, establishes the inverter switching frequency and is generally kept constant along with its amplitude, u_{tri}. The amplitude and the

frequency of the reference signal are desired values, and usually calculated by a control system. The switching moments are determined by the points of intersection between the reference signal and the carrier. If $u_{ref} > u_{tri}$ then the output voltage of the concerned phase is connected to the positive terminal of the dc-link voltage. If $u_{ref} < u_{tri}$ then it is connected to the reference terminal of the dc-link voltage. Each phase is compared with a common carrier. The quotient of the carrier frequency and the frequency of the reference signal is called the *pulse number*, and defined as

$$N_p = \frac{\dot{\alpha}_{tri}}{\dot{\alpha}_{ref}}. \tag{2-3}$$

A pulse number $N_p = n$, means: there are n pulses in each half period of the line voltages. The relation between the amplitude of the reference signal and that of the carrier is called the *modulation index* and defined as

$$M_i = \frac{\hat{u}_{ref}}{\hat{u}_{tri}}. \tag{2-4}$$

In figure 2-5 the modulation index and pulse number are set to a constant value: $M_i = 1$, $N_p = 9$. Dependent of the value of the modulation index, there are three types of modulation:

- *sinus modulation,* if $0 \le M_i \le 1$
- *over modulation,* if $M_i > 1$
- *block modulation,* if $M_i \to \infty$.

In contrast to over modulation or block modulation, the fundamental component of the output voltage of sinusoidal modulation is proportional with the modulation index [Moh '89]

$$u_{sa(1)} = M_i \frac{u_{dc}}{2} \cdot \sin(\dot{\alpha}_s^s t). \tag{2-5}$$

If sinus modulation is assumed, the maximum value of the fundamental output phase voltage is half the dc-link voltage. This means that for $u_{dc} = 515V$ and $M_i = 1$ the maximum value of $u_{sa(1)}$ is 257.5V. Therefore, the motor can not be used at full power.
The output voltage of the inverter not only contains a fundamental component with frequency, $\dot{\alpha}_{ref}$, but harmonic components of the carrier frequency, $\dot{\alpha}_{tri}$, as well.
A selection of the pulse number, N_p, depends on the balance between inverter losses and machine harmonic losses. A higher value of N_p increases the inverter switching losses, but reduces the machine harmonic losses. Adding a *third harmonic* component (figure 2-5) to the reference signals gives a flattened top of the sinusoidals (12% of the fundamental component). It results in less switching actions (less switching losses) and the possibility to choose a higher value of the modulation index. When a floating star connection is applied, the third harmonic component is of no influence on the stator voltages (for example u_{sa} and u_{sab} in figure 2-2) [Buja '75].
A completely different approach for generating PWM results from representing the three-phase inverter output voltages in a space vector system. This approach is quite

convenient to be implemented by microprocessors, being widely used nowadays. However, the space vector method generates virtually the same pulse pattern as the sinusoidal PWM with increased voltage utilisation (third harmonic addition). For this reason, only the sinusoidal PWM technique will be considered in this thesis.

2.2.3. DC-LINK CURRENT

The dc-link of a voltage source converter is characterised by a stiff voltage at the input of the inverter. However, the shape and value of the dc-link current is determined by the load and the switching actions of the power switches (IGBT's).
A typical wave shape of the dc-link current, i_{dc}, is shown in figure 2-6.

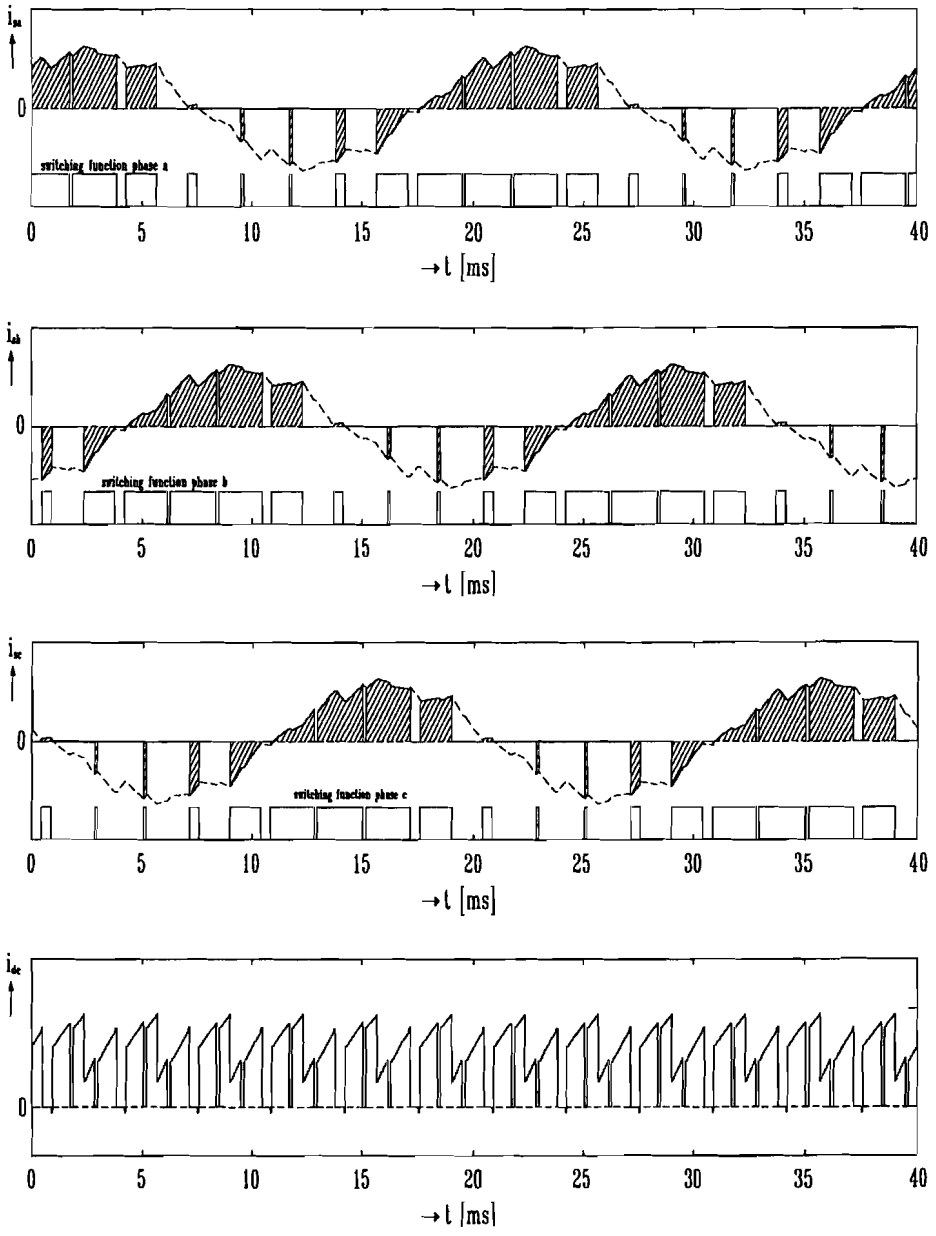

Figure 2-6: Derivation of the dc-link current $N_p = 9$, $M_i = 1$,

Figure 2-6a shows the current, i_{sa}, of 'phase a' of one inverter leg. Figure 2-6a shows also the so called switching function, which shape corresponds to the PWM voltage, u_{aN} (figure 2-2), but the amplitude is either 0 or 1. When the PWM voltage is positive the top switch of the leg 'a' is on and, during these periods, the leg current, i_{sa}, is drawn from the dc-link to the machine if it is positive, and is fed back into the dc-link via the diode if it is negative. Multiplying the current wave form, i_{sa}, by the switching function gives the current of 'phase a' drawn from the dc-link. The resulting pulses of dc-link current, i_{dc}, are shown shaded in figure 2-6a. Figures 2-6b and 2-6c are the current wave forms which are drawn from the other two legs of the inverter. Figure 2-6d is the sum of figures 2-6a, 2-6b, 2-6c and is therefore the total dc-link current, i_{dc}. For the chosen power factor ($\phi = 30°$) the dc-link current appears to be always positive. In general, and especially with lower power factors, the current can be both positive and negative.

The mean value of the dc-link current, $\bar{i}_{dc}$, can be calculated approximately by considering the fundamental stator voltage and stator current in each phase. The power balance between dc-side and ac-side is

$$u_{dc} i_{dc} = u_{sa(1)} i_{sa(1)} + u_{sb(1)} i_{sb(1)} + u_{sc(1)} i_{sc(1)}. \tag{2-6}$$

The stator terms are (assumed) sinusoidal and the current lags the voltage with an angle ϕ. The mean value of the dc-link current, $\bar{i}_{dc}$, is then given by:

$$\bar{i}_{dc} = \frac{3 u_{s(1)} i_{s(1)}}{u_{dc}} \cos\phi. \tag{2-7}$$

Therefore, the mean value of the dc-link current is a measure for the load of a machine. Because the dc-link current is often already measured for protection purposes of the power electronic components in the inverter, the dc-link current is a valuable quantity for control systems. It is a load dependent quantity, which is normally available.

2.2.4. MODELLING THE VOLTAGE SOURCE CONVERTER

For simulation purposes in this thesis, a model of the voltage source converter is needed. The physical scheme of the converter is given in figure 2-2. For modelling the following assumptions are made:

- ideal rectifier and filter, which results in a constant dc-link voltage (equation 2-2)
- ideal inverter, without switching losses and generating sinusoidal output voltages (u_{sa}, u_{sb}, u_{sc}).

Therefore, the model of the voltage source converter is supposed to be ideal. It generates sinusoidal output voltages with amplitude, u_s^*, and frequency, $\dot{\alpha}_s^{s*}$. The model is assumed to be ideal, because the fundamental properties of the control methods are not affected by the *pulse shape* of the stator voltages.

2.3. VOLTAGE FED INDUCTION MACHINE

2.3.1. GENERAL CONSIDERATION

Before describing the machine with mathematical relations, a short description of the structure and the basic principles are given.
In all rotating electrical machines a stationary non-moving part, the stator, and a rotating part, the rotor, are distinguished. Between the rotor and the stator is a small air-gap. First, the following assumptions are made:

- three identical stator windings, separated mechanically by an angle of 120°
- a smooth sinusoidal distribution of turns along the stator's circumference
- small uniform air-gap
- single symmetrical squirrel cage rotor (short-circuited bars)
- no iron and hysteresis losses
- no friction and windage losses
- no saturation effects

The working principle of an induction machine is based on a rotating magnetic field in the air-gap, due to (balanced) three phase currents in the stator windings. The rotating speed of this field is inversely proportional to the number of pole pairs and proportional to the stator voltage frequency. In case the rotor turns slower than the applied stator field (the rotor slips according to the field), a voltage is induced in the shorted winding. This voltage forces current to flow in the rotor bars. The magnetic field penetrating the rotor, combined with these currents, produces torque. In case the rotor revolves at the same frequency as the stator field (synchronous speed), no voltage will be induced in the rotor and no torque is generated.
In this thesis an *orthogonal 2-phase model* of the induction machine is used. This model is also called *semi 4-phase model* or *quadrature-phase model*, because the angle between the two phases equals $90° = 360°/\mathbf{4}$. This corresponds with the intermediate angle in 3-phase models: $120° = 360° / \mathbf{3}$.
There are different possibilities to transform a three phase model in a two phase model. In this thesis a transformation as mentioned in [Blas '91] is used. This transformation is *power invariant* and, if a three phase model is transformed in a two phase model, it results in the following properties:

- current amplitudes are multiplied with a factor 3/2
- voltage amplitudes remain the same
- flux amplitudes remain the same
- impedance's are multiplied with a factor 3/2

The transformation matrices are given in appendix A.

2.3.2. MATHEMATICAL DESCRIPTION

As mentioned before, the single cage induction machine has a stator, fed by a symmetric two phase voltage system, and a short-circuited cage. The voltage fed induction machine is described with the equation system as given below [Blas, '91]:

$$\vec{u}_s^s = r_s \vec{i}_s^s + \frac{d}{dt}\left(\vec{\psi}_s^s\right) \tag{2-8}$$

$$\vec{0} = r_k \vec{i}_k^r + \frac{d}{dt}\left(\vec{\psi}_k^r\right) \tag{2-9}$$

$$\vec{\psi}_s^s = \vec{\psi}_l^s + l_{\sigma s} \vec{i}_s^s \tag{2-10}$$

$$\vec{\psi}_k^a = \vec{\psi}_l^a + l_{\sigma k} \vec{i}_k^a \tag{2-11}$$

$$\vec{\psi}_l^a = l_l \vec{i}_{\mu l}^a \tag{2-12}$$

$$\vec{i}_{\mu l}^a = \vec{i}_s^a + \vec{i}_k^a \tag{2-13}$$

$$m_{el} = \left[R\left(\tfrac{\pi}{2}\right) \cdot \vec{\psi}_l^a\right]^T \vec{i}_s^a \tag{2-14}$$

$$\dot{\rho}^s = \frac{1}{\theta} \int \left(m_{el} - m_{load}\right) dt \tag{2-15}$$

For the sake of compactness, the equation system will be rewritten. The stator flux, $\vec{\psi}_s^s$, and the air-gap flux $\vec{\psi}_l^a$ in (2-8) are eliminated by substitution of (2-10) and (2-11)

$$\vec{u}_s^s = r_s \vec{i}_s^s + \frac{d}{dt}\left(\vec{\psi}_k^s - l_{\sigma k} \vec{i}_k^s + l_{\sigma s} \vec{i}_s^s\right). \tag{2-16}$$

The cage-flux is expressed in terms of stator current, i_s^a, and cage current, i_k^a, by substitution of (2-12) and (2-13) in (2-11)

$$\vec{\psi}_k^a = l_l\left(\vec{i}_s^a + \vec{i}_k^a\right) + l_{\sigma k} \vec{i}_k^a. \tag{2-17}$$

Finally, to calculate the electric torque, the cage-flux is used instead of the air-gap flux by substitution of (2-11) in (2-14)

$$m_{el} = \left[R\left(\tfrac{\pi}{2}\right) \cdot \left(\vec{\psi}_k^a - l_{\sigma k} \vec{i}_k^a\right)\right]^T \vec{i}_s^a. \tag{2-18}$$

The equation system contains different references (s, r, a). For a uniform description of the voltage fed induction machine, a general reference is necessary. As a general reference the cage-flux is chosen, because:

- in relation to the cage-flux axis, in steady state all quantities are dc quantities
- the cage-flux is a central quantity in the machine
- the control methods discussed in chapter 3 of this thesis are derived from field orientation methods, which also uses the cage-flux as a general reference.

The coordinates of the system with the cage-flux as general reference, are called *field coordinates*. Transformation of the equation system ((2-9),(2-15),(2-16),(2-17) and

(2-18)) to the field coordinate system, means that every vector is projected on the cage-flux axis. As seen in figure 2-7, this result in some rotations by a specific angle. Rotor (cage) quantities are rotated by an angle φ^r and stator quantities are rotated by an angle φ^s.

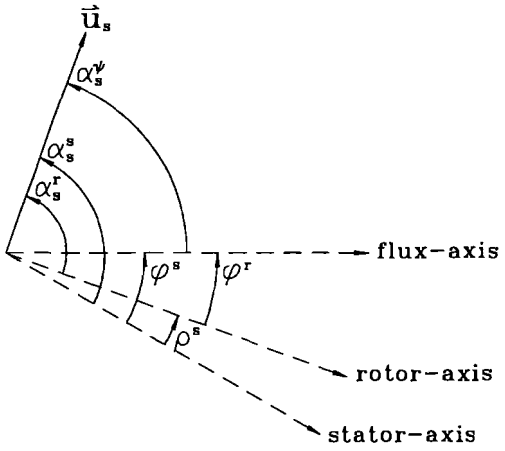

Figure: 2-7: Angle definitions

From figure 2-7 the following angle relations are defined:

$$\varphi^s = \varphi^r + \rho^s \tag{2-19}$$

$$\alpha_s^s = \alpha_s^\psi + \varphi^s \tag{2-20}$$

$$\alpha_s^s = \alpha_s^r + \rho^s. \tag{2-21}$$

The transformed equation system in field coordinates is given by the following set of equations [Blas, '91]:

$$\vec{u}_s^\psi = r_s \vec{i}_s^\psi + \frac{d}{dt}\left(\vec{\psi}_k^\psi + l_{\sigma s}\vec{i}_s^\psi - l_{\sigma k}\vec{i}_k^\psi\right) + R(\tfrac{\pi}{2})\left(\vec{\psi}_k^\psi + l_{\sigma s}\vec{i}_s^\psi - l_{\sigma k}\vec{i}_k^\psi\right)\frac{d}{dt}(\varphi^s) \tag{2-22}$$

$$\vec{0} = r_k \vec{i}_k^\psi + \frac{d}{dt}\left(\vec{\psi}_k^\psi\right) + R(\tfrac{\pi}{2})\vec{\psi}_k^\psi \frac{d}{dt}(\varphi^r) \tag{2-23}$$

$$\vec{\psi}_k^\psi = l_l\left(\vec{i}_s^\psi + \vec{i}_k^\psi\right) + l_{\sigma k}\vec{i}_k^\psi \tag{2-24}$$

$$m_{el} = \left[R(\tfrac{\pi}{2})\cdot\left(\vec{\psi}_k^\psi - l_{\sigma k}\vec{i}_k^\psi\right)\right]^T \vec{i}_s^\psi \tag{2-25}$$

$$\dot{\rho}^s = \frac{1}{\theta}\int (m_{el} - m_{load})\,dt. \tag{2-26}$$

The vector quantities in (2-22)...(2-25) consists of two components:

- a component in the direction of the cage-flux (superscript b)
- a component perpendicular to the direction of the cage-flux (superscript w).

Separating the vector equations in two components results in:

$$u_s^b = r_s i_s^b + \frac{d}{dt}\left(\psi_k + l_{\sigma s} i_s^b - l_{\sigma k} i_k^b\right) - \left(l_{\sigma s} i_s^w - l_{\sigma k} i_k^w\right)\frac{d}{dt}\left(\varphi^s\right) \tag{2-27}$$

$$u_s^w = r_s i_s^w + \frac{d}{dt}\left(l_{\sigma s} i_s^w - l_{\sigma k} i_k^w\right) + \left(\psi_k + l_{\sigma s} i_s^b - l_{\sigma k} i_k^b\right)\frac{d}{dt}\left(\varphi^s\right) \tag{2-28}$$

$$-r_k i_k^b = \frac{d}{dt}\left(\psi_k\right) \tag{2-29}$$

$$-r_k i_k^w = \psi_k \frac{d}{dt}\left(\varphi^r\right) \tag{2-30}$$

$$\psi_k = l_l i_s^b + \left(l_l + l_{\sigma k}\right) i_k^b \tag{2-31}$$

$$0 = l_l i_s^w + \left(l_l + l_{\sigma k}\right) i_k^w \tag{2-32}$$

$$m_{el} = \psi_k i_s^w - l_{\sigma k}\left(i_k^b i_s^w - i_k^w i_s^b\right) = \left(\frac{l_l}{l_l + l_{\sigma k}}\right)\psi_k i_s^w \tag{2-33}$$

$$\dot{\rho}^s = \frac{1}{\theta}\int\left(m_{el} - m_{load}\right) dt. \tag{2-34}$$

The cage-flux has obviously only one component, therefore the superscript, b, has been omitted.

2.3.3. QUASI-STATIONARY BEHAVIOUR

The quasi-stationary state of a voltage fed induction machine with cage rotor is characterised by a constant value of the electrical state quantities: the cage-flux, ψ_k, and both components of the stator current, i_s^b, i_s^w. Therefore the derivatives of them are zero. Accordingly:

$$\left[\frac{d}{dt}\left(\psi_k\right)\right]_0 = 0 \text{ and } \left[\psi_k\right]_0 = \text{constant} \tag{2-35}$$

$$\left[\frac{d}{dt}\left(i_s^b\right)\right]_0 = 0 \text{ and } \left[i_s^b\right]_0 = \text{constant} \tag{2-36}$$

$$\left[\frac{d}{dt}\left(i_s^w\right)\right]_0 = 0 \text{ and } \left[i_s^w\right]_0 = \text{constant}. \tag{2-37}$$

From (2-29) and (2-30) follows that

$$\left[i_k^b\right]_0 = 0 \tag{2-38}$$

$$\left[\frac{d}{dt}\left(i_k^w\right)\right]_0 = 0. \tag{2-39}$$

Equation (2-38) means that there is no magnetising cage current component in the direction of the cage-flux, in other words the cage current stands stationary perpendicular to the cage-flux. Taking (2-35)...(2-39) into account, then the voltage fed induction machine in steady-state is described by the following set of equations:

$$\left[u_s^b\right]_0 = r_s\left[i_s^b\right]_0 - l_l\sigma_s\left[i_s^w\right]_0\left[\dot{\varphi}^s\right]_0 - l_l\left(\frac{\sigma_k}{1+\sigma_k}\right)\left[i_s^w\right]_0\left[\dot{\varphi}^s\right]_0 \tag{2-40}$$

$$\left[u_s^w\right]_0 = r_s\left[i_s^w\right]_0 + \left[\psi_k\right]_0\left[\dot{\varphi}^s\right]_0 + l_l\sigma_s\left[i_s^b\right]_0\left[\dot{\varphi}^s\right]_0 \tag{2-41}$$

$$-r_k\left[i_k^w\right]_0 = \left[\psi_k\right]_0\left[\dot{\varphi}^r\right]_0 \tag{2-42}$$

$$\left[\psi_k\right]_0 = l_l\left[i_s^b\right]_0 \tag{2-43}$$

$$0 = \left[i_s^w\right]_0 + (1+\sigma_k)\left[i_k^w\right]_0 \tag{2-44}$$

$$\left[m_{el}\right]_0 = \left(\frac{1}{1+\sigma_k}\right)\cdot\left[\psi_k\right]_0\left[i_s^w\right]_0 \tag{2-45}$$

$$\left[\dot{\rho}^s\right]_0 = \frac{1}{\theta}\int\left(\left[m_{el} - m_{load}\right]_0\right)dt. \tag{2-46}$$

For write-convenience, the derivatives of quantities have been expressed with the dot-symbol ($\dot{}$), instead of the $\frac{d}{dt}$-symbol and the *absolute* leakage inductances are replaced by *relative* leakage inductances, defined as:

$$\sigma_s = \frac{l_{\sigma s}}{l_l} \tag{2-47}$$

$$\sigma_k = \frac{l_{\sigma k}}{l_l}. \tag{2-48}$$

Both components $\left[u_s^b\right]_0$ and $\left[u_s^w\right]_0$ of the stator voltage vector are constant values, so the voltage vector is also constant (the length, $\left[u_s\right]_0$, as well as the angle between the vector and the flux-axis, $\left[\alpha_s^\psi\right]_0$):

$$\left[\alpha_s^\psi\right]_0 = \text{constant, and } \left[\dot{\alpha}_s^\psi\right]_0 = 0. \tag{2-49}$$

Therefore the derivatives of the angle relations (2-19)...(2-21) become in steady-state:

$$\left[\dot{\alpha}_s^s\right]_0 = \left[\dot{\varphi}^s\right]_0 \tag{2-50}$$

$$\left[\dot{\alpha}_s^r\right]_0 = \left[\dot{\varphi}^r\right]_0 \tag{2-51}$$

$$\left[\dot{\alpha}_s^s\right]_0 = \left[\dot{\alpha}_s^r\right]_0 + \left[\dot{\rho}^s\right]_0. \tag{2-52}$$

From the equations (2-43) and (2-45) it follows that the stator current component $\left[i_s^b\right]_0$ and $\left[i_s^w\right]_0$ are determinative for the cage-flux and the electric torque respectively. This is similar to the decoupled control behaviour of a separately excited dc-machine, where the flux is proportional to the field current and the torque is proportional to product of armature current and flux. Equation (2-52) means that the

angular frequency of the stator voltage, $[\dot{\alpha}_s^s]_0$, is equal to the sum of the slip frequency, $[\dot{\alpha}_s^r]_0$, and the mechanical angular frequency of the rotor, $[\dot{\rho}^s]_0$.
Because of better understanding, the set of stationary equations are graphically represented in the vector diagram of figure 2-8.

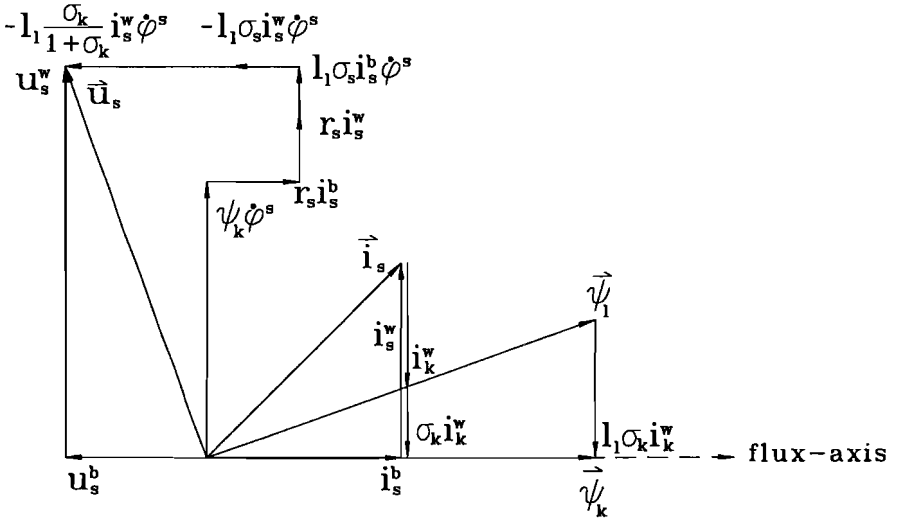

Figure: 2-8: Stationary vector representation of a voltage fed induction machine

2.3.4. CAGE-FLUX

A voltage fed induction machine with a cage-rotor can be seen as a two-port with the *stator voltage*, u_s, and the *angular frequency of the stator voltage*, $\dot{\alpha}_s^s$, as input quantities. A constant cage-flux in the induction machine is important if operation with full torque capability is desired. To maintain a constant cage-flux in the machine, it is important to know the influence of the input quantities on the cage-flux.
The stator current consists of two components: $[i_s^b]_0$ and $[i_s^w]_0$. They are determined by (2-43) and the substitution of (2-42) in (2-44) respectively

$$[i_s^b]_0 = \frac{[\psi_k]_0}{l_1} \tag{2-53}$$

$$[i_s^w]_0 = \left(\frac{1+\sigma_k}{r_k}\right)\cdot[\psi_k]_0[\dot{\varphi}^r]_0. \tag{2-54}$$

Substitution of these stator current components in (2-40) and (2-41) and taking (2-50) and (2-51) into account, results in two important expressions of the voltage fed induction machine:

$$[u_s^b]_0 = [\psi_k]_0\cdot\Omega_1 \tag{2-55}$$

$$[u_s^w]_0 = [\psi_k]_0\cdot\Omega_2, \tag{2-56}$$

with:

$$\Omega_1 = \Omega_1\left(\left[\dot{\alpha}_s^r\right]_0, \left[\dot{\alpha}_s^s\right]_0\right) = \left(\frac{r_s}{l_1} - \frac{l_1}{r_k}\left((1+\sigma_k)(1+\sigma_s)-1\right)\left[\dot{\alpha}_s^r\right]_0\left[\dot{\alpha}_s^s\right]_0\right) \tag{2-57}$$

$$\Omega_2 = \Omega_2\left(\left[\dot{\alpha}_s^r\right]_0, \left[\dot{\alpha}_s^s\right]_0\right) = \left(\frac{r_s}{r_k}(1+\sigma_k)\left[\dot{\alpha}_s^r\right]_0 + (1+\sigma_s)\left[\dot{\alpha}_s^s\right]_0\right). \tag{2-58}$$

The stationary value of the cage-flux is determined by

$$\left[\psi_k\right]_0 = \frac{\left[u_s\right]_0}{\sqrt{\Omega_1^2 + \Omega_2^2}}, \tag{2-59}$$

where $\left[u_s\right]_0$ is the amplitude of the (fundamental) stator voltage:

$$\left[u_s\right]_0 = \sqrt{\left[u_s^b\right]_0^2 + \left[u_s^w\right]_0^2}. \tag{2-60}$$

Relation (2-59) is the corner stone of all scalar control methods of a voltage fed induction machine, which assume a constant flux. A roughly approximation arises if the influences of the stator impedance ($r_s, l_{\sigma s}$) and the cage-leakage inductance ($l_{\sigma k}$) are neglected (paragraph 3.4)

$$\left[\psi_k\right]_0 \approx \frac{\left[u_s\right]_0}{\left|\left[\dot{\alpha}_s^s\right]_0\right|}. \tag{2-61}$$

For a constant cage-flux, it is necessary to hold the relation between stator voltage and stator voltage frequency constant.

2.3.5. ELECTRIC TORQUE

The electric torque of a voltage fed induction machine is an important quantity. The electric torque (Lorentz force) is a result of the current through the conductors (stator windings, rotor bars) and the magnetic field around them (flux).
As mentioned in (2-45) the electric torque in steady-state is determined by:

$$\left[m_{el}\right]_0 = \left(\frac{1}{1+\sigma_k}\right) \cdot \left[\psi_k\right]_0 \left[i_s^w\right]_0. \tag{2-62}$$

If the cage-flux is assumed constant at its rated value, then a maximum torque sensitivity per ampere stator current is achieved. The torque-stator current ratio can be seen as a measure of efficiency. A higher value than the rated value of the cage-flux leads to saturation.
Substitution of (2-54) in (2-62) results in

$$\left[m_{el}\right]_0 = \frac{\left[\psi_k\right]_0^2}{r_k} \cdot \left[\dot{\alpha}_s^r\right]_0, \tag{2-63}$$

and with the cage-flux given by (2-59), this yields

$$[m_{el}]_0 = \frac{[\dot{\alpha}_s^r]_0}{r_k} \cdot \frac{[u_s]_0^2}{\Omega_1^2 + \Omega_2^2}. \tag{2-64}$$

The term $(\Omega_1^2 + \Omega_2^2)$ in the denominator is dependent of both the stator voltage frequency, $[\dot{\alpha}_s^s]_0$, and the slip frequency,$[\dot{\alpha}_s^r]_0$. If (2-57) and (2-58) are substituted in (2-64), and when the higher order terms are neglected, a good approximation of the electric torque is found by

$$[m_{el}]_0 \approx \frac{r_k}{[S]_0 \cdot [\dot{\alpha}_s^s]_0} \frac{[u_s]_0^2}{\left(r_s + \frac{r_k}{[S]_0}\right)^2 + \left(l_l(\sigma_s + \sigma_k)[\dot{\alpha}_s^s]_0\right)^2}, \tag{2-65}$$

where the slip, $[S]_0$, is defined as the relative slip frequency with respect to the stator voltage frequency:

$$[S]_0 = \frac{[\dot{\alpha}_s^r]_0}{[\dot{\alpha}_s^s]_0}. \tag{2-66}$$

The slip, $[S]_{0,max}$, where the electric torque reaches it maximum value is found by differentiation of (2-65) with respect to the slip and then equating it to zero:

$$[S]_{0,max} \approx \pm \frac{r_k}{\sqrt{r_s^2 + \left(l_l(\sigma_s + \sigma_k)[\dot{\alpha}_s^s]_0\right)^2}}. \tag{2-67}$$

The positive value of the slip belongs to the motoring mode of the induction machine, and the negative value of the slip belongs to the regenerating mode of the induction machine. Substitution of (2-67) in (2-65), gives the maximum electric torque value (motoring mode):

$$[m_{el}]_{0,max} \approx \frac{1}{2[\dot{\alpha}_s^s]_0} \frac{[u_s]_0^2}{\sqrt{r_s^2 + \left(l_l(\sigma_s + \sigma_k)[\dot{\alpha}_s^s]_0\right)^2} + r_s}. \tag{2-68}$$

2.3.6. MODELLING THE VOLTAGE FED INDUCTION MACHINE

For modelling the voltage fed induction machine, the model described in [Velt '93] is used. The dynamic model consists of three blocks, a stator block, a rotor block and a mechanical block (figure 2-9).
The blocks are connected by two *vector rotators*. The vector rotators calculate the following coordinate transformations:

$$\bar{\psi}_r^s = \begin{pmatrix} \cos\rho^s & -\sin\rho^s \\ \sin\rho^s & \cos\rho^s \end{pmatrix} \bar{\psi}_r^r \quad \text{and} \quad \bar{i}_s^r = \begin{pmatrix} \cos\rho^s & \sin\rho^s \\ -\sin\rho^s & \cos\rho^s \end{pmatrix} \bar{i}_s^s. \tag{2-69}$$

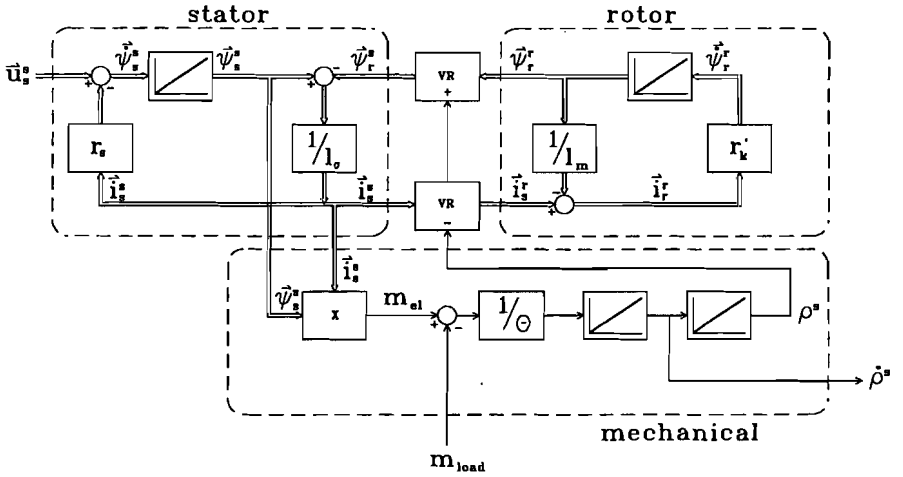

Figure: 2-9: Dynamic model of an induction machine

The mechanical rotor-displacement angle in (2-69), ρ^s, defines the angle between the current-vectors in stator ($\vec{i}_s^s$) and rotor ($\vec{i}_s^r$) coordinates and between the flux-vectors ($\vec{\psi}_r^s$ and $\vec{\psi}_r^r$). The developed electric torque is calculated by the vector product between the stator current and the stator flux:

$$m_{el} = \vec{i}_s^s \times \vec{\psi}_s^s = i_s^{s2}\psi_s^{s1} - i_s^{s1}\psi_s^{s2}. \tag{2-70}$$

The relation between the parameters of figure 2-9 and the machine parameters as used in paragraph 2.3.2. are:

$$l_\sigma = l_1\left(\frac{(1+\sigma_s)(1+\sigma_k)-1}{(1+\sigma_k)}\right) \tag{2-71}$$

$$l_m = l_1\left(\frac{1}{1+\sigma_k}\right) \tag{2-72}$$

$$r_k' = r_k\left(\frac{1}{(1+\sigma_k)^2}\right). \tag{2-73}$$

A detailed description of the induction machine model is given in [Velt '93].

3. SCALAR CONTROL OF INDUCTION MACHINES

In this chapter, some scalar control methods of induction machines fed by a voltage source inverter (pulse-width modulation) are described. As mentioned before, scalar control methods are often used in general purpose (industry) applications, like pumps, blowers, fans, shipping drives, etc.. The stationary and surely the dynamic requirements of scalar control methods are much lower with respect to vector controlled methods. More important requirements for scalar controlled drive systems are the simplicity, robustness, maintenance, costs and efficiency.
The stator voltage of an induction machine can be varied in amplitude and/or frequency. In paragraph 3.1 and 3.2, a short description is given why it is unfavourable to vary only the stator voltage or stator frequency. Paragraph 3.3 pays attention to varying both voltage and frequency.
In the next three paragraphs three drive systems which use speed control and a constant cage-flux are analysed: a constant v/f speed control with slip regulation, using a speed sensor (paragraph 3.5); and two control methods based on the approach proposed by Vuckovic and Vuckosavic (paragraph 3.6 and 3.7), both of which using a dc-link current sensor.

3.1. VARIABLE VOLTAGE OPERATION

The most simple method of induction motor control is to vary the stator voltage at constant stator frequency. The stator voltage at line frequency can be controlled by phase angle control of anti parallel thyristors connected in each phase. The properties of voltage control are:

- extremely simple configuration
- poor dynamic performance
- poor static performance
- high power loss due to high slip (inefficient)

Because of the last three disadvantages it is hardly used. The principle of variable voltage control is explained on the basis of the torque-speed curves of the induction machine. As seen in paragraph 2.3.5., there is a quadratic relation between electric torque, $[m_{el}]_0$, and stator voltage, $[u_s]_0$:

$$[m_{el}]_0 \approx \frac{r_k}{[S]_0 \cdot [\dot{\alpha}_s^s]_0} \frac{[u_s]_0^2}{\left(r_s + \frac{r_k}{[S]_0}\right)^2 + \left(l_l(\sigma_s + \sigma_k)[\dot{\alpha}_s^s]_0\right)^2} \tag{3-1}$$

In figure 3-1, a family of torque curves are plotted where the stator frequency is constant and the stator voltage is a varying parameter. A load curve is also plotted (typical for fans, pumps, blowers).

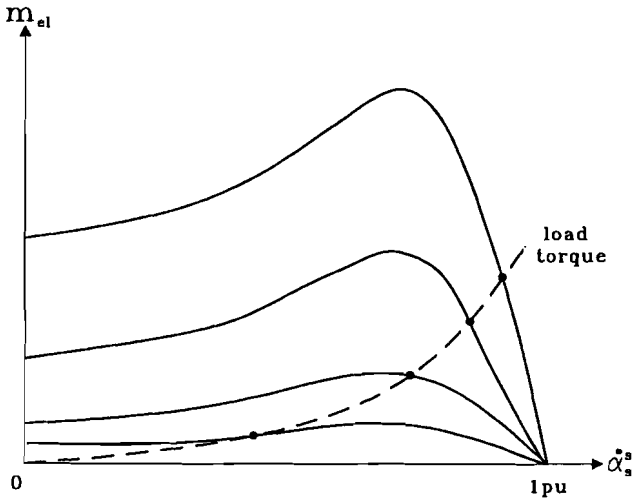

Figure: 3-1: Variable voltage control

By reducing the stator voltage, the torque-speed curve is going down in a quadratic way with respect to the stator voltage (3-1). The slip, $[S_{max}]_0$, where the torque reaches its maximum value, remains at the same value, because it is inversely proportional to the stator frequency ($r_s \to 0$)

$$[S_{max}]_0 \approx \frac{r_k}{l_1(\sigma_s + \sigma_k)[\dot{\alpha}_s^s]_0} \propto \frac{1}{[\dot{\alpha}_s^s]_0}. \tag{3-2}$$

The operating points are defined by the points of intersection between the load-curve and the motor-curves. It is easy to see that an induction machine with a high maximum slip (high cage-resistance, r_k) increases the range of speed variation. However, this causes high copper losses in the cage of the machine.
From (2-61) it follows that reducing the speed (by decreasing the stator voltage), gives a lower value of the flux in the machine. So, the developed torque per ampere of stator current is reduced (2-62). If a constant load torque is assumed , then the stator current increases, resulting in more copper loss. The losses in the machine will cause a severe machine heating problem.

3.2. VARIABLE FREQUENCY OPERATION

Another strategy to control the speed of an induction motor is to vary the stator frequency. However, the efficiency is very low, because the flux in the induction machine decreases if the frequency (speed) increases (2-61). This causes a low torque per ampere stator current ratio.
The principle of variable frequency operation is shown in figure 3-2.
From (2-68), and for convenience assuming $r_s = 0$, it follows that the maximum torque decreases in a quadratic way with respect to the stator frequency $[\dot{\alpha}_s^s]_0$.

$$[m_{el}]_{0,max} \approx \frac{[u_s]_0^2}{2 \cdot l_1(\sigma_s + \sigma_k)} \frac{1}{[\dot{\alpha}_s^s]_0^2} \propto \frac{1}{[\dot{\alpha}_s^s]_0^2} \tag{3-3}$$

The slip, $[S]_{0,max}$, where the maximum torque occurs is given by (3-2). If the stator frequency is decreased at rated voltage, the flux in the machine will saturate, causing an excessive stator current.

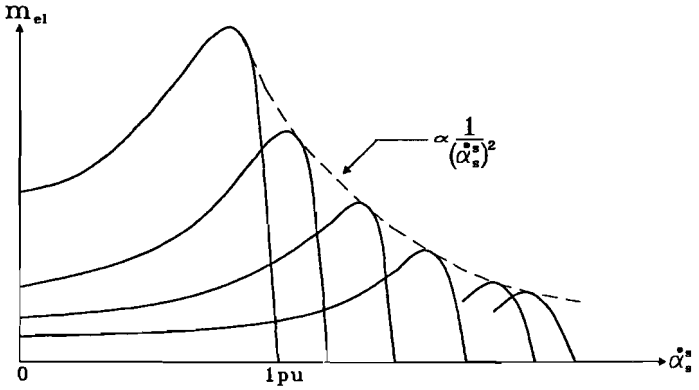

Figure: 3-2: Variable frequency control

3.3. VARIABLE-VOLTAGE VARIABLE-FREQUENCY OPERATION

Nor variable voltage control, neither variable frequency control results in satisfying properties. The main reason is that the cage-flux varies if only voltage or frequency is changed, which results in a bad torque-stator current ratio or saturation. For a constant flux it is necessary to vary both voltage and frequency (see equation (2-61)). This results in *variable-voltage variable-frequency control.* Figure 3-3 shows the torque-frequency curves for variable-voltage variable-frequency control, with the accompanying machine quantities.

By increasing the stator frequency (to increase the speed of the motor), the torque speed curve in figure 3-3 shifts to the right.

The region below the synchronous frequency (1 pu) is called the *constant torque region.* In this region, the ratio between stator voltage and stator frequency is held constant (constant v/f control). This results not only in a constant flux (2-61), but in a constant maximum torque value as well

$$[m_{el}]_{0,max} \approx \frac{1}{2 \cdot l_l(\sigma_s + \sigma_k)} \frac{[u_s]_0^2}{[\dot{\alpha}_s^s]_0^2} \propto \left[\frac{u_s}{\dot{\alpha}_s^s}\right]_0^2 = \text{constant}. \tag{3-4}$$

Now, the motor can deliver its rated torque by drawing its rated current at a constant slip frequency,

$$[m_{el}]_N = \frac{[\psi_k]_N^2}{r_k} \cdot [\dot{\alpha}_s^r]_N. \tag{3-5}$$

Both components of the stator current are also constant:

$$\left[i_s^b\right]_N = \frac{\left[\psi_k\right]_N}{l_l} \tag{3-6}$$

$$\left[i_s^w\right]_N = \frac{(1+\sigma_k)}{\left[\psi_k\right]_k} \cdot \left[m_{el}\right]_N . \tag{3-7}$$

For stator frequencies higher than the rated value, it is possible to increase the motor speed beyond its synchronous speed.

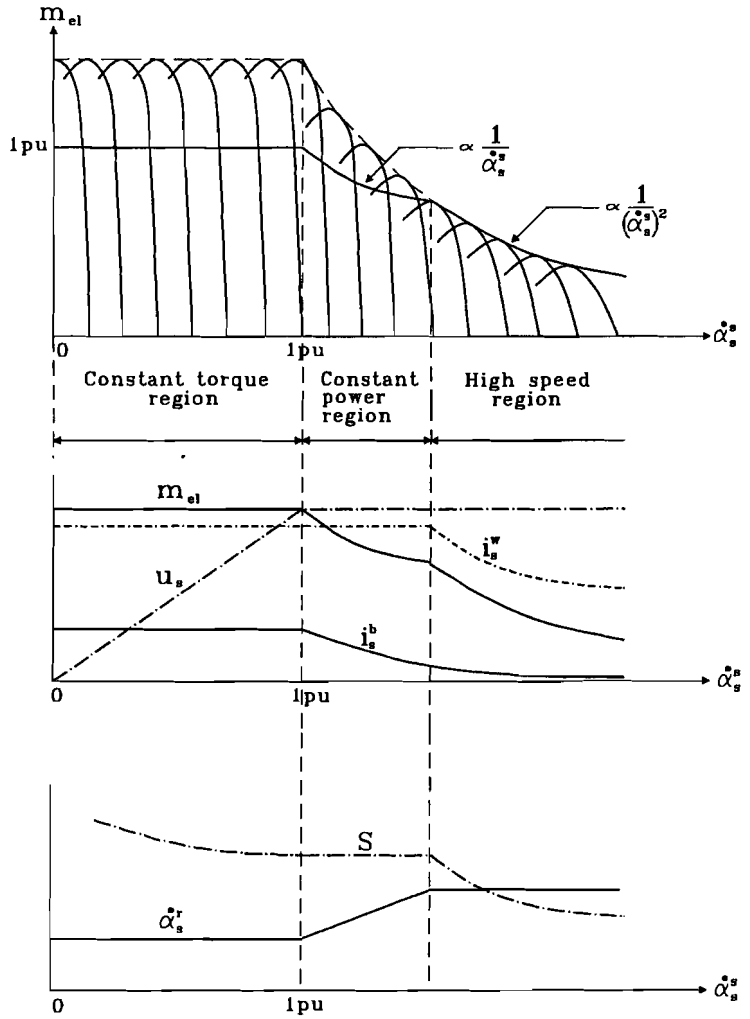

Figure: 3-3: Torque-frequency curves of variable voltage, variable frequency control with accompanying curves of the machine quantities: torque, stator voltage, stator current and slip

Because the stator voltage remains constant at its rated value, a further increasing of the stator voltage results in a reduced cage-flux (field weakening)

$$\left[\psi_k\right]_0 \propto \frac{1}{\left[\dot{\alpha}_s^s\right]_0} . \tag{3-8}$$

The envelope of the maximum torque points decreases in a quadratic way with respect to the stator frequency

$$\left[m_{el}\right]_{0,max} \approx \frac{\left[u_s\right]_N^2}{2 \cdot l_l(\sigma_s + \sigma_k)} \frac{1}{\left[\dot{\alpha}_s^s\right]_0^2} \propto \frac{1}{\left[\dot{\alpha}_s^s\right]_0^2}. \tag{3-9}$$

At the limit of the motor capability in this region, the stator current component, $\left[i_s^w\right]_0$, remains at the same value (to produce electric torque as much as possible), similar to the constant torque region. If (2-61) is substituted in (2-54), it follows that this corresponds to an increase of the slip frequency

$$\left[\dot{\alpha}_s^r\right]_0 = \frac{r_k}{(1+\sigma_k)} \cdot \frac{\left[\dot{\alpha}_s^s\right]_0}{\left[u_s\right]_N} \cdot \left[i_s^w\right]_N \propto \left[\dot{\alpha}_s^s\right]_0, \tag{3-10}$$

or from (2-66), this means that the slip remains constant

$$\left[S\right]_0 = \frac{\left[\dot{\alpha}_s^r\right]_0}{\left[\dot{\alpha}_s^s\right]_0} = \text{constant}. \tag{3-11}$$

The slip frequency increases until the maximum slip frequency is reached; the delivered electric torque changes from its rated- to its maximum value. Considering (3-12), this happens in a inversely proportional way with respect to the stator frequency

$$\left[m_{el}\right]_0 = \frac{\left[i_s^w\right]_N}{(1+\sigma_k)} \cdot \frac{\left[u_s\right]_N}{\left[\dot{\alpha}_s^s\right]_0} \propto \frac{1}{\left[\dot{\alpha}_s^s\right]_0}. \tag{3-12}$$

The magnetising component of the stator current is proportional to the cage-flux (2-43) and decreases therefore in an inversely proportional way with respect to the stator frequency

$$\left[i_s^b\right]_0 = \frac{\left[\psi_k\right]_0}{l} \propto \frac{1}{\left[\dot{\alpha}_s^s\right]_0}. \tag{3-13}$$

In large motors at the limit of the motor capability, the magnetising component of the stator current is relatively small. Therefore, the stator current, is approximately equal to its torque generating component, $\left[i_s^w\right]_0$.

The region is often called the *constant power region*, because the mechanical power remains constant in this region

$$\left[P_{mech}\right]_0 = \left[m_{el}\right]_0 \cdot \left[\dot{\rho}^s\right]_0 \propto \left(1 - \left[S\right]_0\right) = \text{constant}. \tag{3-14}$$

With the stator voltage equal to its rated value and maximum electric torque (at maximum slip frequency), it is still possible to increase the motor speed (*high speed region*). The delivered electric torque decreases in a quadratic way with respect to the stator frequency (3-9). Because the slip frequency, $\left[\dot{\alpha}_s^r\right]_0$ remains constant at its maximum value, the torque generating component of the stator current, $\left[i_s^w\right]_0$, decreases in an inversely proportional way

$$\left[i_s^w\right]_0 = \frac{(1+\sigma_k)}{r_k} \cdot \frac{\left[u_s\right]_N}{\left[\dot{\alpha}_s^s\right]_0} \cdot \left[\dot{\alpha}_s^r\right]_{0,max} \propto \frac{1}{\left[\dot{\alpha}_s^s\right]_0}. \tag{3-15}$$

Because the torque behaviour of a dc series motor is similar, this region is called the *dc series motor region.* The dc series motor region is beyond a frequency somewhere in the range of 1.5 to 2 times the synchronous frequency.
In figure 3-3, any operating point below the maximum torque envelope can be obtained by controlling the voltage and/or frequency of the machine.

3.4. CONSTANT V/F CONTROL

The constant torque region of variable frequency, variable voltage control provides a constant flux and it is the most relevant region for speed control. To keep the cage-flux constant, it is necessary to hold the ratio between stator voltage and stator frequency constant according to (2-59):

$$\left[\psi_k\right]_0 = \frac{\left[u_s\right]_0}{\sqrt{\Omega_1^2 + \Omega_2^2}} \tag{3-16}$$

$$\Omega_1 = \Omega_1\left(\left[\dot{\alpha}_s^r\right]_0, \left[\dot{\alpha}_s^s\right]_0\right) = \left(\frac{r_s}{l_1} - \frac{l_1}{r_k}\left((1+\sigma_k)(1+\sigma_s)-1\right)\left[\dot{\alpha}_s^r\right]_0\left[\dot{\alpha}_s^s\right]_0\right) \tag{3-17}$$

$$\Omega_2 = \Omega_2\left(\left[\dot{\alpha}_s^r\right]_0, \left[\dot{\alpha}_s^s\right]_0\right) = \left(\frac{r_s}{r_k}(1+\sigma_k)\left[\dot{\alpha}_s^r\right]_0 + (1+\sigma_s)\left[\dot{\alpha}_s^s\right]_0\right) \tag{3-18}$$

The denominator of (3-16) is not only non-linear but also a function of the stator voltage-frequency and the slip frequency (load).

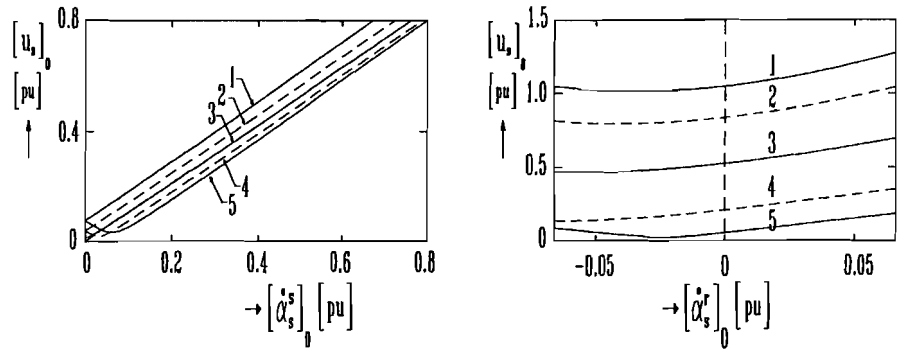

1: load torque = +2 pu	1: frequency = 1 pu
2: load torque = +1 pu	2: frequency = 0.8 pu
3: load torque = 0	3: frequency = 0.5 pu
4: load torque = -1 pu	4: frequency = 0.2 pu
5: load torque = -2 pu	5: frequency = 0.05 pu

Figure 3-4: v/f curves for different load values and voltage/slip frequency curves for different frequencies

For a typical induction machine (appendix C) some characteristics are calculated. Figure 3-4a gives a family of v/f-curves for different load values and figure 3-4b gives a family of voltage/slip frequency curves for different frequencies ($[\psi_k]_0 = 0.8$pu, and for convenience σ_k=0).

Examination of figure 3-4, suggests the following considerations:

- the stator voltage generally increases with the stator frequency in a close to linear fashion, except for regenerative operation at low frequencies which is due to the influence of the stator resistance, r_s;
- the slope of the curves are determined by the air-gap inductance, l_1, and the stator leakage inductance, $l_{\sigma s}$;
- for a certain stator frequency, the stator voltage increases in motoring operation, and decreases in regenerating operation;
- the amount of voltage increase in motoring operation is roughly proportional to the load and fairly independent from the stator frequency
- the amount of voltage decrease in regenerating operation is non-proportional to the load ($[\dot{\alpha}_s^r]_0$) and little dependent from the stator frequency in the range of high frequencies, but changes drastically in the range of low frequencies.

To achieve a constant cage-flux in all cases, it is necessary to match the curves of figure 3-4 as much as possible, in spite of the dependence of the stator voltage, $[u_s]_0$, from frequency, $[\dot{\alpha}_s^s]_0$, and load, $[\dot{\alpha}_s^r]_0$.

3.4.1. OPEN LOOP CONSTANT V/F CONTROL

The most simple voltage/frequency control structure (v/f control structure) arises if the influence of the stator impedance (r_s,$l_{\sigma s}$) and the cage-leakage inductance, $l_{\sigma k}$, are neglected in (3-16). Under this approximation, the cage-flux can be regarded as independent from load and only dependent from the stator frequency, in a linear way:

$$[u_s]_0 \approx [\psi_k]_0 \cdot \left|[\dot{\alpha}_s^s]_0\right| \tag{3-19}$$

The properties of, the so called, *constant v/f-control with a linear characteristic* are:

- cost-effective;
- simple control structure;
- poor dynamic response due to flux variations during transients;
- limited steady-state accuracy with open speed loop, since both flux and slip frequency change with the load;

In spite of these last three shortcomings it is an often applied control structure for voltage fed induction motors, because it is found satisfactory for low-performance, cost effective industrial drives. Accordingly equation (3-19), constant cage-flux with a linear

characteristic is ensured simply by keeping the stator voltage strictly proportional to the stator frequency, $\left[\dot{\alpha}_s^s\right]_0$, (figure 3-5).

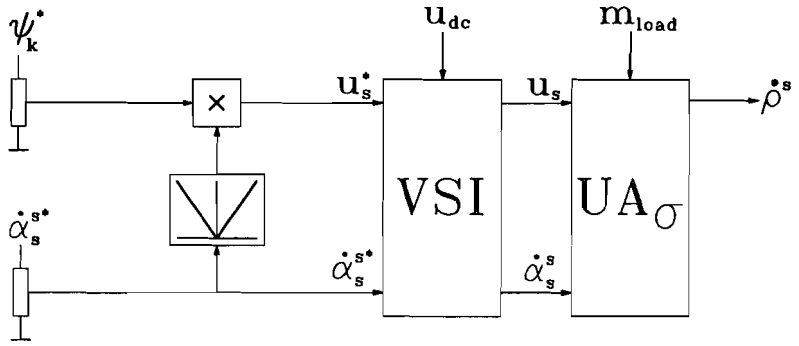

Figure: 3-5: Open loop constant v/f control with linear characteristic

For relatively high (stator)frequencies this approach is valid and leads to moderate under excitation (motoring operation) and over excitation (regenerating operation).
In the low speed region the voltage drop across the (neglected) stator resistance become so important, with respect to the stator voltage, u_s, that ignoring it leads to considerable under excitation (reduced torque/stator current ratio). Techniques to compensate the stator voltage drop are (figure 3-6):

- *linear shift*, realised by adding a constant value to the stator voltage;
- *low speed voltage boost*, realised by adding a frequency dependent voltage to the stator voltage (at low speeds);
- a *combination* of both techniques;

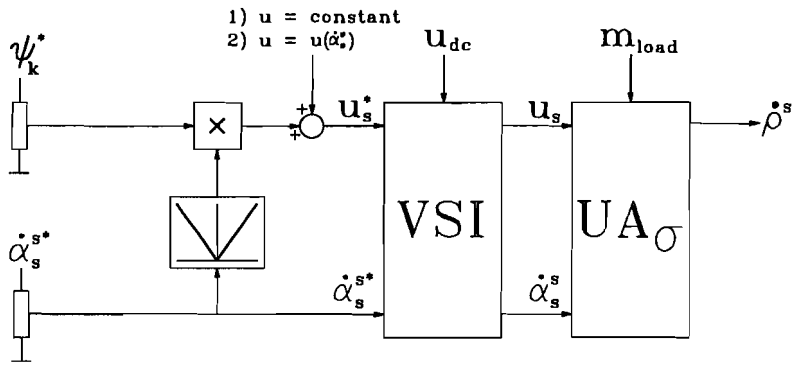

Figure: 3-6: Open loop constant v/f control with linear characteristic and voltage boost (or linear shift)

Because a voltage boost is still present if the machine is not loaded, the compensation methods lead to over excitation, particularly at low speeds. Over excitation causes saturation and therefore motor heating problems.

In the configurations above, the dependency of the load is not included. In reality the cage-flux decreases with increasing motor load, because of the increasing voltage drop across the stator resistance, r_s, caused by the stator current, i_s. As seen in figure 3-4, to neutralise this effect it is necessary to increase the stator voltage, u_s, nearly proportional to a *load-dependent parameter*. Both stator current, i_s, and slip frequency, $\dot{\alpha}_s^r$, are possible candidates (figure 3-7 and 3-8).
If the stator current, i_s, is used, feedback of the stator current amplitude (rectified value), $|i_s|$, is inaccurate. It is required to take the phase-relation of u_s and i_s into account, in order to decern the magnetising current, i_s^b, from the load current, i_s^w. In addition, the sign of the feedback has only one polarity (generally the wrong one for regenerative loads, because this never results in under excitation). The so called *current-dependent boost* (figure 3-7), exhibits poor stability characteristics, gives machine saturation at zero load and needs not only a current sensor, but a voltage sensor as well [Abbo '77].

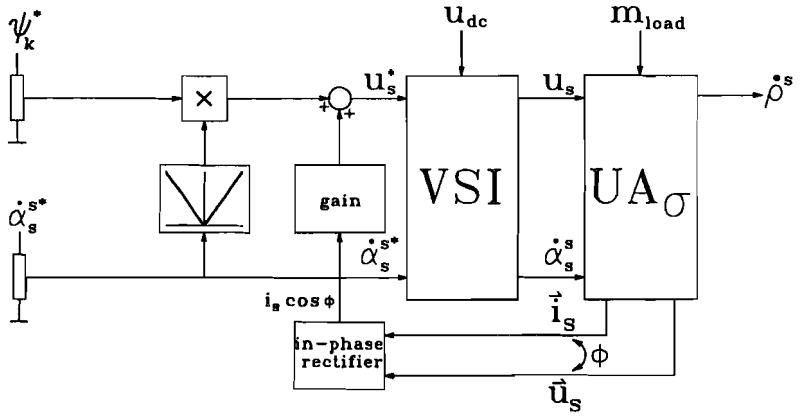

Figure 3-7: Open loop constant v/f control with linear characteristic and the stator current as load dependent parameter

A *slip-dependent boost* technique (figure 3-8) gives a better stability, has no saturation problems at no load but requires a speed sensor (dc tachometer). When the speed sensor is not needed for speed regulation, maybe this solution is expensive and impractical.

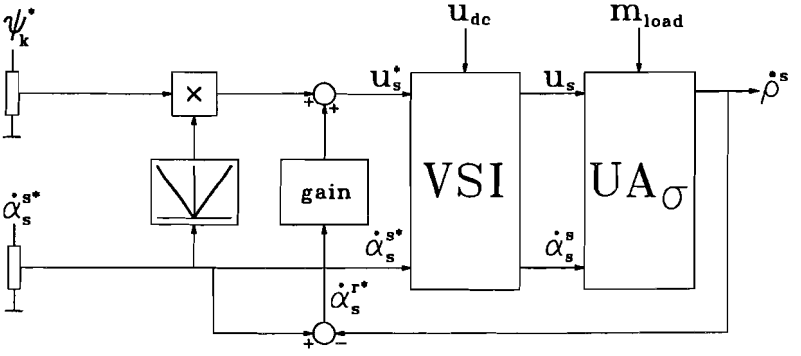

Figure: 3-8: Open loop constant v/f control with linear characteristic and the slip frequency as load dependent parameter

3.4.2. CLOSED LOOP CONSTANT V/F CONTROL

To obtain a constant cage-flux, approximations of the ideal v/f-characteristics (figure 3-4), as mentioned before, are not sufficient. It is necessary to make duplicates of the characteristics, taking the influence of the load into account and making no neglects. In this case, only a closed loop flux regulation technique complies (figure 3-9). It regulates the flux to its desired level in any situation, without the drawbacks of the previously described methods.
However, *flux-sensors* (Hall elements) are expensive and impractical, because of the special mechanical work on the motor. It would make the drive impractical to handle as a standard commercial drive.
Other methods to obtain a flux (related) signal are available:

- *Probing coils* (small stator windings) are simpler to implement but are also incompatible with the use of standard motors.
- *Synthesis of the air-gap voltage*, by subtraction the magnitude of the stator impedance voltage drop from the stator voltage, is temperature sensitive due to the variations in the stator resistance.
- *A method proposed by A. Abbondanti* [Abbo, 77] determines a flux related signal from the reactive power. The flux related signal is independent of the stator resistance, but requires measured values of stator phase voltages and -currents in order to calculate the reactive power signal.

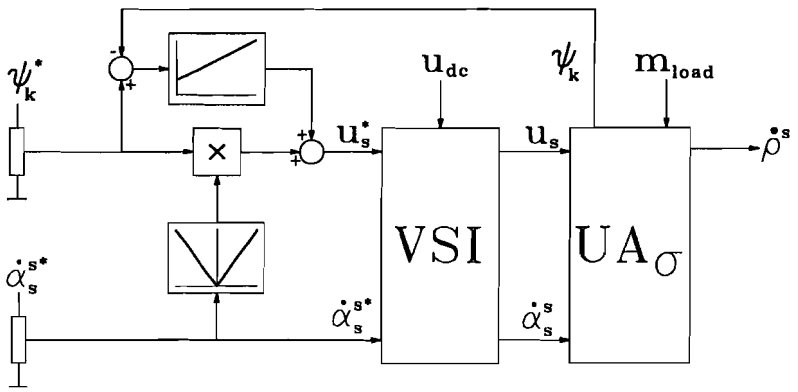

Figure: 3-9: Closed loop constant v/f control with flux control

It should be emphasised that closed loop constant v/f-control is used for electrical drives where a constant steady-state flux in *any* situation is necessary.

3.5. CONSTANT V/F SPEED CONTROL WITH SLIP REGULATION

Constant v/f speed control with slip regulation [Bose '87] make use of an ideal non-linear v/f-characteristic to ensure a stationary constant cage-flux. To compensate the stationary speed error, caused by a load change, the slip frequency is taken into account. The control system uses the measured speed value (dc tachometer).

3.5.1. CONTROL STRUCTURE

A block diagram of the speed control system is shown in figure 3-10.

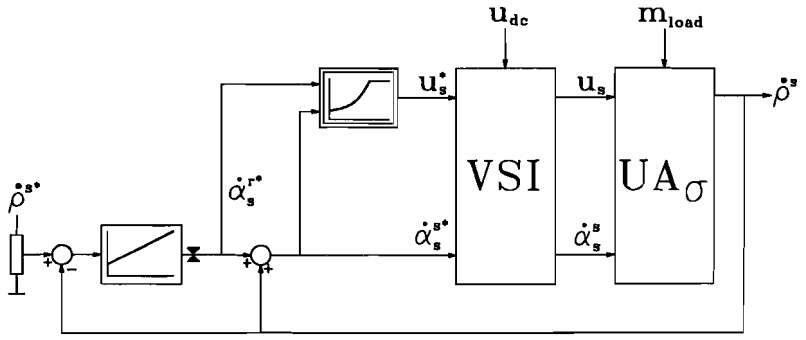

Figure: 3-10: Control structure of constant v/f speed control with slip regulation

The slip frequency signal, $\left[\dot{\alpha}_s^{r*}\right]_0$, which is proportional to the torque (2-63) is regulated by the speed loop error $\left(\dot{\rho}^{s*} - \dot{\rho}^s\right)$. The slip frequency is added with the measured speed signal, $\left[\dot{\rho}^s\right]_0$, to generate the stator voltage frequency (2-52):

$$\left[\dot{\rho}^s\right]_0 = \left[\dot{\alpha}_s^{s*}\right]_0 - \left[\dot{\alpha}_s^{r*}\right]_0 \tag{3-20}$$

The desired stator voltage signal, $\left[u_s^*\right]_0$ is generated from the frequency signal through the non-linear v/f-characteristic (3-16) to maintain a constant desired cage-flux, $\left[\psi_k^*\right]_0$. The drive system accelerates with a clamped value of the slip frequency, which corresponds to maximum torque (2-68), and settles down to a stationary value as required by the load. If the desired speed, $\left[\dot{\rho}^{s*}\right]_0$, is reduced , the slip frequency, $\left[\dot{\alpha}_s^{r*}\right]_0$, becomes negative and the drive system goes into regenerative mode.
Since the slip frequency is proportional to the developed electrical torque, the scheme can be considered as torque-control within a speed control loop. In contrast with figure 3-10, torque control is often realised using the stator current. The advantage of the scheme in figure 3-10 is that an (expensive) current sensor is avoided; the measured speed signal is used in both loops.

3.5.2. CONTROL PARAMETERS

In the control structure of figure 3-10 only the values of the integration time constant, τ_i, and the gain, κ_p, of the ordinary PI-controller are control parameters. A PI-controller has a transfer function given by (where s is the Laplace operator)

$$H_{PI}(s) = \kappa_p \frac{(1+\tau_i s)}{\tau_i s}. \tag{3-21}$$

The control parameters are determinative for the dynamics of the drive system. Integral action of the PI-controller is necessary to eliminate the stationary speed error.
To tune the controller, first an (approximated) system description is needed. The input of the system to be controlled is the slip frequency, $\dot{\alpha}_s^{r*}$, and the output is the speed, $\dot{\rho}^s$. Because the electrical time constants are relative small with respect to mechanical time constant, the transfer function of the process to be controlled is divided in a mechanical part and an electrical part

$$H_{process}(s) = H_{mech}(s) \cdot H_{el}(s) \tag{3-22}$$

$$\left(\frac{\dot{\rho}^s}{\dot{\alpha}_s^{r*}}\right)_{process} = \left(\frac{\dot{\rho}^s}{m_{el}}\right)_{mechanical} \cdot \left(\frac{m_{el}}{\dot{\alpha}_s^{r*}}\right)_{electrical}. \tag{3-23}$$

The mechanical part is determined by (2-46). The dynamics of the electrical part are approximated by simulation, because an analytical description leads to complex expressions due to the high order dynamic character of an induction machine. A first order approximation was sufficient. So, the electrical part is determined by (at 80% of rated cage-flux)

$$\left(\frac{m_{el}}{\dot{\alpha}_s^r}\right) \approx \frac{\kappa_{el}}{1+\tau_{el}s} = \frac{32}{1+14s}. \tag{3-24}$$

The gain, κ_{el}, is easy to find analytically using (2-63):

$$\kappa_{el} = \left[\frac{m_{el}}{\dot{\alpha}_s^r}\right]_0 = \frac{[\psi_k]_0^2}{r_k}. \tag{3-25}$$

The simplified drive system is given in figure 3-11.

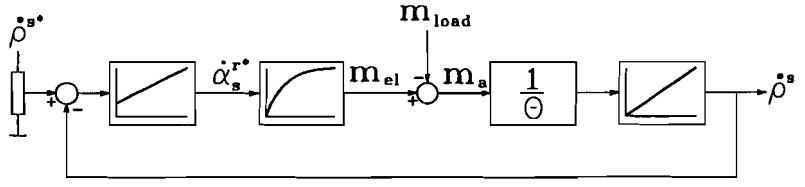

Figure: 3-11: Simplified scheme of constant v/f speed control with slip regulation

The transfer function of the open loop system is:

$$\left(\frac{\dot{\rho}^s}{\dot{\rho}^{s*}}\right)_{open\ loop} = \frac{\kappa_p \kappa_{el}}{\Theta \tau_{el}} \frac{(s+1/\tau_i)}{s^2(s+1/\tau_{el})} \tag{3-26}$$

The PI-controller is tuned by the 'symmetric optimum (SO)' standard. The SO-standard realises a closed loop transfer function which value is equal to unity, for a bandwidth as great as possible [Vput '92]. This results in parameter conditions as given below:

$$\kappa_p = \frac{\theta}{2\kappa_{el}\tau_{el}} = 0.48 \tag{3-27}$$

$$\tau_i = 4\tau_{el} = 56\,\text{pu} = 178.2\,\text{ms}. \tag{3-28}$$

The closed loop transfer function of the controlled system is:

$$\left(\frac{\dot{\rho}^s}{\dot{\rho}^{s*}}\right) = \frac{1+4\tau_{el}s}{1+4\tau_{el}s+8\tau_{el}^2s^2+8\tau_{el}^3s^3}, \tag{3-29}$$

in the time domain this means (inverse Laplace transformation):

$$\left(\frac{\dot{\rho}^s}{\dot{\rho}^{s*}}\right) = 1+e^{-t/2\tau_{el}}-2e^{-t/4\tau_{el}}\cos\left(\frac{\sqrt{3}}{4\tau_{el}}t\right). \tag{3-30}$$

Therefore, the percentage overshoot, PO = 43.3%, the *rise time* at which the response reaches the first time the steady-state value, $T_{rise} = 3.1\tau_{el} = 43.4\,\text{pu} = 137.8\,\text{ms}$, and the *settling time* at which the response comes permanently in a 2% band around the steady-state value, $T_{set} = 16.5\tau_{el} = 231\,\text{pu} = 735.3\,\text{ms}$.
The percentage overshoot is unacceptable, so a smoothing of the control command, $\left[\dot{\rho}^{s*}\right]_0$, is needed. If a smoothing filter with a time constant, $\tau_{smooth} = 4\tau_{el} = 56\,\text{pu}$, is put in front of the control command

$$\frac{\dot{\rho}^{s*}}{\dot{\rho}^{s**}} = \frac{1}{1+\tau_{smooth}s}, \tag{3-31}$$

the closed loop transfer function of the controlled system becomes

$$\left(\frac{\dot{\rho}^{s*}}{\dot{\rho}^{s**}}\right) = \frac{1}{1+4\tau_{el}s+8\tau_{el}^2s^2+8\tau_{el}^3s^3}. \tag{3-32}$$

Hence, in the time domain:

$$\left(\frac{\dot{\rho}^{s*}}{\dot{\rho}^{s**}}\right) = 1+e^{-t/2\tau_{el}}-\frac{2}{\sqrt{3}}e^{-t/4\tau_{el}}\cos\left(\frac{\sqrt{3}}{4\tau_{el}}t\right), \tag{3-33}$$

this results in the following properties:

$$\begin{aligned} &PO = 8.1\% \\ &T_{rise} = 7.6\tau_{el} = 106.4\,\text{pu}\,(\approx 338\,\text{ms}) \\ &T_{set} = 13.3\tau_{el} = 186.2\,\text{pu}\,(\approx 593\,\text{ms}) \end{aligned} \tag{3-34}$$

In the simulations, the slip value is clamped to the maximum slip value ($S_{max} = \pm 0.066\,\text{pu}$) and the stator voltage is clamped to the maximum value determined by the voltage source inverter ($|u_s| = 1\,\text{pu}$). The simulation results of the constant v/f speed control method with slip regulation are given and discussed in paragraph 4.1.

3.6. NON-LINEAR CONTROL METHOD USING THE DC-LINK CURRENT

A control algorithm that uses the dc-link current of a converter has been proposed by V. Vuckovic and S. Vuckosavic [Vuck '91]. Feedback of the dc-link current is very attractive, because it is nearly always measured for protection purposes. Moreover, a relative expensive and sensitive speed sensor can be avoided. The control structure is derived of field orientation theory, and aimed to obtain the constant cage-flux amplitude and proportionality between the electrical torque, the slip frequency and the torque generating component of the stator current. In this way the problems of slip compensation, stator voltage drop compensation and v/f characteristic correction are solved at the same time. The method is very accurate at stationary operation, because no neglections are made. The control structure contains non-linear calculations, therefore a (simple) micro-controller in necessary.
Figure 3-12 shows the control principle. There are two different loops: *a voltage control loop* and a *slip-compensation loop.*

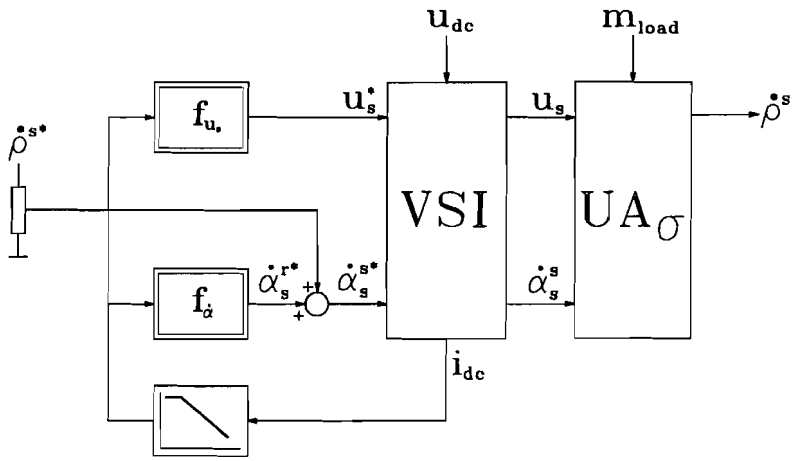

Figure: 3-12: General scheme of the non-linear control method using the dc-link current

3.6.1. STATOR CURRENT

The input power of a voltage fed induction machine, described in field coordinates, is given by

$$[p_s]_0 = [u_s^b]_0[i_s^b]_0 + [u_s^w]_0[i_s^w]_0. \tag{3-35}$$

Substitution of (2-40) and (2-41) yields an expression without voltage components

$$[p_s]_0 = r_s\left([i_s^b]_0^2 + [i_s^w]_0^2\right) + [\dot{\varphi}^s]_0 l_l\left(\frac{1}{1+\sigma_k}\right)\cdot[i_s^b]_0[i_s^w]_0. \tag{3-36}$$

If the magnetising stator current component, $[i_s^b]_0$, is assumed constant (cage-flux is constant), then the torque generating stator current component, $[i_s^w]_0$, can be calculated from the input power, $[p_s]_0$, and the stator frequency, $[\dot{\varphi}^s]_0\left(=[\dot{\alpha}_s^s]_0\right)$ as being:

$$\left[i_s^w\right]_0 = -\frac{\left[\dot{\varphi}^s\right]_0 l_l \left[i_s^b\right]_0}{2r_s(1+\sigma_k)} + \sqrt{\left(\frac{\left[\dot{\varphi}^s\right]_0 l_l \left[i_s^b\right]_0}{2r_s(1+\sigma_k)}\right)^2 + \frac{[p_s]_0}{r_s} - \left[i_s^b\right]_0^2} \tag{3-37}$$

$$\left[i_s^w\right]_0 = f_i\left(p_s, i_s^b, \dot{\varphi}^s\right). \tag{3-38}$$

The motor input power is calculated using the measured dc-link current. Assuming that there are no inverter losses (or, if they are, added to the stator resistance), the motor input power is:

$$[p_s]_0 = [u_{dc}]_0 [i_{dc}]_0. \tag{3-39}$$

For a voltage source (PWM-)inverter with constant dc-link voltage, the input power is proportional with the dc-link current, $[i_{dc}]_0$.

3.6.2. VOLTAGE CONTROL LOOP

The amplitude of the stator voltage is obtained by substitution of (2-40) and (2-41) in (3-40):

$$[u_s]_0^2 = \left[u_s^b\right]_0^2 + \left[u_s^w\right]_0^2 \tag{3-40}$$

$$[u_s]_0^2 = r_s^2 [i_s]_0^2 + \left[\dot{\varphi}^s\right]_0^2 l_l^2 (1+\sigma_s)^2 \left(\left[i_s^b\right]_0^2 + \sigma^2 \left[i_s^w\right]_0^2\right) + 2r_s \left[\dot{\varphi}^s\right]_0 l_l \left(\frac{1}{1+\sigma_k}\right) \cdot \left[i_s^b\right]_0 \left[i_s^w\right]_0 \tag{3-41}$$

with the amplitude of the fundamental component of the stator current:

$$[i_s]_0 = \sqrt{\left[i_s^b\right]_0^2 + \left[i_s^w\right]_0^2} \tag{3-42}$$

and for convenience, the leakage factor, σ, is defined as:

$$\sigma = 1 - \frac{1}{(1+\sigma_s)(1+\sigma_k)} \tag{3-43}$$

If (3-36) is substituted in (3-41), the amplitude of the fundamental stator voltage, $[u_s]_0$, can be expressed as function of the input power, the stator frequency and the flux component of the stator current:

$$[u_s]_0 = \sqrt{2r_s [p_s]_0 + \left[\dot{\varphi}^s\right]_0^2 l_l^2 (1+\sigma_s)^2 \left(\left[i_s^b\right]_0^2 + \sigma^2 \left[i_s^w\right]_0^2\right) - r_s^2 \left(\left[i_s^b\right]_0^2 + \left[i_s^w\right]_0^2\right)} \tag{3-44}$$

$$[u_s]_0 = f_u\left(p_s, i_s^b, \dot{\varphi}^s\right) \tag{3-45}$$

The torque generating component of the stator current, $\left[i_s^w\right]_0$, will be calculated by (3-38).

3.6.3. SLIP COMPENSATION LOOP

When an induction motor operates with constant stator frequency, $[\dot{\alpha}_s^s]_0$, the increase of the load torque reduces the speed, $\dot{\rho}^s$. The speed reduces to a level, where the slip frequency, $[\dot{\alpha}_s^r]_0$ reaches a value that produces an electrical torque equal to the load-torque. As mentioned earlier (2.3.3.), in steady-state, the stator frequency is equal to the sum of the desired speed and the actual slip frequency (2-52):

$$[\dot{\alpha}_s^s]_0 = [\dot{\varphi}^s]_0 = [\dot{\rho}^{s*}]_0 + [\dot{\alpha}_s^r]_0 \tag{3-46}$$

If the cage-flux is constant, the slip frequency is proportional to the torque generating component of the stator current (2-54):

$$[\dot{\alpha}_s^r]_0 = \frac{r_k}{(1+\sigma_k)[\psi_k]_0}[i_s^w]_0 \tag{3-47}$$

Substitution of (3-47) in (3-46) and taking (2-43) into account, yields:

$$[\dot{\alpha}_s^s]_0 = [\dot{\rho}^{s*}]_0 + \frac{1}{[i_s^b]_0 \tau_k}[i_s^w]_0 \tag{3-48}$$

with the cage time constant, τ_k, defined as

$$\tau_k = l_l(1+\sigma_k)/r_k . \tag{3-49}$$

Again, the torque generating component of the stator current, $[i_s^w]_0$, will be calculated by (3-38). If (3-38) is substituted in (3-48), the stator voltage frequency $[\dot{\alpha}_s^s]_0$ is determined according to (3-50):

$$[\dot{\alpha}_s^s]_0 = [\dot{\rho}^{s*}]_0 + f_{\dot{\alpha}}(p_s, i_s^b, \dot{\varphi}^s) \tag{3-50}$$

with:

$$f_{\dot{\alpha}}(p_s, i_s^b, \dot{\varphi}^s) = \frac{1}{[i_s^b]_0 \tau_k} \cdot f_i(p_s, i_s^b, \dot{\varphi}^s) \tag{3-51}$$

3.6.4. CONTROL STRUCTURE

The general control structure of figure (3-12) is extended in more detail. Resumed, the control structure is determined by (3-52)....(3-55):

$$[i_s^w]_0 = f_i(p_s, i_s^b, \dot{\varphi}^s) \tag{3-52}$$

$$[p_s]_0 = [u_{dc}]_0 [i_{dc}]_0 \tag{3-53}$$

$$[u_s]_0 = f_u(p_s, i_s^b, \dot{\varphi}^s) \tag{3-54}$$

$$[\dot{\alpha}_s^s]_0 = [\dot{\rho}^{s*}]_0 + f_{\dot{\alpha}}(p_s, i_s^b, \dot{\varphi}^s) \tag{3-55}$$

The final control structure is given in figure 3-13. In both loops the filters W_1 and W_2 were introduced for adjusting the dynamics in both loops. The filter W_2 is also necessary to avoid an arithmetic loop, due to the recursive character of (3-55). Before the filter W_1, a limiter is employed, limiting the stator voltage in order to protect the system in case of large load torque steps at low speeds. Filter W_3 is introduced for the purpose of inverter noise elimination.

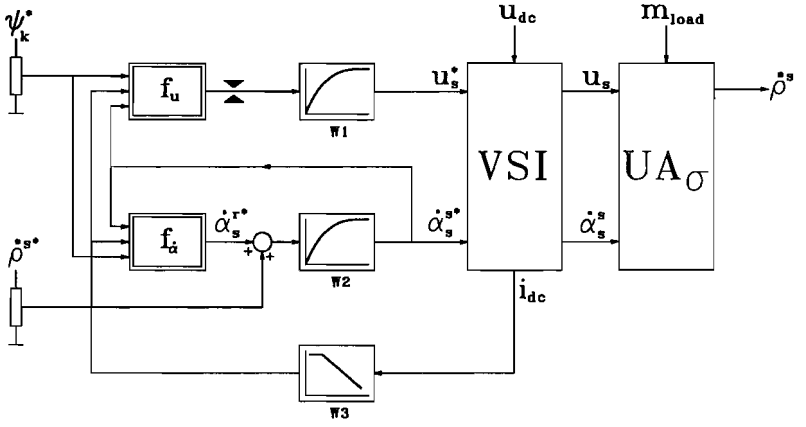

Figure: 3-13: Resulting scheme of non-linear control method using the dc-link current

3.6.5. CONTROL PARAMETERS

Both W_1 and W_2 are first order filters, whose harmonic spectrum are respectively:

$$|W_1| = \frac{1}{\sqrt{1+(\omega/\omega_{\text{cut-off},w_1})}} \tag{3-56}$$

$$|W_2| = \frac{1}{\sqrt{1+(\omega/\omega_{\text{cut-off},w_2})}} \tag{3-57}$$

Filter W_1 mainly influences the dynamics of the load responses and filter W_2 mainly influences the dynamics of the speed responses. The lower the cut-off frequency, the more the accompanying response is damped. Filter W_2 has also influence on the stator current: a low cut-off frequency results in a lower value of the stator current. The values are found by simulations (trail and error), and set to successively 0.125 pu (6.25 Hz) and 0.0104 pu (0.52 Hz). Filter W_3 is a third order Butterworth filter which is applied for eliminating PWM-noise. The pass band of a Butterworth filter is without ripples, but it has a wide transition band. The harmonic spectrum is defined by (unity gain)

$$|W_3| = \frac{1}{\omega^3_{\text{cut-off},w_3}} \cdot \frac{1}{\sqrt{1+(\omega/\omega_{\text{cut-off},w_3})^6}} \tag{3-58}$$

The maximum stator voltage is limited to 1 pu. Simulation results are given and discussed in paragraph 4.2.

3.7. LINEARISED CONTROL METHOD USING THE DC-LINK CURRENT

The control structure of paragraph 3.6 makes use of complex non-linear calculations. In this paragraph the non-linear structure is linearized [Vuck '92], to achieve a simpler structure which can be implemented by analogue hardware. The method also uses only one current sensor to measure the dc-link current within the voltage source inverter. The control scheme is simple, low-cost, without non-linear v/f-characteristic and without feedback information from the induction motor to the control part.
A general scheme is given in figure 3-14 As shown, the control scheme consists of two loops: *a voltage control loop* and a *slip-compensation loop.*

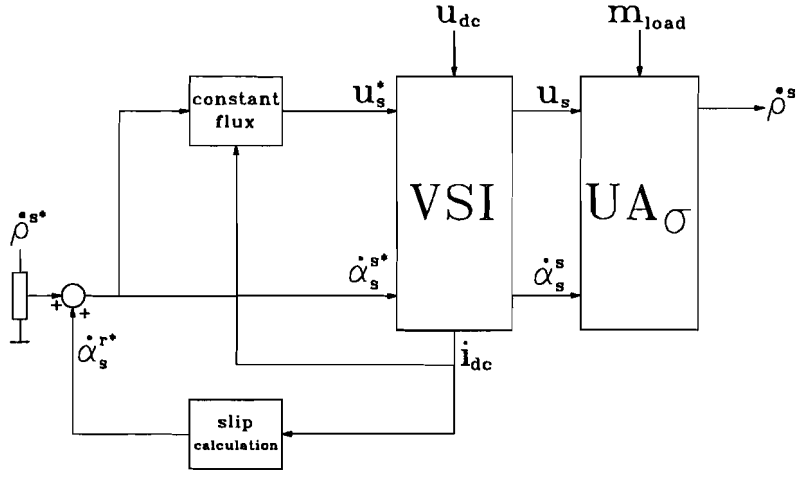

Figure: 3-14: General scheme of linearised control method using the dc-link current

3.7.1. VOLTAGE CONTROL LOOP

The amplitude of the stator voltage and the motor input power are previously described by (3-41) and (3-39):

$$[u_s]_0^2 = r_s^2[i_s]_0^2 + [\dot{\varphi}^s]_0^2 l_1^2(1+\sigma_s)^2\left([i_s^b]_0^2 + \sigma^2[i_s^w]_0^2\right) + 2r_s[\dot{\varphi}^s]_0 l_1\left(\frac{1}{1+\sigma_k}\right)\cdot[i_s^b]_0[i_s^w]_0 \qquad (3\text{-}59)$$

$$[p_s]_0 = [u_{dc}]_0[i_{dc}]_0. \qquad (3\text{-}60)$$

For an inverter with variable dc-link voltage (PAM-inverter), the stator voltage,$[u_s]_0$, is proportional to the dc-link voltage. In case of a PWM-inverter, the dc-link voltage is normally kept constant, while the fundamental component of the stator voltage is varied through different switching patterns. If the inverter losses are neglected (or added to the stator resistance), equation (3-60) can be written as

$$[p_s]_0 = [u_s]_0\frac{[u_{dc}]_0}{[u_s]_0}[i_{dc}]_0 = [u_s]_0[i'_{dc}]_0. \qquad (3\text{-}61)$$

In contrast with a PAM-inverter, in equation (3-61), the factor $[u_{dc}]_0/[u_s]_0$ of a PWM-inverter is not a constant value. When a PWM-inverter is used it is necessary to substitute, the dc-link current by a related quantity, $[i'_{dc}]_0$

$$[i'_{dc}]_0 = \frac{[u_{dc}]_0}{[u_s]_0}[i_{dc}]_0. \tag{3-62}$$

Using (2-40) and (2-41) the machine input power can also be written as:

$$[p_s]_0 = [u_s^b]_0[i_s^b]_0 + [u_s^w]_0[i_s^w]_0 = r_s[i_s]_0^2 + [\dot{\varphi}^s]_0 l_l \left(\frac{1}{1+\sigma_k}\right)\cdot[i_s^b]_0[i_s^w]_0 \tag{3-63}$$

Multiplication of (3-63) with $2r_s$ results in two equal terms of equation (3-59)

$$2r_s[p_s]_0 - r_s^2[i_s]_0^2 = r_s^2[i_s]_0^2 + 2r_s[\dot{\varphi}^s]_0 l_l \left(\frac{1}{1+\sigma_k}\right)\cdot[i_s^b]_0[i_s^w]_0 \tag{3-64}$$

Substitution of (3-64) in (3-59) and taking (3-61) into account, yields a new expression:

$$[u_s]_0^2 = 2r_s[u_s]_0[i'_{dc}]_0 + [\dot{\varphi}^s]_0^2 l_l^2(1+\sigma_s)^2\left([i_s^b]_0^2 + \sigma^2[i_s^w]_0^2\right) - r_s^2[i_s]_0^2, \tag{3-65}$$

with the leakage factor, σ, defined as

$$\sigma = 1 - \frac{1}{(1+\sigma_s)(1+\sigma_k)}. \tag{3-66}$$

If the following relations are valid:

$$r_s[i_s]_0^2 << 2[u_s]_0[i'_{dc}]_0 = 2[p_s]_0 \tag{3-67}$$

$$\sigma^2[i_s^w]_0^2 << [i_s^b]_0^2, \tag{3-68}$$

then (3-65) can be simplified to

$$[u_s]_0^2 = 2r_s[u_s]_0[i'_{dc}]_0 + [\dot{\varphi}^s]_0^2 l_l^2(1+\sigma_s)^2[i_s^b]_0^2. \tag{3-69}$$

The current $[i_s^b]_0$ is assumed to be constant, since the cage-flux is supposed constant.

For small deviations around a certain operation point, $P_l = \left([u_s]_0, [i'_{dc}]_0, [\dot{\varphi}^s]_0\right)$, a first order linear approximation of (3-69) is allowed:

$$f(u_s, i'_{dc}, \dot{\varphi}^s) = u_s^2 - 2r_s u_s i'_{dc} - [\dot{\varphi}^s]_0^2 l_l^2(1+\sigma_s)^2[i_s^b]_0^2 = 0, \tag{3-70}$$

$$df(u_s, i'_{dc}, \dot{\varphi}^s) = \left.\frac{\partial f}{\partial u_s}\right|_{P_l} du_s + \left.\frac{\partial f}{\partial i'_{dc}}\right|_{P_l} di'_{dc} + \left.\frac{\partial f}{\partial \dot{\varphi}^s}\right|_{P_l} d\dot{\varphi}^s = 0. \tag{3-71}$$

This results in:

$$\left(2[u_s]_0 - 2r_s[i'_{dc}]_0\right)du_s - 2r_s[u_s]_0 di'_{dc} - 2[\dot{\varphi}^s]_0 l_l^2(1+\sigma_s)^2[i_s^b]_0^2 d\dot{\varphi}^s = 0, \tag{3-72}$$

or, after simple manipulation,

$$du_s = \frac{[u_s]_0}{[u_s]_0 - r_s[i'_{dc}]_0} r_s di'_{dc} + \frac{[\dot{\varphi}^s]_0 l_l^2 (1+\sigma_s)^2 [i_s^b]_0^2}{[u_s]_0 - r_s[i'_{dc}]_0} d\dot{\varphi}^s. \tag{3-73}$$

For a linear expression of (3-73), an additional restriction is necessary:

$$[u_s]_0 >> r_s[i'_{dc}]_0 \Leftrightarrow [u_s]_0^2 / r_s >> [p_s]_0. \tag{3-74}$$

The validity is dependent of the speed and the value of r_s.it is only in the (very) low speed region of importance. Restriction (3-74) results in two approximations:

$$\frac{[u_s]_0}{[u_s]_0 - r_s[i'_{dc}]_0} \approx 1 \tag{3-75}$$

$$[u_s]_0 - r_s[i'_{dc}]_0 \approx [\dot{\varphi}^s]_0 l_l (1+\sigma_s)[i_s^b]_0 \tag{3-76}$$

Approximation (3-76) is derived from (3-70). Hence, taking (3-75) and (3-76) into account in the region where $[u_s]_0 >> r_s[i'_{dc}]_0$, equation (3-73) will be approximated by:

$$du_s = r_s di'_{dc} + l_l (1+\sigma_s)[i_s^b]_0 d\dot{\varphi}^s. \tag{3-77}$$

The signal to control the stator voltage, u_s, is determined by a variation around P_1:

$$\begin{aligned} u_s &= [u_s]_0 + du_s \\ i'_{dc} &= [i'_{dc}]_0 + di'_{dc} \\ \dot{\varphi}^s &= [\dot{\varphi}^s]_0 + d\dot{\varphi}^s \end{aligned} \tag{3-78}$$

Using (3-77) and (3-78) results in an expression, which is equal to voltage/frequency control with load dependent voltage boost

$$u_s = r_s i'_{dc} + l_l (1+\sigma_s)[i_s^b]_0 \dot{\varphi}^s. \tag{3-79}$$

3.7.2. SLIP COMPENSATION LOOP

As mentioned before (3.6.3.), in a slip calculation loop the stator frequency is calculated by the sum of the desired speed and the slip frequency

$$\dot{\varphi}^s = \dot{\rho}^{s*} + \frac{r_k}{\psi_k (1+\sigma_k)} i_s^w. \tag{3-80}$$

The torque generating component of the stator current, i_s^w, will be derived from the measured current in the dc-link. First an exact stationary expression of the dc-link current is needed. Substitution of (3-59) and (3-63) in (3-61) results in

$$[i'_{dc}]_0 = \frac{[i_s]_0^2 + [\dot{\varphi}^s]_0 \tau_s (1-\sigma)[i_s^b]_0 [i_s^w]_0}{\sqrt{[i_s]_0^2 + [\dot{\varphi}^s]_0^2 \tau_s^2 ([i_s^b]_0^2 + \sigma^2 [i_s^w]_0^2) + 2[\dot{\varphi}^s]_0 \tau_s (1-\sigma)[i_s^b]_0 [i_s^w]_0}}, \tag{3-81}$$

with the stator time constant defined as

$$\tau_s = l_l(1+\sigma_s)/r_s . \tag{3-82}$$

Again a first order linear approximation around $P_2 = \left(\left[i_s^b\right]_0, \left[i_s^w\right]_0\right) = \left(\left[i_s^b\right]_0, 0\right)$ is needed for a linear expression:

$$i'_{dc} = \frac{\left[i_s\right]_0^2 + \left[\dot{\varphi}^s\right]_0 \tau_s (1-\sigma) i_s^b i_s^w}{\sqrt{\left[i_s\right]_0^2 + \left[\dot{\varphi}^s\right]_0^2 \tau_s^2 \left(\left(i_s^b\right)^2 + \sigma^2 \left(i_s^w\right)^2\right) + 2\left[\dot{\varphi}^s\right]_0 \tau_s (1-\sigma) i_s^b i_s^w}} \tag{3-83}$$

$$di'_{dc} = \left.\frac{\partial i'_{dc}}{\partial i_s^b}\right|_{P_2} di_s^b + \left.\frac{\partial i'_{dc}}{\partial i_s^w}\right|_{P_2} di_s^w . \tag{3-84}$$

This results in:

$$di'_{dc} = \frac{1}{\sqrt{1+\left(\left[\dot{\varphi}^s\right]_0 \tau_s\right)^2}} di_s^b + \frac{(1-\sigma)}{\sqrt{\left(1+\left(\left[\dot{\varphi}^s\right]_0 \tau_s\right)^{-2}\right)^3}} di_s^w \tag{3-85}$$

In most cases, (motors with relative small stator resistance) it is allowed to assume

$$\left(\left[\dot{\varphi}^s\right]_0 \tau_s\right)^{-2} << 1. \tag{3-86}$$

Then the torque generating component of the stator current is approximated by:

$$di_s^w = \frac{1}{(1-\sigma)} \left(di'_{dc} - \frac{1}{\sqrt{1+\left(\left[\dot{\varphi}^s\right]_0 \tau_s\right)^2}} di_s^b \right) \tag{3-87}$$

In this case, i_s^w is equal to di_s^w because it is linearized around $\left[i_s^w\right]_0 = 0$

$$i_s^w = \frac{1}{(1-\sigma)} \left(i'_{dc} - \frac{1}{\sqrt{1+\left(\left[\dot{\varphi}^s\right]_0 \tau_s\right)^2}} \left[i_s^b\right]_0 \right) \tag{3-88}$$

Substitution of (3-88) and (2-53) in (3-80) results in an expression for controlling the stator frequency

$$\dot{\varphi}^s = \dot{\rho}^{s*} + \frac{1}{(1-\sigma)\tau_k \left[i_s^b\right]_0} \left(i'_{dc} - \frac{1}{\sqrt{1+\left(\left[\dot{\varphi}^s\right]_0 \tau_s\right)^2}} \left[i_s^b\right]_0 \right), \tag{3-89}$$

with the cage time constant defined as:

$$\tau_k = l_l(1+\sigma_k)/r_k . \tag{3-90}$$

3.7.3. CONTROL STRUCTURE

The general scheme of figure (3-14) will be worked out in more detail. The modified dc-link current, i'_{dc}, is determined by (3-62) and the voltage control and slip compensation loop are mathematically described by (3-79) and (3-89). As mentioned in (2.3.3.), in steady-state $[\dot{\varphi}_s]_0$ is equal to $[\dot{\alpha}_s^s]_0$. Resumed:

$$i'_{dc} = \frac{u_{dc}}{u_s} i_{dc} \tag{3-91}$$

$$u_s = K_u i'_{dc} + K_{vf} \dot{\alpha}_s^s \tag{3-92}$$

$$\text{with: } K_u = r_s \text{ and } K_{vf} = l_l(1+\sigma_s)[i_s^b]_0 \tag{3-93}$$

$$\dot{\alpha}_s^s = \dot{\rho}^{s*} + K_f(i'_{dc} - I_f) \tag{3-94}$$

$$\text{with: } K_f = \frac{1}{\tau_k [i_s^b]_0 (1-\sigma)} \text{ and } I_f = \frac{[i_s^b]_0}{\sqrt{1+([\dot{\varphi}^s]_0 \tau_s)^2}} \tag{3-95}$$

Both (3-92) and (3-94) are linearised approximations. They are only valid in stationary case, provided that:

$$\begin{aligned} &r_s[i_s]_0^2 << 2[u_s]_0[i'_{dc}]_0 = 2[p_s]_0 \\ &\sigma^2[i_s^w]_0^2 << [i_s^b]_0^2 \\ &[u_s]_0 >> r_s[i'_{dc}]_0 \Leftrightarrow [u_s]_0^2/r_s >> [p_s]_0 \\ &([\dot{\alpha}_s^s]_0 \tau_s)^{-2} << 1 \end{aligned} \tag{3-96}$$

Figure 3-15 gives the finally control structure:

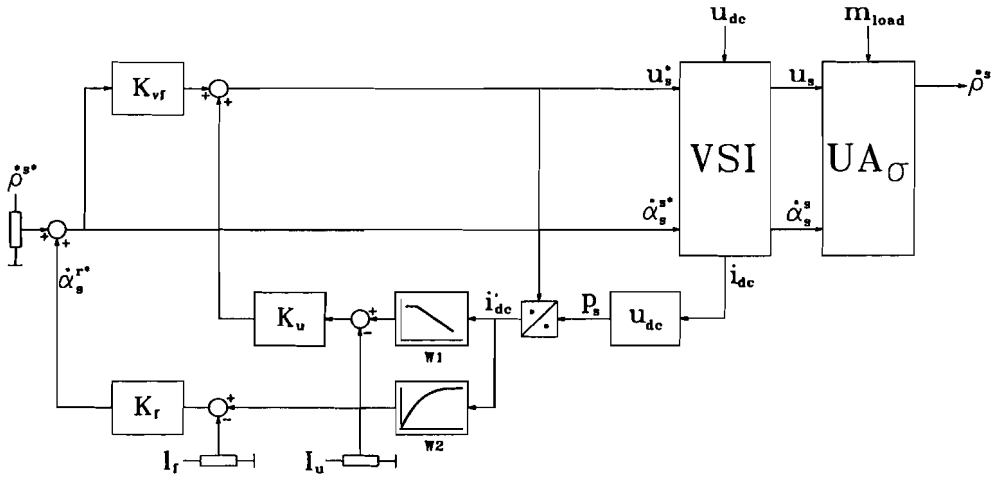

Figure: 3-15: Control structure of linearised control method using the dc-link current

The voltage control loop contains three parameters (K_{vf}, K_u, I_u)) and a filter W_1. The gains K_{vf} and K_u agree with the slope of the linear v/f characteristic and a load dependent voltage boost respectively. The parameter I_u is a bias-current in order to achieve the best linear fitting of the (in reality non-linear) relation between stator voltage, u_s, and modified dc-link current, i'_{dc}. Filter W_1 eliminates PWM-noise, contained in the measured dc-link current.
The slip compensation loop contains two parameters and a filter W_2. The gain K_f calculates the slip frequency from the modified dc-link current, i'_{dc}. Parameter I_f is actually a non-linear function of the stator frequency. To avoid a non-linear block into the control structure, the parameter I_f is assumed to be constant. Filter W_2 is not only eliminating PWM-noise, but determines the dynamic speed response, as well.
The control system is completely linear and therefore easy to realise with analogue hardware. Only the block used for the calculation of the adapted dc-link current, i'_{dc}, is non-linear. A linear approximation of a division is only possible in a small region. However, an exponential approximation satisfies in a wide range and is also easy to realise with analogue hardware.
In the control scheme, the parameters of the voltage control loop are independent of the parameters of the slip compensation loop.

3.7.4. CONTROL PARAMETERS

The values of the control parameters are given below (desired cage-flux, $\left[\psi_k^*\right]_0 = 0.8\,\text{pu}$):

Table 3-1: Control parameters

Parameter	Value [pu]
K_u	0.84
K_{vf}	0.04
K_f	0.02625
I_u	0
I_f	0.034
$\omega_{\text{cut-off},w_1}$	20
$\omega_{\text{cut-off},w_2}$	0.0667

The parameter settings in table 3-1 are calculated according to (3-93) and (3-95). These values are close to the optimal values [Vuck '92] (optimal here means that the resulting flux and speed steady-state errors have a minimum quadratic sum).
Filter W_1 is a third order filter with Butterworth characteristics. The filter is defined by the following harmonic spectrum (unity gain):

$$|W_1| = \frac{1}{\omega^3_{\text{cut-off},w_1}} \cdot \frac{1}{\sqrt{1+\left(\omega/\omega_{\text{cut-off},w_1}\right)^6}} \tag{3-97}$$

The cut-off frequency, $\omega_{cut-off,w_1}$, is set to 20 pu (1 kHz), the switching frequency of the PWM-inverter. Filter W_2 is a simple first order lag with spectrum:

$$|W_2| = \frac{1}{\sqrt{1+\left(\omega/\omega_{cut-off,w_2}\right)}} \tag{3-98}$$

The cut-off frequency determines the dynamic response. The lower the cut-off frequency, the more the response is damped. Its value is found by simulations (trail and error), and set to 0.0667 pu (3.33 Hz). Simulation results are given and discussed in paragraph 4.3.

4. SIMULATION RESULTS

The control methods, which are discussed in paragraph 3.5, 3.6 and 3.7, are analysed by computer simulations. The induction motor simulation model is described in paragraph 2.3.6, while the model of the PWM-inverter is assumed to be ideal (2.2.4.). Simulations (using the simulation tool, PSI/c [Bosch '93]) of the control methods are made to examine their (quasi)-stationary and dynamic properties. The simulation results are represented in per unit. A survey of the used per unit system (PUS) is given in appendix B. The parameters of the *fictive* induction machine are given in appendix C.
Table 4-1 gives an overview of the used test signals:

Table 4-1: Simulation test signals

	speed command: $\dot{\rho}^{s*}$[pu]		load: m_{load}[pu]	
nr	type	value	type	value
1	constant	1	ramp*	0→1
2	constant	0.15	ramp*	0→1
3	ramp**	1→0→1	quadratic	$0.5\cdot(\dot{\rho}^s)^2$
4	constant	1	step	0→1
5	constant	0.15	step	0→1
6	staircase	0.1→0.4→0.7→1	quadratic	$0.5\cdot(\dot{\rho}^s)^2$

* the slope of the ramp function is equal to the mechanical time constant
** the slope of the ramp function is twice the mechanical time constant

Ramp shaped test signals are used to determine the quasi-stationary behaviour of the control structure, while step shaped test signals are used to determine the dynamic behaviour of the control structure. A quadratic load is chosen, because it represents a practical load with a centrifugal character (pumps, fans, blowers).
Examination of the parameter sensitivities are also made by simulations. The influence of variations in stator and cage resistance (temperature dependent), air-gap inductance (saturation effects) and leakage inductance are determined with respect to the cage-flux and the speed. The parameters are varied with plus and minus 10%, both in half and full load situation.
The PSI/c simulation models, which are used in this chapter, are given in appendix D.

4.1. CONSTANT V/F SPEED CONTROL WITH SLIP REGULATION

4.1.1. QUASI-STATIONARY BEHAVIOUR

The quasi-stationary simulations of the constant speed control method with slip regulation (paragraph 3.5.) are given in the figures 4-1, 4-2 and 4-3.

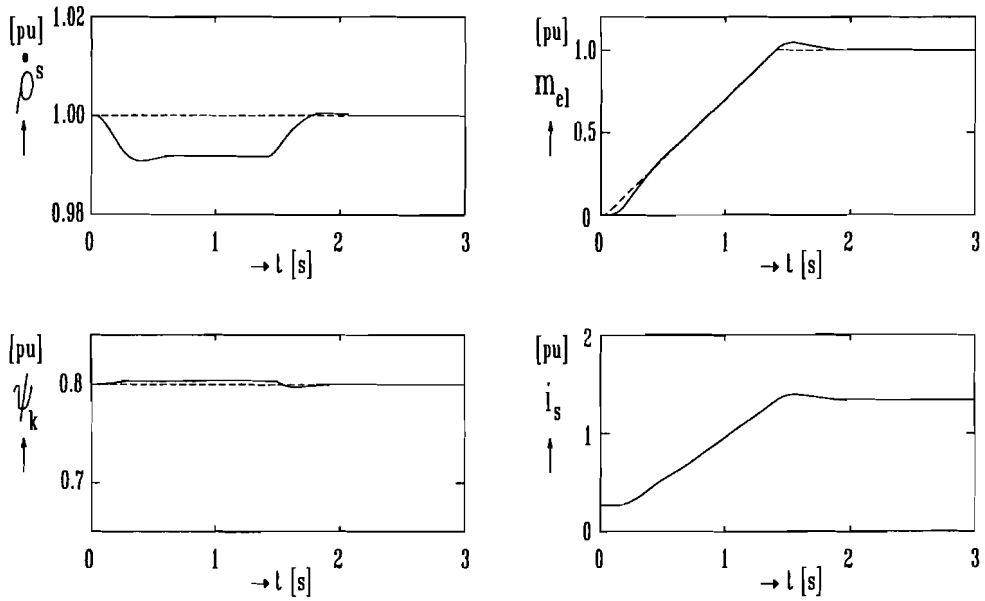

Figure 4-1: Response of a ramp shaped load change at a speed of 1 pu $\left(\frac{d}{dt}(m_{load})=0.731\,pu\cdot s^{-1}\right)$

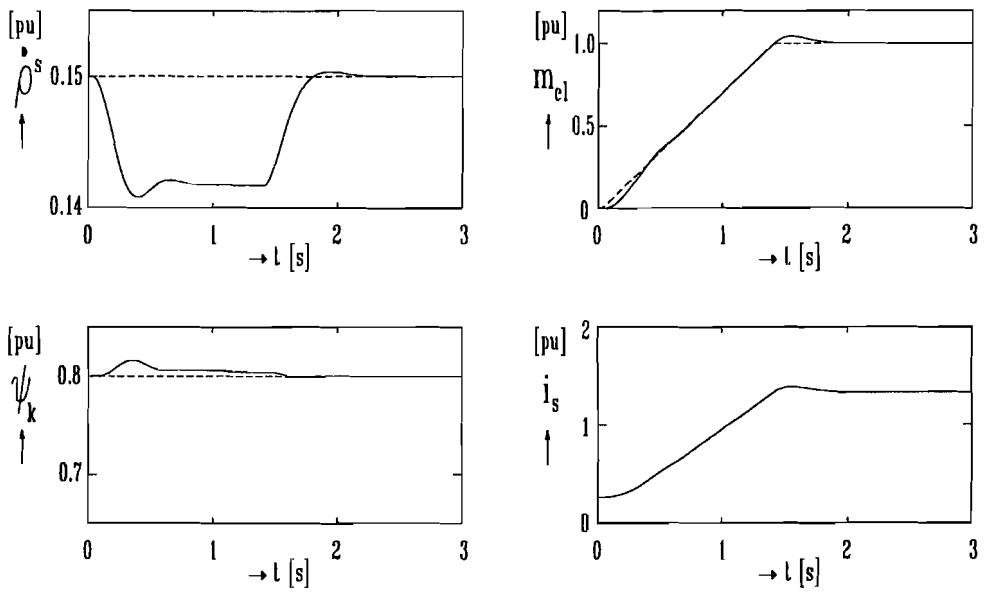

Figure 4-2: Response of a ramp shaped load change at a speed of 0.15 pu $\left(\frac{d}{dt}(m_{load})=0.731\,pu\cdot s^{-1}\right)$

As expected, there are no stationary speed deviations, because the PI-controller eliminates the difference between the desired speed, $[\dot{\rho}^{s*}]_0$, and the shaft speed, $[\dot{\rho}^{s}]_0$. During the increase of the load torque, (figure 4-1 and 4-2) a temporarily speed-deviation arises. In the high speed region ($\dot{\rho}^{s*} = 1\,\text{pu}$) the deviation is about -0.8% and in the low speed region ($\dot{\rho}^{s*} = 0.15\,\text{pu}$) the deviation is about -5.5%. The difference is due to the amount of kinetic energy stored in the inertia, which is proportional to the quadratic of the frequency ($E_{kin} = \frac{1}{2}\theta \cdot (\dot{\rho}^{s})^2$). Variations of the cage-flux are negligible (less than 2%). The electric torque of the induction machine follows the ramp shaped load torque very accurate without excessive stator current.

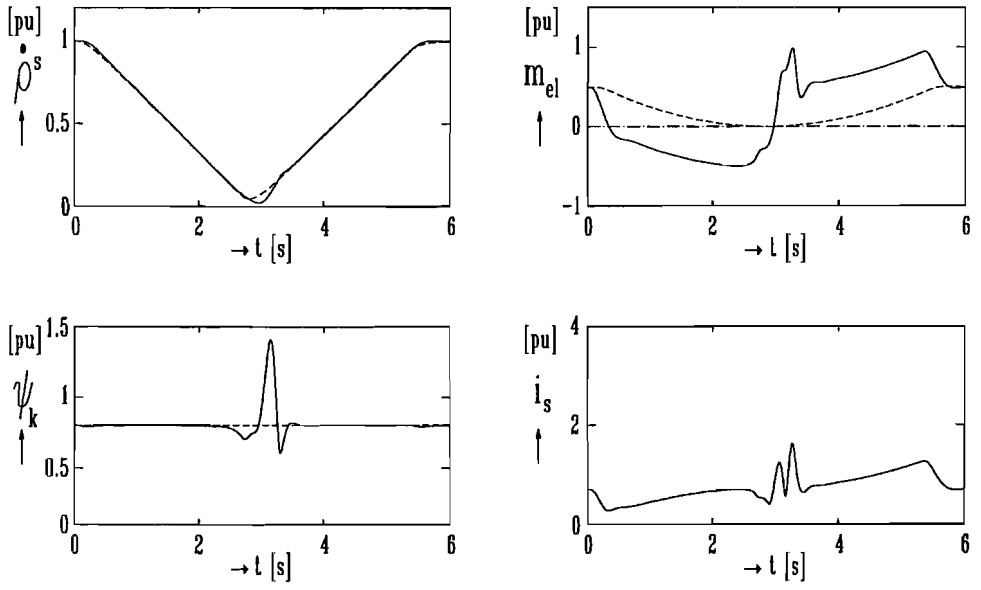

Figure 4-3: Response of a ramp shaped speed change with a quadratic load $\left(\frac{d}{dt}(\dot{\rho}^{s*}) = \pm 0.365\,\text{pu}\cdot\text{s}^{-1}\right), \left(m_{load} = 0.5\cdot(\dot{\rho}^{s})^2\right)$

The response of the ramp shaped speed change with a quadratic load (figure 4-3), has only a deviation in the speed region around standstill. This is due to the resistive character of the stator impedance in the low speed region: the voltage drop across the stator resistance is then no longer negligible. The cage-flux increases considerable ($\psi_k(\dot{\rho}^{s} \approx 0) = 1.4\,\text{pu}$), in practice this will lead to saturation. The delay between the desired speed and the shaft speed is due to the smoothing filter, needed to restrict the overshoot during step changes.

4.1.2. DYNAMIC BEHAVIOUR

The results of the dynamic simulations of the constant v/f speed control method with slip regulation (paragraph 3.5) are depicted in figure 4-4, 4-5, and 4-6.
In both the high- and low speed region of the load response (figure 4-4 and 4-5), the response of the upwards going edge differs from the downwards going edge. This is caused by the strongly non-linear character of the control system and the induction

machine. The rise time of the speed in both the high speed region ($\dot{\rho}^s = 1\,\text{pu}$) as in the low speed region ($\dot{\rho}^s = 0.15\,\text{pu}$) is about 515 ms. The temporarily speed decrease is respectively about 5.4% and 32% (the difference is due to the kinetic energy stored in the inertia, which is quadratic related with the speed).

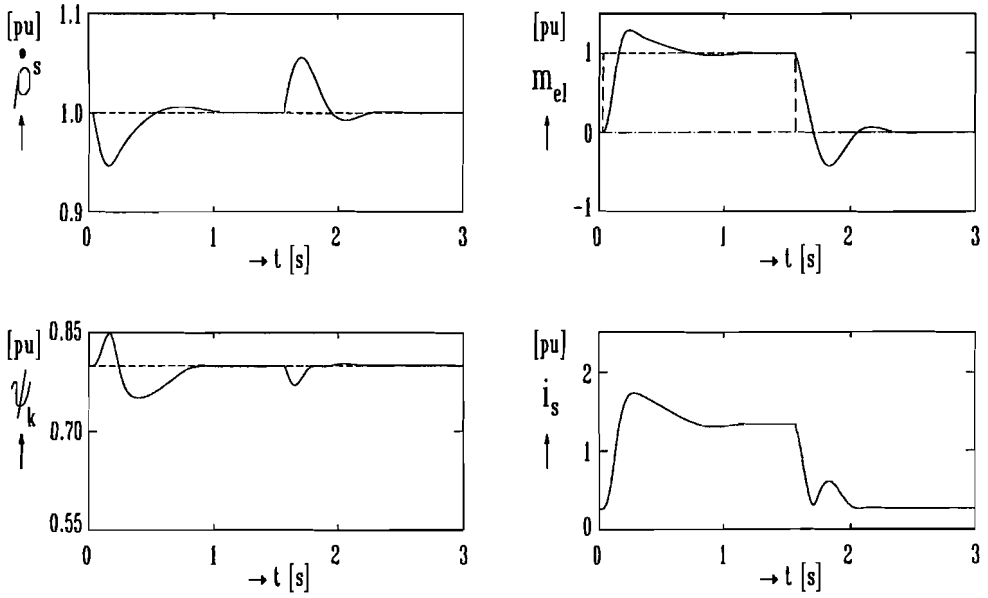

Figure 4-4: Response of a unit load step at a speed of 1 pu (m_{load}:0→1pu)

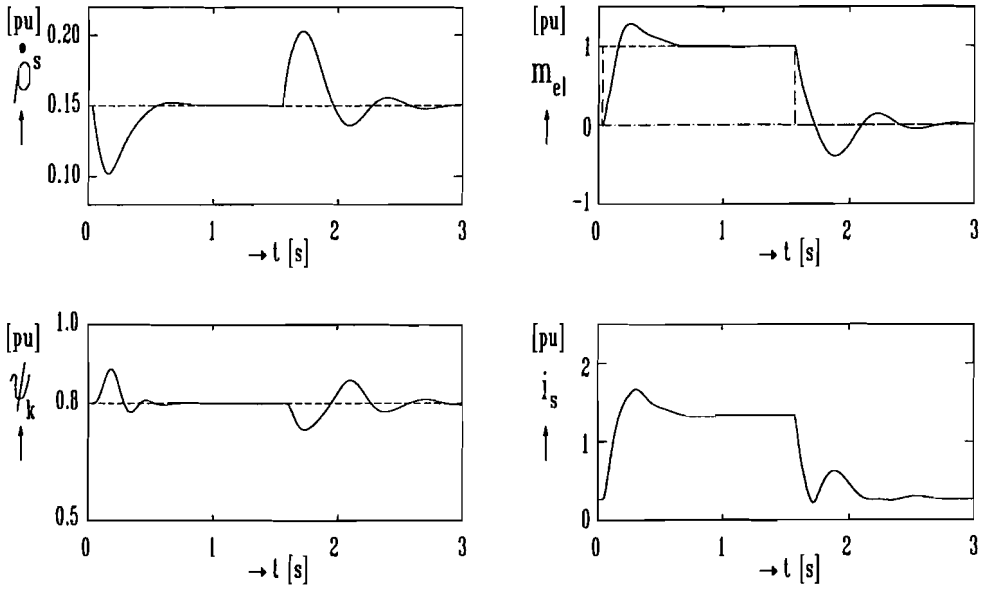

Figure 4-5: Response of a unit load step at a speed of 0.15 pu (m_{load}:0→1pu)

The speed responses of the staircase test signal with quadratic load (figure 4-6) have in all cases an overshoot of approximately 5% with a rise time of 400 ms. This

corresponds roughly with (3-34). No saturation of the cage-flux occurs, but in practice a current limitation will be required (to protect the semiconductors of the inverter).
The responses (figure 4-4, 4-5 and 4-6) are stable and well damped.

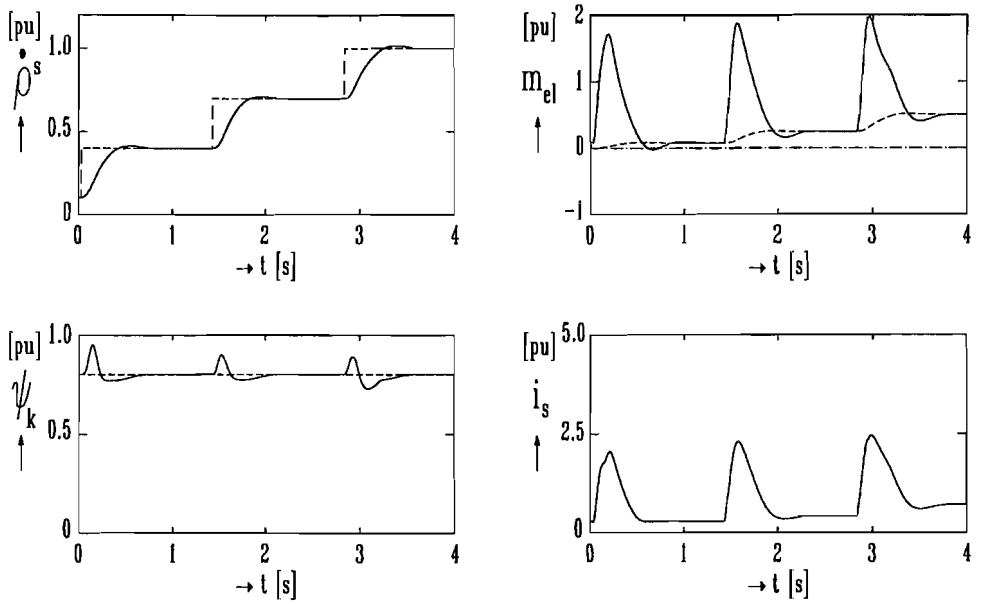

Figure 4-6: Response of staircase speed change with quadratic load

$$\left(\dot{\rho}^{s*} = (0.1 \rightarrow 0.5 \rightarrow 0.7 \rightarrow 1)\text{pu}\right), \left(m_{load} = 0.5 \cdot \left(\dot{\rho}^{s}\right)^2\right)$$

4.1.3. PARAMETER SENSITIVITY

The results of varying the stator and cage resistance $(r_s \pm 10\%, r_k \pm 10\%)$, the air-gap inductance $(l_l \pm 10\%)$ and the leakage inductances $(l_{\sigma s} \pm 10\%, l_{\sigma k} \pm 10\%)$ are shown in figures (4-7), (4-8) and (4-9).

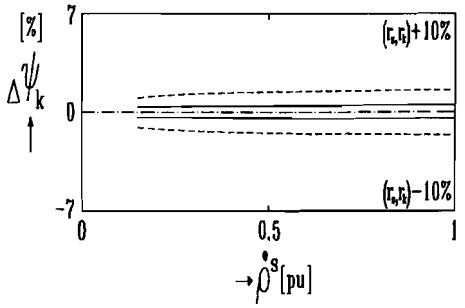

Figure 4-7: Deviation of the cage-flux due to variations of r_s and r_k $(\pm 10\%)$ at half load (—) and full load (---)

In case of the v/f speed control with slip regulation, only the deviation of the cage-flux is relevant because the speed is controlled in a closed loop with a PI-controller.

The parameter sensitivity is very small. Deviations due to the air-gap inductance are about 1% (figure (4-8)). During full load, flux-deviations due to resistance and leakage inductance variations are about 1.5% (figure 4-7 and 4-9). An increase of the resistances results in an increase of the cage-flux. An increase of the leakage inductances results in a reduced cage-flux.

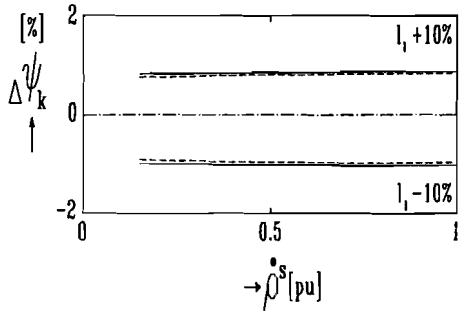

Figure 4-8: Deviation of the cage-flux due to variations of l_1 $(\pm 10\%)$ at half load (—) and full load (---)

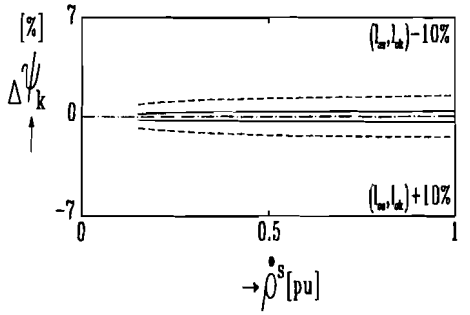

Figure 4-9: Deviation of the cage-flux due to variations of $l_{\sigma s}$ and $l_{\sigma k}$ $(\pm 10\%)$ at half load (—) and full load (---)

4.2. NON-LINEAR CONTROL METHOD USING THE DC-LINK CURRENT

4.2.1. QUASI-STATIONARY BEHAVIOUR

The quasi-stationary simulation results of the non-linear control method using the dc-link current (paragraph 3.6) are shown in figure 4-10, 4-11 and 4-12.
Although, the control structure is an open loop system, there are no stationary deviations, caused by load changes. This is due to the accurate calculation of the control signals without approximations.

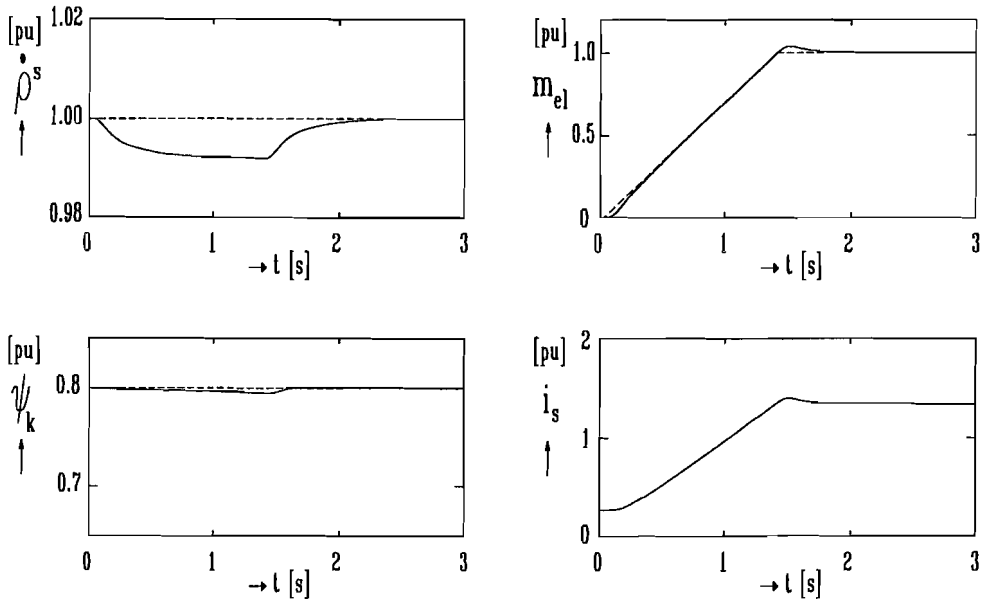

Figure 4-10: Response of a ramp shaped load change at a speed of 1 pu $\left(\frac{d}{dt}(m_{load})=0.731\,pu\cdot s^{-1}\right)$

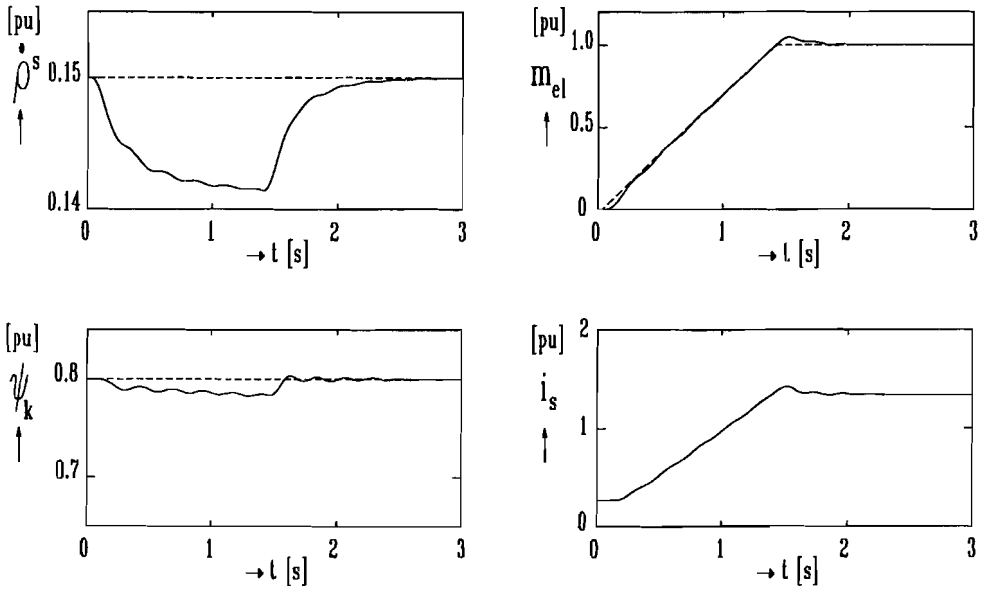

Figure 4-11: Response of a ramp shaped load change at a speed of 15% $\left(\frac{d}{dt}(m_{load})=0.731\,pu\cdot s^{-1}\right)$

During the increase of the load-torque (figure 4-10 and 4-11), there is a temporarily speed deviation. In the high speed region ($\dot{\rho}^{s*}=1\,pu$) the deviation is about -0.8% and in the low speed region ($\dot{\rho}^{s*}=0.15\,pu$) the deviation is about -5.5%. The difference in speed deviation is caused by the amount of kinetic energy stored in the inertia ($E_{kin}=\frac{1}{2}\theta\cdot(\dot{\rho}^{s})^2$). The cage-flux remains almost constant, however in the low speed region there is a resonance caused by the motor which is badly damped. For speeds

higher than 0.15 pu, the electric torque follows the ramp shaped load very accurately, for lower speeds the system become unstable.

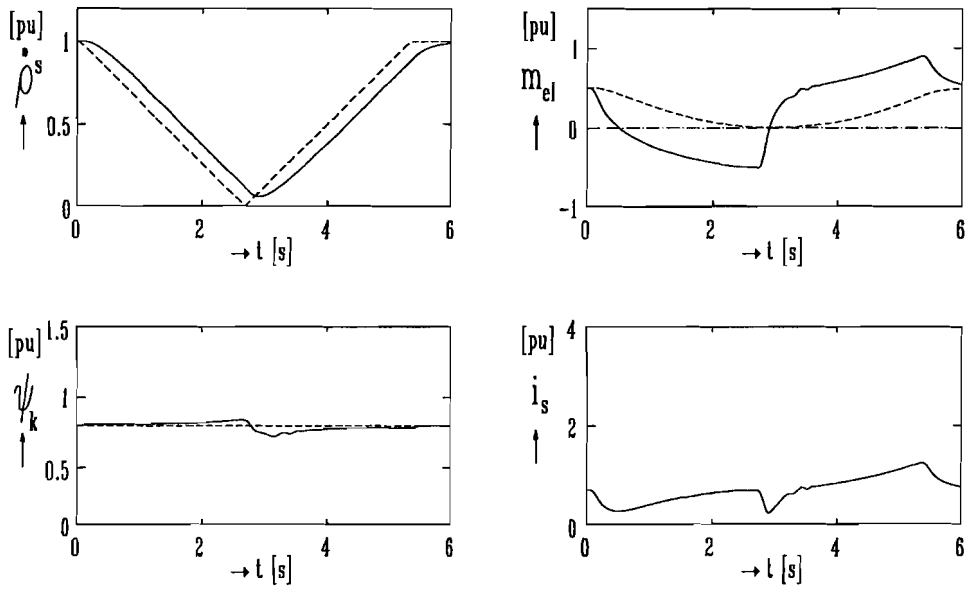

Figure 4-12: Response of a ramp shaped speed change with a quadratic load $\left(\frac{d}{dt}\left(\dot{\rho}^{s*}\right) = \pm 0.365\,\text{pu}\cdot\text{s}^{-1}\right), \left(m_{load} = 0.5\cdot\left(\dot{\rho}^{s}\right)^2\right)$

The response of the ramp shaped speed change with a quadratic load (figure 4-12), has only a deviation in the very low speed region. This is due to the voltage drop across the stator resistance, which becomes relatively important in the very low speed region. The flux around standstill varies from 0.72 till 0.84 pu and is well damped. Saturation will have no influence. The delay between the desired speed and the shaft speed is due to low cut-off frequency of the filter, W_2, necessary for damping in the low speed region and reducing the stator current.

4.2.2. DYNAMIC BEHAVIOUR

The dynamic simulations of the non-linear control algorithm that uses the dc-link current (paragraph 3.6) are given in figure 4-13, 4-14 and 4-15.

The load response in the high speed region ($\dot{\rho}^s = 1\,\text{pu}$, figure 4-13) is much better damped, than the response in the low speed region ($\dot{\rho}^s = 0.15\,\text{pu}$, figure 4-14). The difference between the responses of the upwards and downwards going load edge is due to the non-linear behaviour of the induction machine. The temporarily speed decrease is respectively about 4% and 33%, moreover, there is no speed overshoot (the difference is due to the kinetic energy stored in the inertia, which is quadraticaly related with the speed).

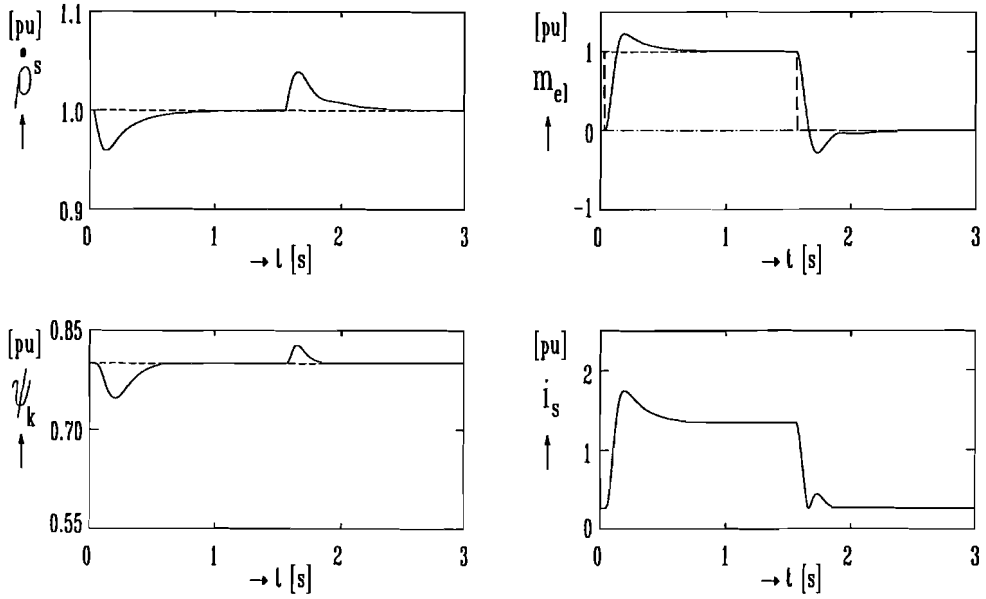

Figure 4-13: Response of a unit load step at a speed of 1 pu
(m_{load}:0→1pu)

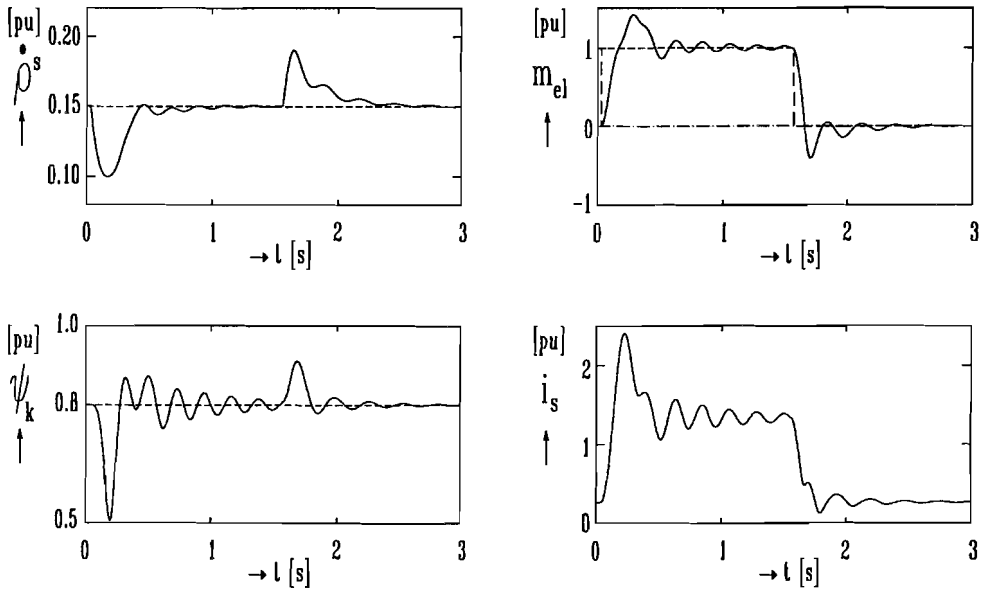

Figure 4-14: Response of a unit load step at a speed of 0.15 pu
(m_{load}:0→1pu)

The speed responses of the staircase test signal with quadratic load (figure 4-15) have no overshoot. No saturation of the cage-flux occurs, but in practice maybe a current limitation will be required (to protect the semiconductors of the inverter).
For speeds values higher than 0.15 pu, the responses are stable and well damped.

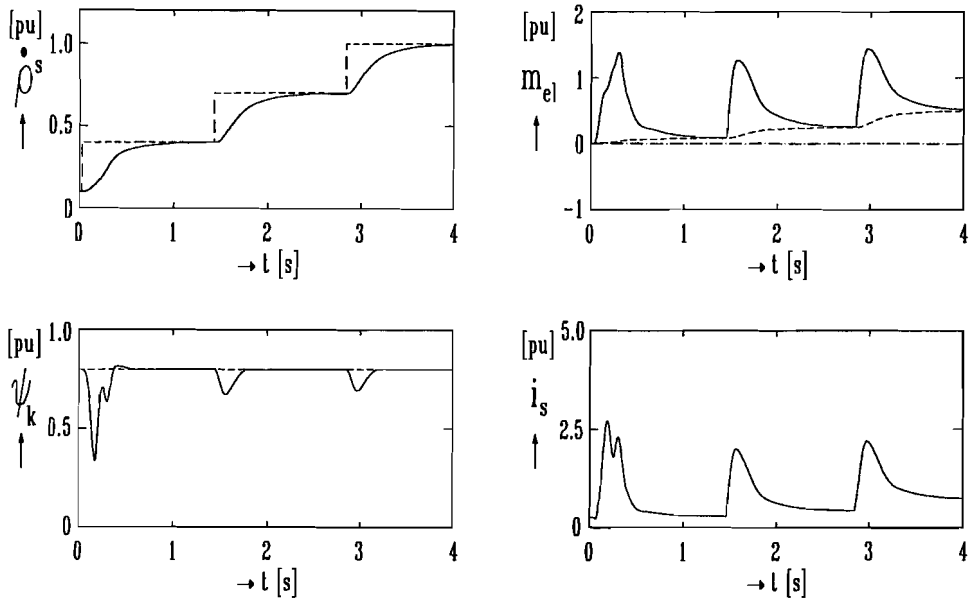

Figure 4-15: Response of staircase speed change with quadratic load

$$\left(\dot{\rho}^{s*} = (0.1 \rightarrow 0.5 \rightarrow 0.7 \rightarrow 1)\text{pu}\right), \left(m_{load} = 0.5 \cdot \left(\dot{\rho}^s\right)^2\right)$$

4.2.3. PARAMETER SENSITIVITY

In figure (4-16), (4-17) and (4-18), the results of successively resistance, air-gap inductance and leakage inductance variations are shown.

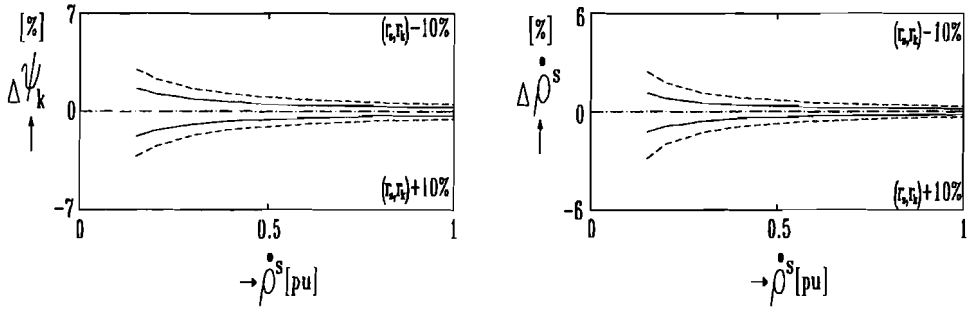

Figure 4-16: Deviation of the cage-flux and the speed due to variations of r_s and r_k $(\pm 10\%)$ at half load (—) and full load (---)

In the low speed region, variation of the stator and cage resistance is more sensitive than in the high speed region (figure 4-16). Around standstill the deviation will become larger (at 15% of rated speed and full load, the cage-flux deviation is about 3%). An increase of resistance causes a reduced cage-flux. In the high speed region, the deviations are negligible (at full load $\psi_k \leq 1\%$ and $\dot{\rho}^s \leq 0.5\%$). In the whole speed range flux deviations due to the air-gap inductance are about 1% and speed deviations are negligible (figure 4-17). An increase of the leakage-inductance results in a decrease of the cage-flux which is less than 3% in the whole speed region. The speed deviation due to the leakage inductances is only sensitive in the low speed region (figure 4-18).

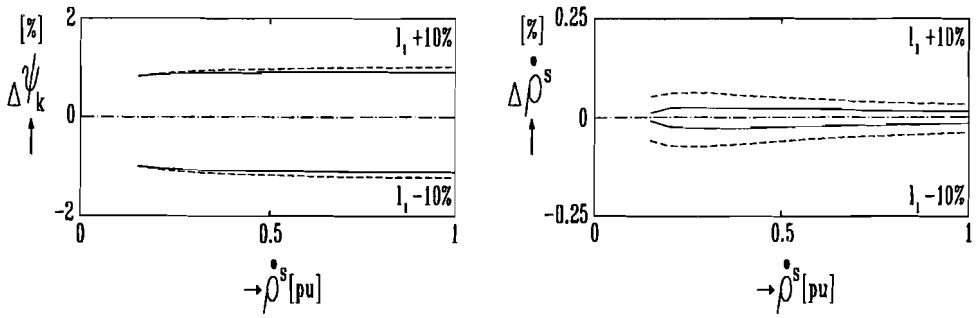

Figure 4-17: Deviation of the cage-flux and the speed due to variations of l_1 (±10%) at half load (—) and full load (---)

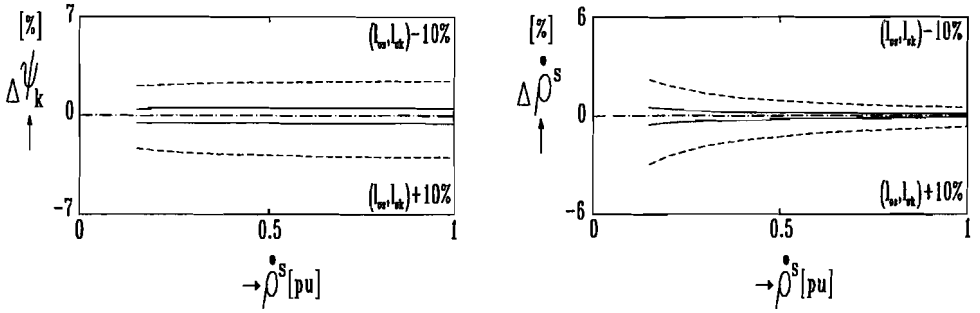

Figure 4-18: Deviation of the cage-flux and the speed due to variations of $l_{\sigma s}$ and $l_{\sigma k}$ (±10%) at half load (—) and full load (---)

4.3. LINEARISED CONTROL METHOD USING THE DC-LINK CURRENT

4.3.1. QUASI-STATIONARY BEHAVIOUR

The results of the quasi-stationary simulations of the linearised control method using the dc-link current (paragraph 3.7) are shown in figure 4-19, 4-20 and 4-21.
Because the control structure is an open loop system with linearised approximations, there are steady state deviations caused by load changes. The load torque responses (figure 4-19 and figure 4-20) results in both a stationary cage-flux deviation and a stationary speed deviation: in the high speed region -16% and -1.3%, respectively
in the low speed region -12.7% and -4.5%, respectively.
Decreasing of the cage-flux is mainly due to the influence of the cage leakage inductance, $l_{\sigma k}$, because the load dependent voltage drop across the cage leakage inductance is not included in the (linearised) v/f constant, K_{vf}. The difference in speed deviation is caused by the amount of kinetic energy stored in the inertia ($E_{kin} = \frac{1}{2}\theta\cdot(\dot{\rho}^s)^2$). The electric torque of the induction machine follows the ramp shaped load torque very accurately. In this case, no stator current limitation is needed.

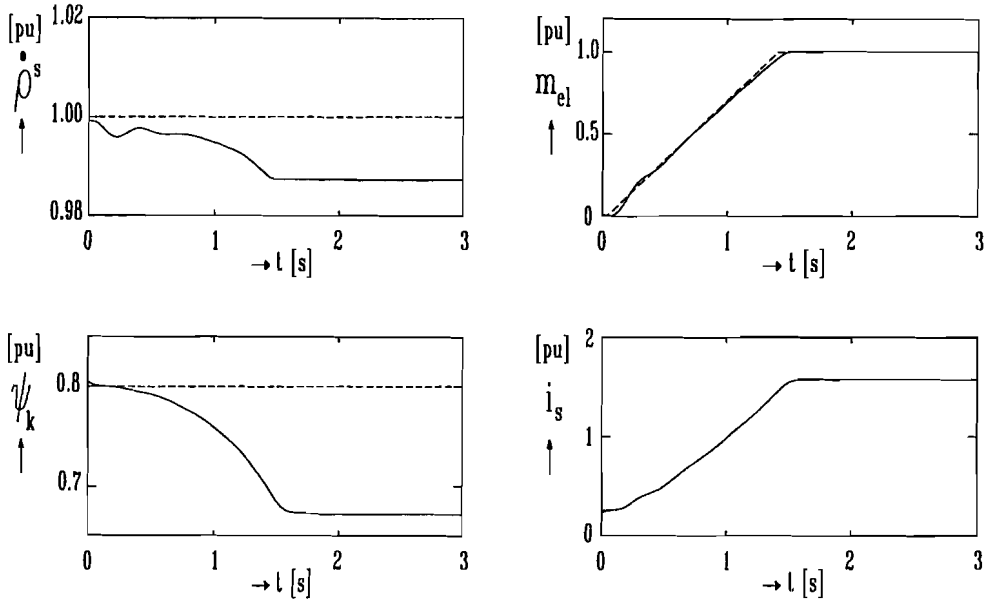

Figure 4-19: Response of a ramp shaped load change at a speed of 1 pu $\left(\frac{d}{dt}(m_{load})=0.731\,pu{\cdot}s^{-1}\right)$

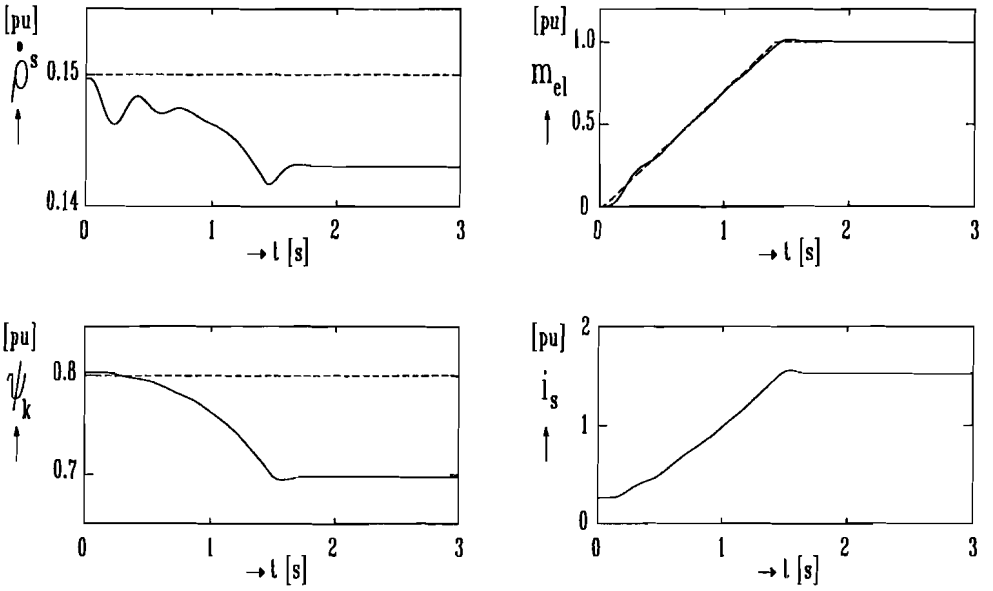

Figure 4-20: Response of a ramp shaped load change at a speed of 0.15 pu $\left(\frac{d}{dt}(m_{load})=0.731\,pu{\cdot}s^{-1}\right)$

The response of the ramp shaped speed change with a quadratic load (figure (4-21)), has only difficulties in the speed region around standstill. This is due to the voltage drop across the stator resistance, which become relatively important in the very low speed region. The value of the cage-flux around standstill oscillates from about 0.2 till 1.4 pu, but it is well damped. Because the duration of the flux peaks are short, saturation will have little effect. To protect the power electronic components of the inverter, a stator current limitation seems necessary.

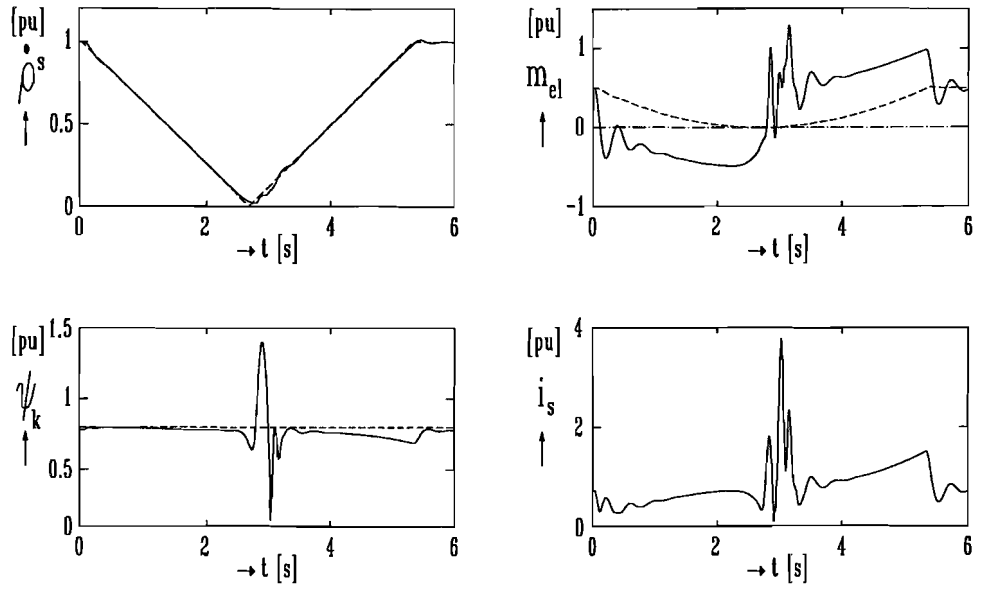

Figure 4-21: Response of a ramp shaped speed change with a quadratic load $\left(\frac{d}{dt}\left(\dot{\rho}^{s*}\right) = \pm 0.365\,\text{pu}\cdot\text{s}^{-1}\right), \left(m_{load} = 0.5\cdot\left(\dot{\rho}^{s}\right)^2\right)$

4.3.2. DYNAMIC BEHAVIOUR

The dynamic simulation results of the linear control algorithm that uses the dc-link current (paragraph 3.7) are depicted in figure 4-22, 4-23 and 4-24.

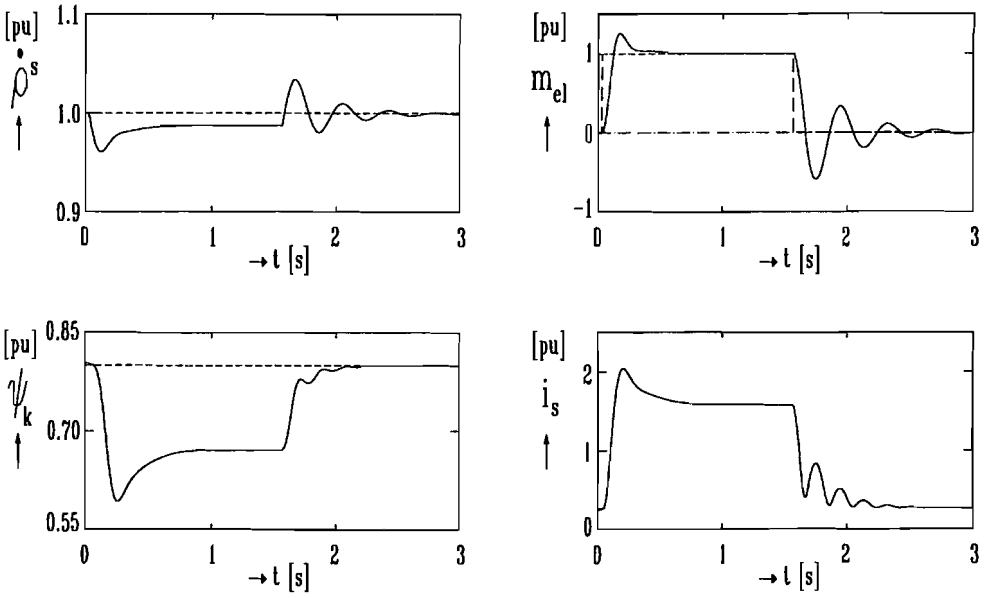

Figure 4-22: Response of a unit load step at a speed of 1 pu (m_{load}:0→1 pu)

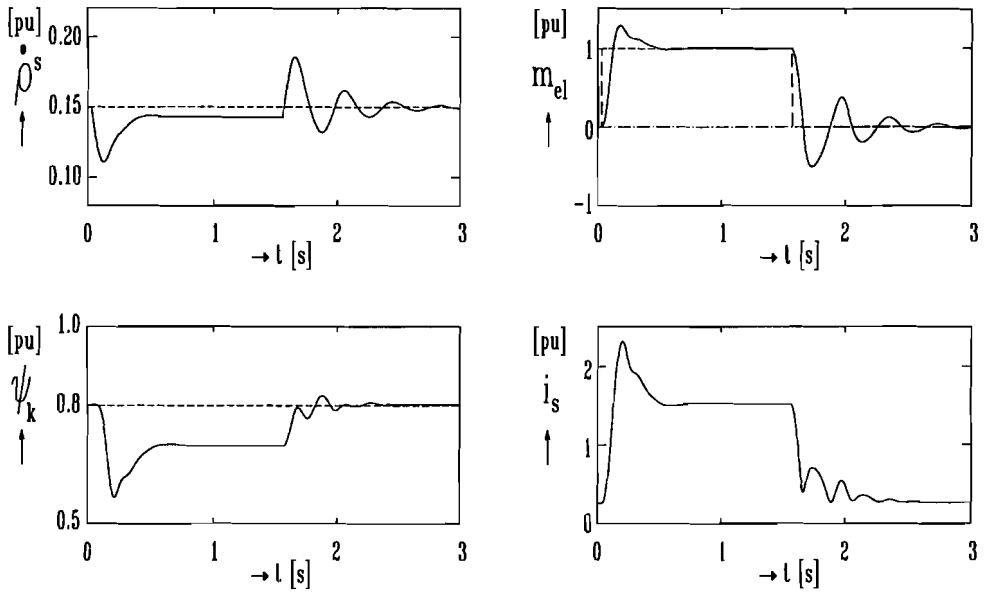

Figure 4-23: Response of a unit load step at a speed of 0.15 pu
(m_{load}:0→1pu)

The shape of the dynamics in the high speed region ($\dot{\rho}^s = 1$pu, figure 4-22) differs little from those in the low speed region ($\dot{\rho}^s = 0.15$pu, figure 4-23). However, the 'speed dip' is about 4% and 26% respectively (the difference is due to the energy stored in the inertia). The response of the upwards going load edge is much better damped than the response of the downwards going load edge, caused by the non-linear behaviour of the induction machine.

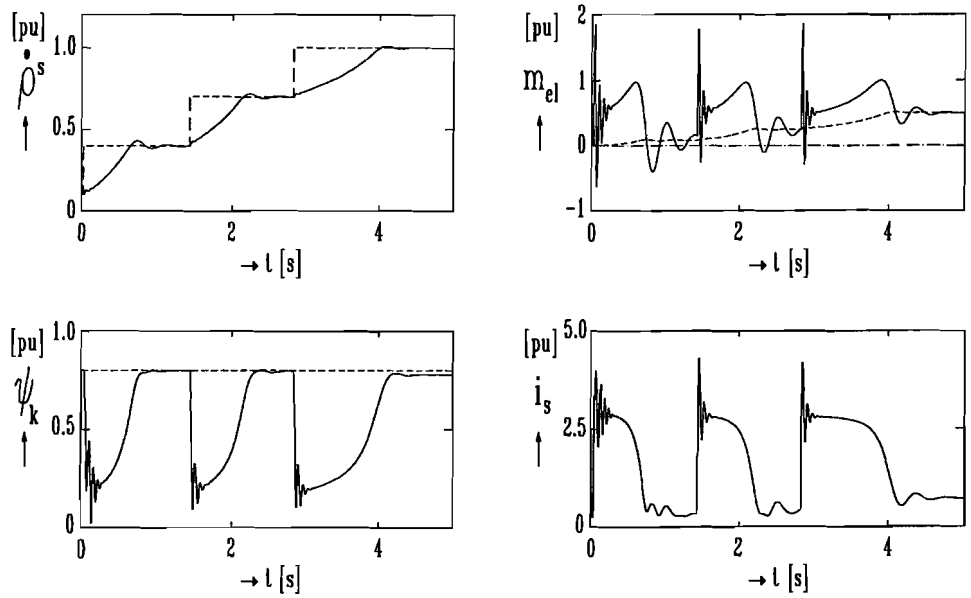

Figure 4-24: Response of staircase speed change with quadratic load

$$\left(\dot{\rho}^{s*} = (0.1 \rightarrow 0.5 \rightarrow 0.7 \rightarrow 1)\text{pu}\right), \left(m_{load} = 0.5 \cdot \left(\dot{\rho}^s\right)^2\right)$$

The speed responses of the staircase test signal with quadratic load (figure (4-24)) are different. The lower the speed, the faster the response (with more overshoot):

for $\dot{\rho}^{s*} = 0.4$ pu, the rise time is about 620 ms and the overshoot 9%

for $\dot{\rho}^{s*} = 0.7$ pu, the rise time is about 720 ms and the overshoot 7%

for $\dot{\rho}^{s*} = 1.0$ pu, the rise time is about 1180 ms and the overshoot 3%.

During the speed steps, the cage-flux decreases to a value of approximately 0.2 pu, which causes the high rise time. Because of the low flux value, the behaviour of the machine during the speed steps is comparable with start ups with constant values of stator voltage and stator frequency. Due to the low flux value, there is more stator current needed to comply with the electric torque to accelerate the machine. It will be necessary to limit the stator current (protection of the inverter semiconductors).

4.3.3. PARAMETER SENSITIVITY

The results of varying the stator and cage resistance $(r_s \pm 10\%, r_k \pm 10\%)$, the air-gap inductance $(l_l \pm 10\%)$ and the leakage inductances $(l_{\sigma s} \pm 10\%, l_{\sigma k} \pm 10\%)$ are shown in figure (4-25), (4-26) and (4-27) respectively. The linearised control method using the dc-link current is more sensitive for parameter variations than the non-linear method (paragraph 4.3.2) but the curves have the same tendency. During full load, an increase of the leakage inductances results in demagnetising the machine.

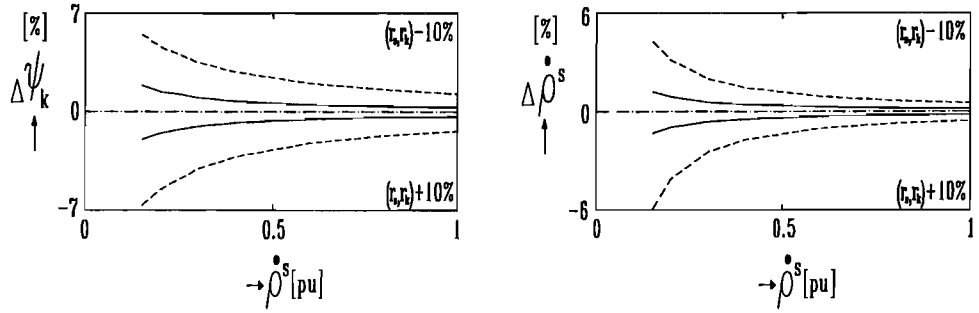

Figure 4-25: Deviation of the cage-flux and the speed due to variations of r_s and r_k $(\pm 10\%)$ at half load (—) and full load (---)

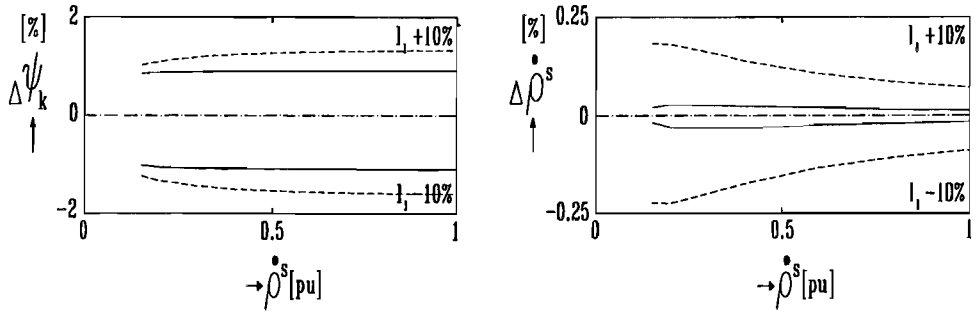

Figure 4-26: Deviation of the cage-flux and the speed due to variations of l_l $(\pm 10\%)$ at half load (—) and full load (---)

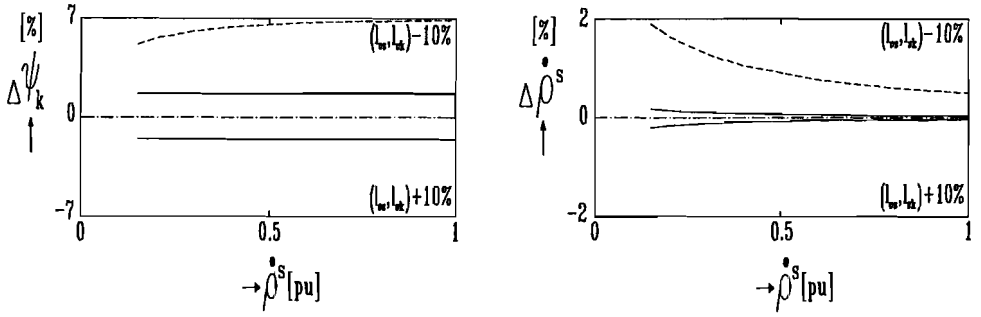

Figure 4-27: Deviation of the cage-flux and the speed due to variations of $l_{\sigma s}$ and $l_{\sigma k}$ $(\pm 10\%)$ at half load (—) and full load (---)

4.4. COMPARISON OF THE CONTROL ALGORITHMS

With the simulation results of paragraph 4.1, 4.2 and 4.3 a comparison of the three control structures is made.

Comparing the control structures (figure 3-10, 3-13 and 3-15), gives the following results:

Table 4-2: Properties of control structures

constant v/f speed control with slip regulation	linearised control using the dc-link current	non-linear control using the dc-link current
closed loop structure	open loop structure	open loop structure
speed control and slip compensation	slip compensation	slip compensation
measurement of speed	measurement of dc-link current	measurement of dc-link current
non-linear control structure	linearised control structure	non-linear control structure
analogue or digital implementation	analogue implementation	digital implementation

In particular, the speed measurement in the constant v/f speed control structure is a drawback. The speed sensor is expensive and susceptible for disturbances, while the dc-link current sensor is almost always present for protection purposes of the semiconductors of the inverter. The linear control structure using the dc-link current is characterised by its simple structure.

Looking at the stationary qualities of the control structures, only the linear control structure has a stationary speed error with respect to the desired speed (about 1-5% in the speed range 0.15-1 pu). However, in scalar control applications, small speed deviations are often of no importance.

The dynamic characteristics are shown in figure 4-28. The curves are a result of a unit load step in both the high speed region (4-28a) and the low speed region (4-28b). In the high speed region, the non-linear control structure that uses the dc-link current results in the best performance. The speed deviation (4%) is relatively small, there is no speed overshoot. Because of the stationary error, the linear control structure that uses the dc-link current, never reaches the desired speed (speed=1, torque=1).

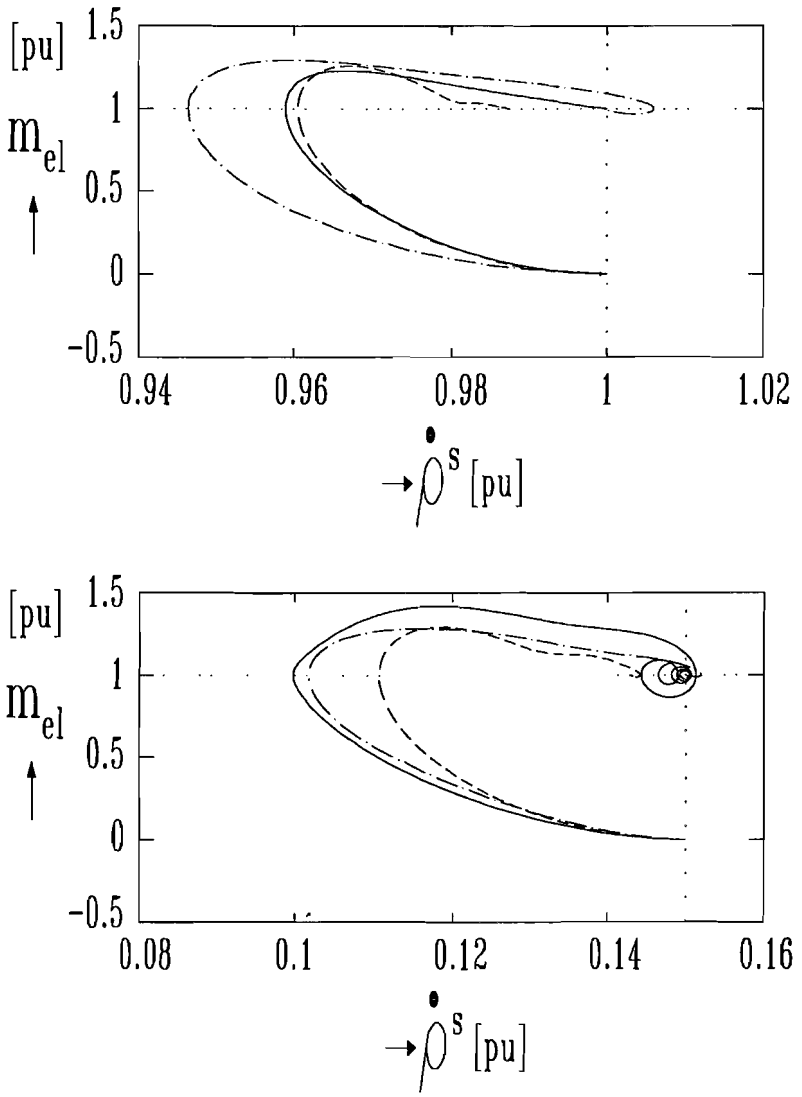

Figure 4-28: Speed-torque curves for a unit load step in the high and low speed region
(-.- = voltage frequency speed control with slip regulation,
— = non-linear control using the dc-link current,
--- = linearised control using the dc-link current)

In the low speed region, the badly damped resonance of the non-linear structure is clear. For this reason, the performance of the constant v/f speed control with slip regulation is better.

Each response convergates to its steady-state value and is, except the non-linear control structure at low speeds, well damped.

The parameter sensitivity of the v/f speed control with slip regulation is very small. The sensitivity of the linear control method shows the same tendency as the non-linear control method, but the deviations are larger. Especially in the low speed region, the deviations of the cage-flux and speed due to variations in the resistances and leakage inductances become more important.

5. IMPLEMENTATION OF THE NON-LINEAR CONTROL METHOD USING THE DC-LINK CURRENT

The non-linear control method with feed back dc-link current is implemented in a digital control system. The control method is tested with an induction machine, fed by a pulse width modulated voltage source converter. Responses of step shaped speed and load changes are measured and compared with simulation results.
An overview of the used electrical drive system is shown in figure 5.1.

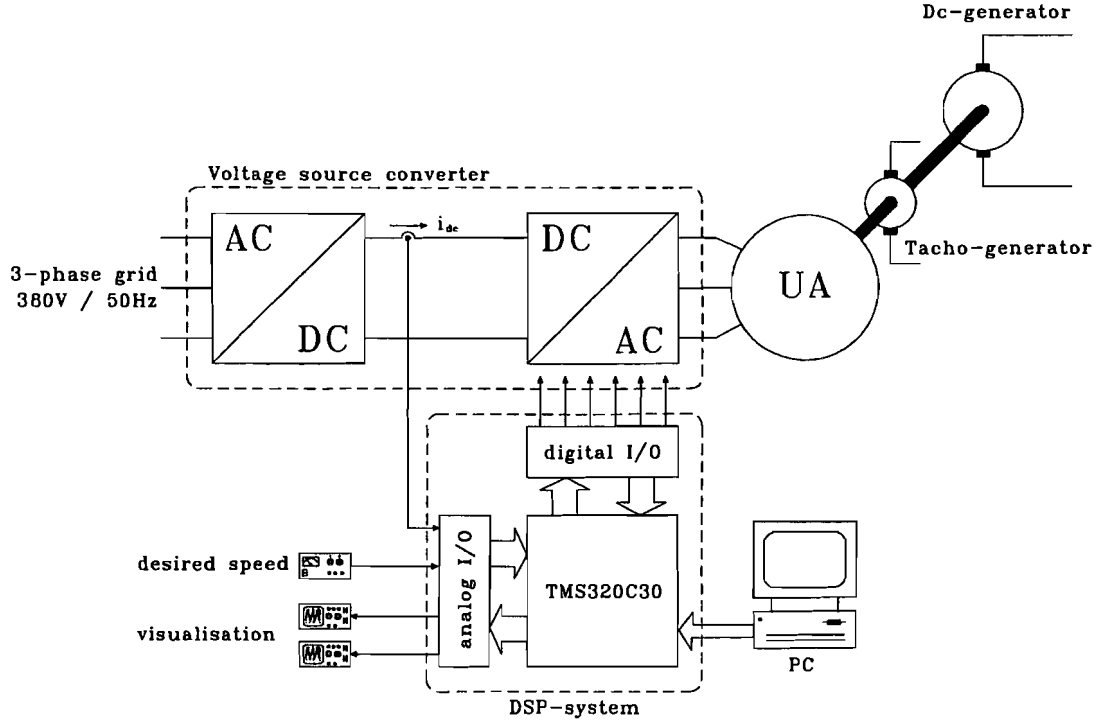

Figure 5-1: Overview of the experimental electrical drive system

In paragraph 5.1 the power part of the drive system as depicted in figure 5.1 is discussed, while in paragraph 5.2 the control system is discussed. The measured responses are shown and compared with simulated responses in paragraph 5.3. All quantities are calculated and shown in per unit. The per unit system and the used references are discussed in appendix B.

5.1. POWER PART OF THE DRIVE SYSTEM

The power part of the drive system (figure 5.1) consists of a voltage source converter (rectifier, inverter), an induction machine and a load.
The rectifier is a variable dc-voltage supply (Electronic Measurements Inc., type 500T20) which converts the three phase grid voltages (380V, 50Hz) to a dc-voltage which is adjustable between 0 and 500 V (0-20 A). During the experiments the voltage is set to 500 V (1.6 pu).

The three phase inverter is a modular construction (5 kVA), which converts the constant dc-link voltage to a pulse width modulated three phase voltage with adjustable amplitude and frequency. The switching devices are high speed Insulated Gate Bipolar Transistors (IGBT) of type IXGH25N100A (1000 V, 25 A, 20 kHz) whose gates are controlled by the digital output of the DSP-system. To avoid undesirable disturbance signals the connection between the IGBT's and the DSP system is made by fibreglass cables. A freewheel diode is anti-parallel connected to each IGBT.
To stabilise the dc-link voltage, a dissipative braking chopper is implemented[1]. The braking chopper dissipates the energy stored in the system inertia during regenerative operation of the induction machine.
A 2.2 kW single cage induction machine (Brook Crompton, UD90LN-2 S680584) with two poles is used for experiments. The parameters of the motor are calculated by means of three simple measurements. Appendix E shows both the calculation method (appendix E1) and the results of the parameter determination (appendix E2).
A dc-machine (type G621 nr 877501) is used as a load of the induction machine. The maximum current of the machine is 5 A. Therefore, the induction machine can not operate at its rated power. However, for testing the non-linear control method this it not really a problem.

5.2. CONTROL SYSTEM

5.2.1. HARDWARE

The control method is implemented in a digital signal processing system (DSP-system). which consists of three cards:

- DSP-card (TMS320C30)
- analogue I/O card
- digital I/O card.

A TMS320C30 assembly program (paragraph 5.2.2) is down loaded via an interface in the 16 k memory of the DSP-card.
Eight analogue input signals (measured values, set points) can be read and eight analogue output signals (control signals, visualisation of intern variables) can be written synchronously. The analogue to digital conversion and visa versa takes place with a sample frequency which is defined in the DSP-assembly program. The sample frequency is dependent of the length of the (control) program. The amplitude of the I/O signals are between -10 V and 10 V, but scaled in such a way that an analogue input signal of 0-10V results in a digital number between 0-2048.
From the digital card, only six of the eight outputs are used for firing the IGBT's of the inverter.
The non-linear control method (paragraph 3.6) uses the dc-link current as feedback signal. Therefore, a current sensor (LEM-module, nr EM1236) is applied in the dc-link of the converter. A LEM-sensor converts a current to a proportional current signal

[1]The braking chopper is designed by M.B.J. Leusenkamp and described in his report 'Ontwerp van een remchopper voor een 5 kW spanningsinverter', EMV 94-06.

which is galvanically separated from the power part. This current can be converted to any desired voltage using an (accurate) resistor. The transfer function of the applied current measurement is

$$u(i_{dc}) = \frac{i_{dc}}{K_{LEM}} R = \frac{i_{dc}}{1000} 2000 = 2i_{dc}. \qquad (5\text{-}1)$$

5.2.2. DSP-PROGRAM

The control rules (3-52)...(3-55) of the non-linear control method are translated to a TMS320C30 assembly program [Texas '91]. The flow-chart of the program 'Vuckovic.asm' is given in appendix F1. The listing of the assembly program is shown in appendix F2.

The sample frequency, f_s, is set to 15kHz ($T_s = 66\frac{2}{3}\mu s$). The whole control cycle takes about 50μs, which is comparable with the cycle time of indirect field orientation. As can be seen in the time sequence diagram of figure 5.2, there is enough time for executing a control cycle.

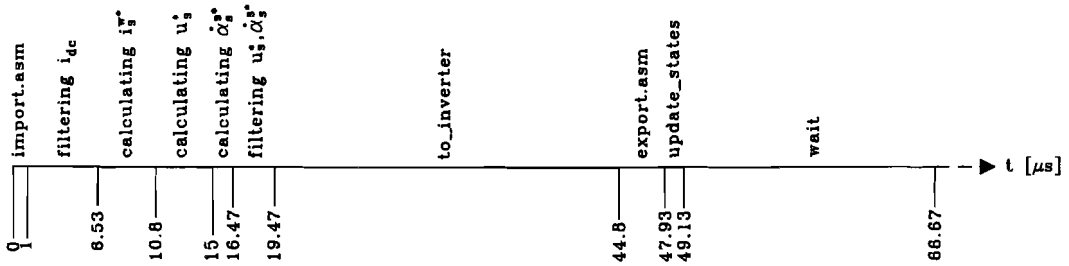

Figure 5-2: Time sequence diagram of the control cycle

As mentioned in paragraph 3.6.5 a third order Butterworth filter is needed for eliminating PWM-noise. For implementing a digital Butterworth filter, a general filter macro 'filter' of the library MATLIB.asm is used[2]. The cut-off frequency is set to 200 Hz (4 pu).

After calculating the desired stator voltage, u_s^*, and the desired stator frequency, $\dot{\alpha}_s^{s*}$, by means of the control rules (3-52)...(3-55), both quantities are filtered to smooth the command signals of the inverter. For these purposes two ordinary first order lags are used, with cut-off frequencies of 200Hz (4 pu) and 5Hz (0.1 pu), respectively. Both values are found by simulations (see paragraph 3.6.5).

The filtered quantities of u_s^* and $\dot{\alpha}_s^{s*}$ are the amplitude and the frequency of the fundamental component of the three pulse width modulated stator voltages, which are generated by switching the IGBT's in a certain pattern. This pattern is calculated in the macro 'to_inverter.asm'[3]. The macro adds 12% third harmonic to the fundamental component (paragraph 2.2.2).

---

[2]The general filter macro is written by Ir. S.G. Bosga for TMS320C40 purposes, the filter coefficients for the Butterworth characteristics are calculated with the MATLAB tool 'Butter'.

[3]The macro 'to_inverter.asm' is written by Dr. ir. J.L. Duarte for general purposes

Finally, the DSP-program waits for an interrupt, which is generated when the next A/D conversion is finished. The interrupt starts the next control cycle.

5.3. RESULTS

The implemented control structure uses the machine parameters as calculated in appendix E. Due to the maximum dc-link voltage of 1.6 pu (500 V) the amplitude of the triangular carrier is set to 0.8 pu. Therefore it is possible to reach a maximum value of the fundamental component of the stator voltage of 1 pu (see equation (2-5))

$$\hat{u}_{sa(1)} = M_i \frac{u_{dc}}{2} = \frac{\hat{u}_{ref}}{\hat{u}_{tri}} \cdot \frac{u_{dc}}{2} \quad \Leftrightarrow \quad \hat{u}_{sa(1)} = \hat{u}_{ref}. \tag{5-2}$$

A drawback of the relative small amplitude of the carrier is less switching actions in the region where the stator voltage amplitude exceeds the carrier amplitude (0.8 pu). This results in more harmonic content in the block shaped stator voltages (it looks more and more like block modulation). The pulse number, N_p, is set to 15.

To verify the measured results of the implemented control structure, simulations of the same situations are carried out. For simulation purposes, the simulation model of appendix D3 is used, however with the machine parameters as calculated in appendix E. Because the pull-off torque of the machine with load is not negligible, it is measured and set to a constant value of 0.0476 pu (0.45 Nm). For simulation purposes, other losses (iron losses, friction, switching losses) are neglected.

Four experiments are carry out. Both the speed and load behaviour are tested by step shaped changes as shown in table 5-1.

Table 5-1: Trigger signals

Experiment	$\dot{\rho}_s^*$ [pu]	m_{load} [pu]
1	step 0.8 → 1	constant 0.0476
2	step 0.4 → 0.5	constant 0.0476
3	constant 1	step 0.0476 → 0.318
4	constant 0.5	step 0.0476 → 0.318

A sudden load change is done by switching on the armature current of the dc-generator. The value of the load torque is adjusted with an analogue balance system. Step changes of the desired speed are generated by the DSP-system.

During the four experiments of table 5-1, the speed is measured by means of a tachometer (0.1564 V/Hz). In case of the last two experiments, not only the speed is measured, but the filtered dc-link current as well. Therefore, the filtered dc-link current (third order Butterworth filter in the DSP-program) is put to an analogue output of the DSP-system.

The measured data is stored in a NICOLET oscilloscope (type NIC320). Because the measured signals contain a large dc-component, the quantisation of this oscilloscope is relative large. Therefore, the data is processed by MATLAB, using a first order digital Butterworth filter ($f_{cut-off} = 0.01 \cdot f_{nyquist}$). The measured data is hardly affected, because

the spectrum of the measured signals is situated in the low frequency region and the quantisation noise is situated in a much higher frequency region.
Figure 5-3, shows the result of the first experiment.

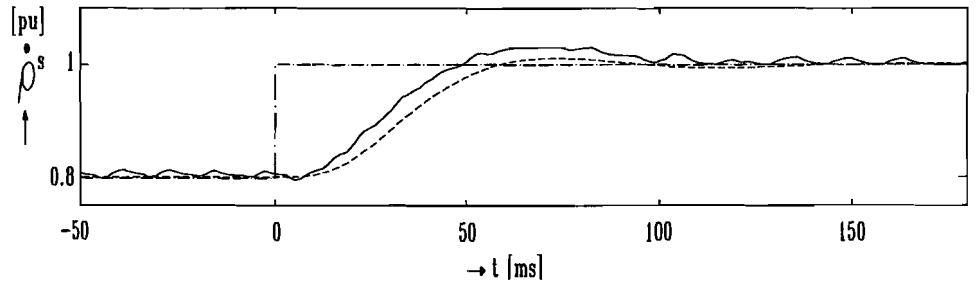

Figure 5-3: Measured (—) and simulated (---) speed response of a step shaped change of the desired speed (-.-.) in no-load situation $\left(\dot{\rho}_s^*: 0.8\text{pu} \rightarrow 1\text{pu},\ m_{load}=0.0476\text{pu}\right)$

In figure 5-3, there is hardly difference between the steady state values of the measured speed response and the simulated speed response. There is only a small deviation between the dynamics of the responses. The rise time of the measured and simulated response is about 49 ms and 58 ms, respectively. The ripple of the measured response is due to the pulse shaped stator voltages of the PWM-inverter.
The result of the step shaped speed change at half speed is shown in figure 5-4.

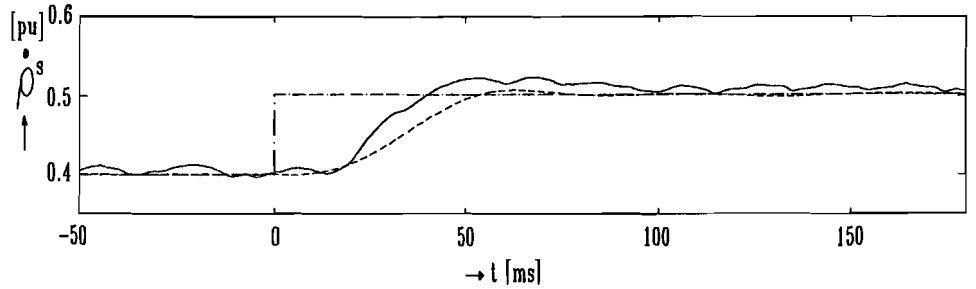

Figure 5-4: Measured (—) and simulated (---) speed response of a step shaped change of the desired speed (-.-.) in no-load situation $\left(\dot{\rho}_s^*: 0.4\text{pu} \rightarrow 0.5\text{pu},\ m_{load}=0.0476\text{pu}\right)$

Stationary there is a small error between both responses (discussed at the end of this paragraph). Again the measured response is little faster than the simulated response (rise time 40 ms and 54 ms, respectively).
It can be concluded that the measured speed responses of figure 5-3 and 5-4 fairly agree with the simulated responses.
The result of the experiment with a step shaped load change at a speed of 1pu is shown in figure 5-5. The speed deviation at the moment of the load change is both in the measured and simulated responses visible (-2.3% and -2.7% respectively). The rise time of the responses are 72 ms and 58 ms, respectively. Therefore the simulated speed response is about 14 ms faster than the measured response. The steady state value of the simulated filtered dc-link current is both in no-load and load situation about 0.035pu

lower than the measured steady state value. This is due to the losses in the drive system, which are not taken fully into account in the simulations (switch losses, iron losses, friction).The measured response is therefore more damped than the simulated response. The ripple in the measured responses is due to the pulse shaped stator voltages.

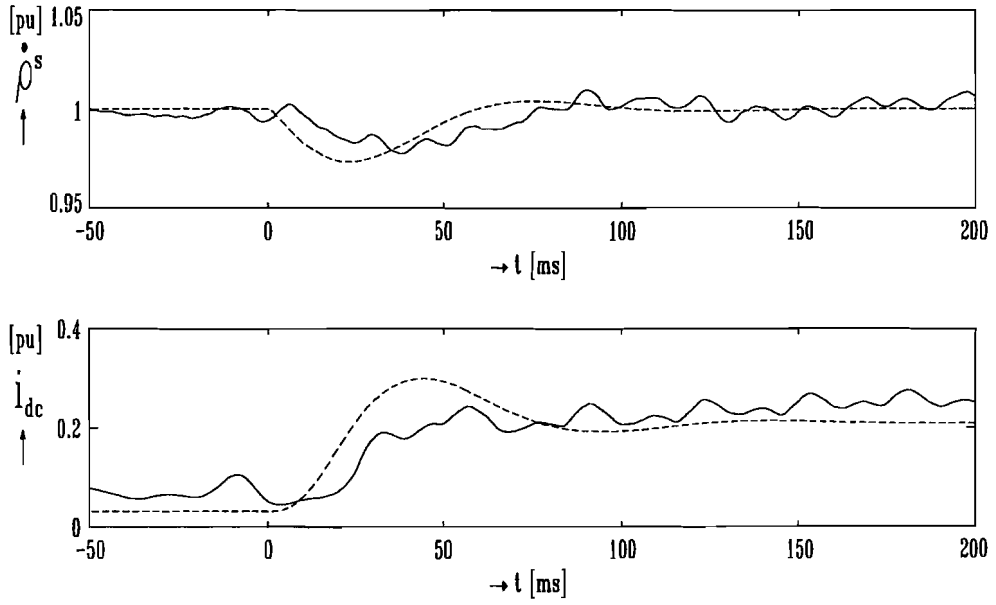

Figure 5-5: Measured (—) and simulated (---) responses of a step shaped load change at a speed of 1 pu
$\left(m_{load}: 0.0476 \rightarrow 0.318pu,\ \dot{\rho}_s^* = 1pu\right)$

Figure 5-6 shows the result of the fourth experiment. At a speed of 0.5 pu, the dynamics of the measured speed response are slower than the simulated responses. The speed dips of the responses are -3.8% and -5.4%, respectively. The steady-state deviation of the speed is very small. The simulated filtered dc-link current is again lower than the measured current (0.019 pu), which is due to the losses of the drive system. The dynamics of the filtered dc-link current are quite different.
It can be concluded that, in spite of the deviations in the dynamics of the load responses (figure 5-5 and 5-6), the steady-state behaviour satisfies the expected results.

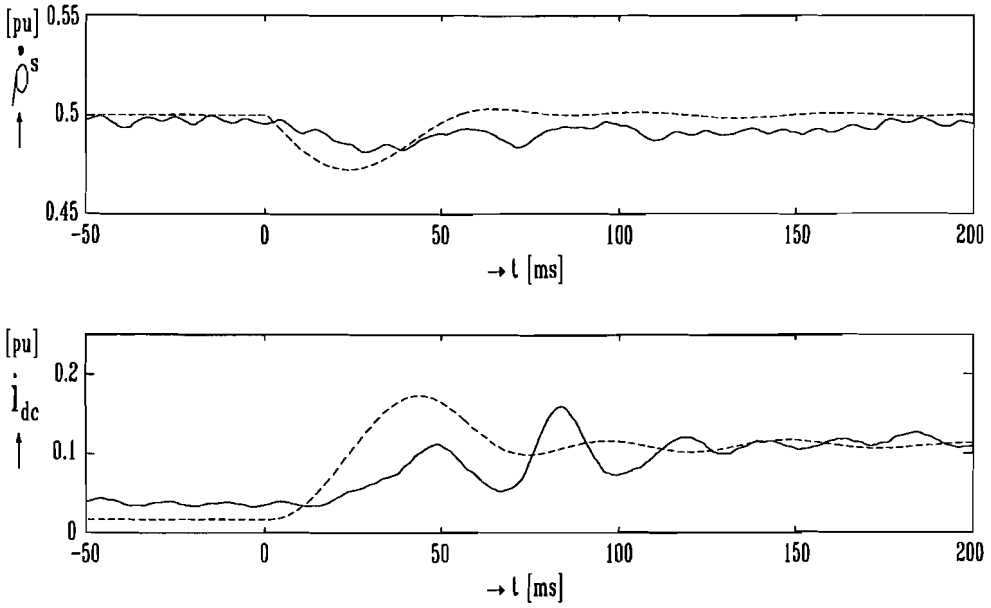

Figure 5-6: Measured (—) and simulated (---) responses of a step shaped load change at a speed of 0.5 pu
(m_{load}:0.0476 → 0.318pu, $\dot{\rho}_s^* = 0.5$pu)

Finally, the speed behaviour in a wide speed range (0-3000 rpm) for different load values (0, 0.11pu and 0.32pu) is measured. The results are shown in figure 5-7.

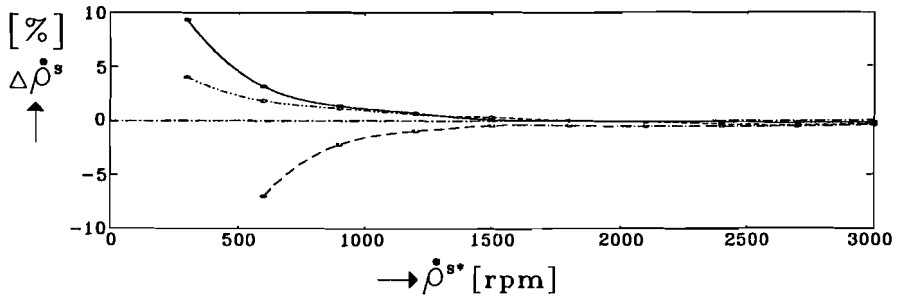

Figure 5-7: Speed behaviour in the speed region 0-3000rpm for different load values
(—— = 0; —-·- = 0.11pu; – – = 0.32pu)

Figure 5-7 shows that the speed deviation between the desired speed and the measured speed is load-dependent. The speed deviation at $m_{load} = 0$ and $m_{load} = 0.11$ pu is less than 5% in the speed region 600-3000rpm (0.2-1pu). If the load of the machine is larger, ($m_{load} = 0.32$pu) the speed deviation at 600rpm is about -7%. It can be concluded that the steady-state error in the low speed region is not in fully agreement with the simulated results. The deviations in the low speed region are mainly due to the (temperature) sensitivity of the machine parameters. Another cause could be the constancy of the dc-link voltage. Deviations of the dc-link voltage, which is supposed to be constant, become relative more important in the low speed region.

6. CONCLUSIONS

- *Scalar control methods* are widely used for (rugged) general ac drive applications. They are characterised by a simple control structure, low costs, satisfactory steady-state behaviour and moderate controlled transient responses. Efficient scalar control of voltage fed induction machines is based on the principle of maintaining a constant voltage/frequency ratio, which results in an approximated *constant flux*. Suiting this principle for operation in the low speed region and for high load situations, has resulted in many adapted structures (low speed voltage boost, load dependent voltage boost).

- Because of the absence of transducers (expensive, sensitive for disturbances, maintenance), *variable speed drives without feedback* of measured machine quantities become more important. Higher accuracy of speed is achieved by *slip compensation*. If an induction machine is fed by a voltage source converter with constant dc-link voltage, the *dc-link current* is a very useful quantity for control structures. The dc-link current is a load-dependent quantity which is normally available for inverter protection purposes.

- Derivation of a scalar control structure, based on the stationary equations of the voltage fed induction machine in field oriented coordinates, which uses the dc-link current, results in a *non-linear control structure*. Implementation is only possible in a microprocessor based control system. Linearisation of the non-linear control structure leads to a simple control structure which is easy to implement with analogue hardware. In case of the *linearised control structure*, the voltage/frequency control structure with a load-depended voltage boost is clearly recognizable..

- Simulations have proved that the steady-state behaviour of the *non-linear control structure using the dc-link current* is excellent and equals the qualities of closed loop control. In the high speed region, machine dynamics are well damped, but in the low speed region (<15% of synchronous speed) resonances appear, which are a result of badly damped machine dynamics. Parameter sensitivity of the stator and cage resistance and the leakage inductance is only important in the very low speed region.

- Simulations show that the steady-state behaviour of the *linearised control structure using the dc-link current* results in speed deviations (at a load torque of 1 pu, the speed deviation in the low speed region is about -1.3% and in the high speed region about -4.5%). During load or speed changes the flux deviations are considerable. The machine dynamics are hardly affected by the control method. In spite of these shortcomings the control method can be useful in applications where small speed deviations are of no importance. The linearised control method is more sensitive for parameter variations than the non-linear control method.

- *Implementation of the non-linear control structure* using the dc-link current in a DSP-system (TMS320C30) and testing the qualities with a 2.2kW induction machine fed by a PWM voltage source converter (IGBT's) result in steady-state errors in the low speed region (<20% of synchronous speed). The deviations in the low speed region are mainly due to the (temperature) sensitivity of the machine parameters and the constancy of the dc-link voltage. When the shape of the measured responses and simulated responses are compared, there is a lot of conformity.

- Although simulation results are not in fully agreement with the experimental results in the low-speed region, the main working principle of the non-linear control method using the dc-link current is proven to be valid in the high-speed region.

BIBLIOGRAPHY

[Abb '77] **Abbondanti. A.**
Method of flux control in induction motors driven by variable frequency, variable voltage supplies
In: IEEE-IAS, Int. Semiconductor Power Converter Conf., 28-31 march 1977, Lake Buena Vista (USA): IEEE, (New York), 1977, P177-184

[Blas '91] **Blaschke, F. and A. Vandenput**
Electrische aandrijvingen II - Regeltechnieken voor draaiveldmachines - Ontwikkeling van de fundamentele regelstructuur en regeltechniek
Oktober 1991, Leuven: Katholieke Universiteit Leuven, Dep. E - afd. VIT - Lab. voor Electrische machines en aandrijvingen

[Bosch '93] **Bosch, van den P.P.J., H. Butler, A.R.M. Soeterboek and M.M.W.G. Zaat**
Modelling and Simulation with PSI/c
Delft: University of Technology Delft, 1993
BOZA automatisering BV, Nuenen. ISBN 90-71898-17-2

[Bose '86] **Bose, B.K.**
Power Electronics and AC Drives
London: Prentice Hall International, 1986, ISBN 0-13-686882-7

[Buja '75] **Buja, G. and G. Indri**
Improvement of Pulse-width Modulation Techniques
Archiv für Elektrotechnik, Band 57 (1975), P281-289

[Evan '86] **Evans, P.D. and R.J. Hill-Cottingham**
DC link current in PWM inverters
IEE Proceedings, Pt B, Vol. 133 (1986), No. 4, P217-224

[Fin '90] **Finch, J.W., D.J. Atkinson and P.P. Acarnley**
Scalar to Vector: General principles of modern induction motor control
In: 4th Int. Conf. on Power Electronics and Variable Speed Drives 17-19 July 1990, London (UK): IEE, London (UK), 1990 P364-369

[Hein '89] **Heinemann, G.**
Comparison of several control schemes for AC induction motors under steady-state and dynamic conditions
In: EPE'89, Eur. Conf. on Power Electronics and Applications, 9-12 Oct. 1989, Aachen (Germany): EPE'89 Secretariat, Dusseldorf, 1989, Vol. 2, P843-848

[Leon '85] **Leonhard, W.**
Control of Electrical Drives
Berlin: Springer Verlag, 1985, ISBN 3-540-13650-9
Translation of: *Regelung in der electrischen Antriebstechnik,*
Stuttgart: Teubner, 1974

[Moh '89] **Mohan, N., T.M. Undeland, W.P. Robbins**
Power Electronics: Converters, Applications and Design
New York: John Wiley & Sons, 1989, ISBN 0-471-61342-8

[Sen '90] **Sen, P.C.**
Electric Motor Drives and Control - Past, Present and Future
IEEE Trans. on Industrial Electronics, Vol. 37 (1990), No. 6, P562-575

[Stef '92] **Stefanovic, V.R.**
Industrial AC drives, status of technology
In: EPE'92, Eur. Conf. on Power Electronics and Applications
March 1992, Germany, 1992
Vol. 2, No.1, P7-24

[Texas '91] **Texas Instruments**
TMS320C3x User's guide
June 1991, Texas Instruments

[Vput '92] **Vandenput, A.**
Electrische aandrijftechniek I
Collegedictaat: Electrische Aandrijftechniek (5P120))
Maart 1992, Eindhoven: Technische Universiteit Eindhoven,
Fac. E, Vakgroep EMV

[Velt '93] **Veltman, A.**
The Fish Method, Interaction between AC-machines and Switching Power Converters
Delft: University of Technology Delft, 1993, Doctoral Dissertation
Delft University Press, ISBN 90-9006763-9

[Vuck '91] **Vuckovic, V. and S. Vukosavic**
A low cost variable speed induction motor drive with improved static and dynamic properties
In: EPE '91, Eur. Conf. on Power Electronics and Applications,
3-6 Sept. 1991, Firenze (Italy): Litografia GEDA, Torino (Italy),
1991, Vol. 2, P406-411

[Vuck '92] **Vuckovic, V. and S. Vukosavic**
Control algorithm for the inverter fed induction motor drive with DC current feedback loop based on principles of the vector control
Electric Machines and Power Systems,
Sept. - Oct 1992,
Vol. 20 Iss. 5, P405-424

[Werf '94] **Werf, Johan van der**
Het toepassen van een spannings/stroom-model voor directe koppelregeling van een asynchrone machine
Afstudeerverslag EMV 94-13
December 1994, Eindhoven: Technische Universiteit Eindhoven, Faculteit der Elektrotechniek, Vakgroep Elektromechanica en vermogenselektronica

[Wil '76] **Wilson, J.W.A. and J.A. Yeamans**
Intrinsic harmonics of idealized inverter PWM systems
In: IEEE-Industry Applications Society (IEEE-IAS), Annual Meeting, 11-14 Oct. 1976, Chigaco (USA): IEEE, New York, 1976, P967-973

APPENDIX A: Transformation matrices

In this thesis the following transformation matrices are used to transform the three-phase model to a two-phase model and visa versa. The matrices are derived in [Blas '91].

Current transformations

Current transformation matrix from 3 phase to 2+1 phase model:

$$\begin{bmatrix} i_s^{s1} \\ i_s^{s2} \\ i_{s0} \end{bmatrix} = \begin{bmatrix} 1 & -\frac{1}{2} & -\frac{1}{2} \\ 0 & \frac{\sqrt{3}}{2} & -\frac{\sqrt{3}}{2} \\ 1 & 1 & 1 \end{bmatrix} \cdot \begin{bmatrix} i_{sa} \\ i_{sb} \\ i_{sc} \end{bmatrix} \tag{A1}$$

Current transformation matrix from 2+1 phase to 3 phase model:

$$\begin{bmatrix} i_{sa} \\ i_{sb} \\ i_{sc} \end{bmatrix} = \begin{bmatrix} \frac{2}{3} & 0 & \frac{1}{3} \\ -\frac{1}{3} & \frac{1}{\sqrt{3}} & \frac{1}{3} \\ -\frac{1}{3} & -\frac{1}{\sqrt{3}} & \frac{1}{3} \end{bmatrix} \cdot \begin{bmatrix} i_s^{s1} \\ i_s^{s2} \\ i_{s0} \end{bmatrix} \tag{A2}$$

Voltage transformations

Voltage transformation matrix from 3 phase to 2+1 phase model:

$$\begin{bmatrix} u_s^{s1} \\ u_s^{s2} \\ u_{s0} \end{bmatrix} = \begin{bmatrix} \frac{2}{3} & -\frac{1}{3} & -\frac{1}{3} \\ 0 & \frac{1}{\sqrt{3}} & -\frac{1}{\sqrt{3}} \\ \frac{1}{3} & \frac{1}{3} & \frac{1}{3} \end{bmatrix} \cdot \begin{bmatrix} u_{sa} \\ u_{sb} \\ u_{sc} \end{bmatrix} \tag{A3}$$

Voltage transformation matrix from 2+1 phase to 3 phase model:

$$\begin{bmatrix} u_{sa} \\ u_{sb} \\ u_{sc} \end{bmatrix} = \begin{bmatrix} 1 & 0 & 1 \\ -\frac{1}{2} & \frac{\sqrt{3}}{2} & 1 \\ -\frac{1}{2} & -\frac{\sqrt{3}}{2} & 1 \end{bmatrix} \cdot \begin{bmatrix} u_s^{s1} \\ u_s^{s2} \\ u_{s0} \end{bmatrix} \tag{A4}$$

Flux transformations

Flux transformation matrix from 3 phase to 2+1 phase model:

$$\begin{bmatrix} \psi_s^{s1} \\ \psi_s^{s2} \\ \psi_{s0} \end{bmatrix} = \begin{bmatrix} \frac{2}{3} & -\frac{1}{3} & -\frac{1}{3} \\ 0 & \frac{1}{\sqrt{3}} & -\frac{1}{\sqrt{3}} \\ \frac{1}{3} & \frac{1}{3} & \frac{1}{3} \end{bmatrix} \cdot \begin{bmatrix} \psi_{sa} \\ \psi_{sb} \\ \psi_{sc} \end{bmatrix} \tag{A5}$$

Flux transformation matrix from 2+1 phase to 3 phase model:

$$\begin{bmatrix} \psi_{sa} \\ \psi_{sb} \\ \psi_{sc} \end{bmatrix} = \begin{bmatrix} 1 & 0 & 1 \\ -\frac{1}{2} & \frac{\sqrt{3}}{2} & 1 \\ -\frac{1}{2} & -\frac{\sqrt{3}}{2} & 1 \end{bmatrix} \cdot \begin{bmatrix} \psi_s^{s1} \\ \psi_s^{s2} \\ \psi_{s0} \end{bmatrix} \tag{A6}$$

The index 's0' ($i_{s0}, u_{s0}, \psi_{s0}$) in A1...A6 refers to the star point of the three phase system. The quantities with index 's0' are supposed to be zero.

APPENDIX B: Per unit system

B1: Standard quantities

A *physical quantity*, $\langle a \rangle$, is defined as an expression with a dimension. It is possible to write this expression as a product of a *reference quantity with dimension*, $[\langle a \rangle]_{ref}$, and a *value without dimension*, a. This value indicates how many times the physical quantity contains the reference quantity

$$\langle a \rangle = a \cdot [\langle a \rangle]_{ref}. \tag{B1}$$

In the so called Giorgi unity system (SI-system) all reference quantities are set to unity (for example: $[\langle u \rangle]_{ref} = 1\,V$ or $[\langle i \rangle]_{ref} = 1\,A$). In this thesis, the per unit system (PUS) is used. PUS uses rated quantities as reference quantities. Therefore, the values of most variables are between -1 and +1, there is little difference in the parameter values of several machines and the performance of different machines is easy to compare.
For the per unit system in this thesis, four basic reference quantities are chosen:

$$[\langle u \rangle]_{ref} = [\langle u \rangle]_N \tag{B2}$$

$$[\langle i \rangle]_{ref} = [\langle i \rangle]_N \tag{B3}$$

$$[\langle \alpha \rangle]_{ref} = [\langle \alpha \rangle]_{SI} \tag{B4}$$

$$[\langle \dot{\alpha} \rangle]_{ref} = [\langle \dot{\alpha} \rangle]_N. \tag{B5}$$

The references of both the voltage and the current are the rated value of the two dimensional stator vectors (appendix A). However, these values are in most cases unknown. Easier is to use the rated values of the stator windings. Therefore the voltage reference (B2) retains the same value, but the current reference is multiplied by a factor 3/2 [Blas '91]. Therefore B(2) and (B3) become

$$[\langle u \rangle]_{ref} = [\langle u_{sq} \rangle]_N \tag{B6}$$

$$[\langle i \rangle]_{ref} = \tfrac{3}{2}[\langle i_{sq} \rangle]_N. \tag{B7}$$

Using the basic references (B4), B(5), B(6) and B(7), more references can be derived:

$$[\langle r \rangle]_{ref} = \frac{[\langle u \rangle]_{ref}}{[\langle i \rangle]_{ref}} \tag{B8}$$

$$[\langle t \rangle]_{ref} = \frac{[\langle \alpha \rangle]_{ref}}{[\langle \dot{\alpha} \rangle]_{ref}} \tag{B9}$$

$$[\langle\psi\rangle]_{ref} = \frac{[\langle u\rangle]_{ref}}{[\langle\dot{\alpha}\rangle]_{ref}} \tag{B10}$$

$$[\langle l\rangle]_{ref} = \frac{[\langle u\rangle]_{ref}}{[\langle\dot{\alpha}\rangle]_{ref}[\langle i\rangle]_{ref}} \tag{B11}$$

$$[\langle m_{el}\rangle]_{ref} = \frac{[\langle u\rangle]_{ref}[\langle i\rangle]_{ref}}{[\langle\dot{\alpha}\rangle]_{ref}} \tag{B12}$$

$$[\langle\theta\rangle]_{ref} = \frac{[\langle u\rangle]_{ref}[\langle i\rangle]_{ref}}{\left([\langle\dot{\alpha}\rangle]_{ref}\right)^3}. \tag{B13}$$

From B(1), per unit values are calculated by

$$a = \frac{\langle a\rangle}{[\langle a\rangle]_{ref}}, \quad \text{with } a \in \{u, i, \dot{\alpha}, t, r, l, \psi, m, \theta\}. \tag{B14}$$

B2: Reference quantities of test-machine

Using B4...B13, the reference quantities of the test-machine (appendix E2) are calculated. The results are given in table B1.

Table B1: Reference quantities of test-machine

Reference quantity	Reference value	Reference dimension
$[\langle u\rangle]_{ref}$	$3.1113 \cdot 10^{2}$	[V]
$[\langle i\rangle]_{ref}$	9.5460	[A]
$[\langle\alpha\rangle]_{ref}$	1	[rad]
$[\langle\dot{\alpha}\rangle]_{ref}$	$3.1416 \cdot 10^{2}$	[rad / s]
$[\langle r\rangle]_{ref}$	$3.2593 \cdot 10^{1}$	[Ω]
$[\langle t\rangle]_{ref}$	$3.1831 \cdot 10^{-3}$	[s]
$[\langle\psi\rangle]_{ref}$	$9.9035 \cdot 10^{-1}$	[Vs]
$[\langle l\rangle]_{ref}$	$1.0375 \cdot 10^{-1}$	[H]
$[\langle m_{el}\rangle]_{ref}$	9.4538	[Nm]
$[\langle\theta\rangle]_{ref}$	$9.5787 \cdot 10^{-5}$	$[kg \cdot m^2]$

APPENDIX C: Parameters of the fictive machine

Table E4: Parameters of the fictive machine

Parameter	Value
l_l	3 pu
$\sigma_s = \sigma_k$	0.05 pu
r_k	0.02 pu
r_s	0.04 pu
θ	430 pu

APPENDIX D: Simulation programs (PSI/c)

In appendix D, the PSI/c simulation programs used in chapter 3 are given. For more information about the PSI/c commands see [Bosch '93].

D1: Induction machine

```
%*******************************************************************************
%              Link one of the control methods of appendix D
%              above this line
%*******************************************************************************
%UA MACHINE MODEL
%see 'The fish method' par 3.6; A. Veltman 1993
%*******************************************************************************
%UA-MACHINE PARAMETERS:
l               =   PAR(3);          %   main inductance
l_sig_k         =   PAR(0.15);       %   cage leakage inductance
l_sig_s         =   PAR(0.15);       %   stator leakage inductance
r_k             =   PAR(0.02);       %   cage resistance
r_s             =   PAR(0.04);       %   stator resistance
J               =   PAR(430);        %   inertia
%*******************************************************************************
%PWM-INVERTER PARAMETERS:
u_dc            =   PAR(2);          %   dc-link voltage
%*******************************************************************************
%IDEAL CONVERTER
alfa_s_s_des    =   INTMOD(alfaP_s_s_des PAR: 1.52899E-2,pi);
u1              =   u_s_des*cos(alfa_s_s_des);              %   ideal u_s_s1_des
u2              =   u_s_des*sin(alfa_s_s_des);              %   ideal u_s_s2_des
i_dc            =   (u1*i_s_s1 + u2*i_s_s2)/u_dc;           % power balance
%*******************************************************************************
%MODEL PARAMETERS
k               =   PAR(l/(l+l_sig_k));
l_sigma         =   PAR(l_sig_s + l*l_sig_k/(l+l_sig_k));
l_m             =   PAR(k*k*(l+l_sig_k));
r_r             =   PAR(k*k*r_k);
%*******************************************************************************
%STATOR SECTION
flux_s_s1       =   INT(u1 - i_s_s1*r_s PAR: 2.35045E-2);
flux_s_s2       =   INT(u2 - i_s_s2*r_s PAR: -0.839671);
flux_r_s1       =   flux_r_r1*cos(theta) - flux_r_r2*sin(theta);
flux_r_s2       =   flux_r_r1*sin(theta) + flux_r_r2*cos(theta);
i_s_s1          =   (flux_s_s1-flux_r_s1)/l_sigma;
i_s_s2          =   (flux_s_s2-flux_r_s2)/l_sigma;
i_s             =   sqrt(i_s_s1*i_s_s1 +  i_s_s2*i_s_s2);
%*******************************************************************************
%ROTOR SECTION
flux_r_r1       =   INT(i_r_r1*r_r PAR: .760898);
flux_r_r2       =   INT(i_r_r2*r_r PAR: 3.92096E-2);
i_s_r1          =   i_s_s1*cos(theta) + i_s_s2*sin(theta);
i_s_r2          =  -i_s_s1*sin(theta) + i_s_s2*cos(theta);
i_r_r1          =   i_s_r1 - flux_r_r1/l_m;
i_r_r2          =   i_s_r2 - flux_r_r2/l_m;
%*******************************************************************************
%MECHANICAL SECTION
mel             =   i_s_s2*flux_s_s1 - i_s_s1*flux_s_s2;
rhoP_s          =   INT(1/J*(mel-mload) PAR: 1);
theta           =   INTMOD(rhoP_s PAR: -1.5943, pi);
%*******************************************************************************
%CALCULATION OF AIR-GAP FLUX
flux_l_s1       =   flux_s_s1 - i_s_s1*l_sig_s;
flux_l_s2       =   flux_s_s2 - i_s_s2*l_sig_s;
flux_l          =   sqrt(flux_l_s1*flux_l_s1 + flux_l_s2*flux_l_s2);
%*******************************************************************************
%CALCULATION OF CAGE FLUX
i_k_s1          =   flux_l_s1/l - i_s_s1;
i_k_s2          =   flux_l_s2/l - i_s_s2;
i_k             =   sqrt(i_k_s1*i_k_s1 + i_k_s2*i_k_s2)*l_sig_k;
flux_k_s1       =   flux_l_s1 + i_k_s1*l_sig_k;
flux_k_s2       =   flux_l_s2 + i_k_s2*l_sig_k;
flux_k          =   sqrt(flux_k_s1*flux_k_s1 + flux_k_s2*flux_k_s2);
%*******************************************************************************
```

D2: Constant v/f speed control with slip regulation

```
%*************************************************************************************
%Constant v/f speed control with slip regulation
%*************************************************************************************
%CONTROL PARAMETERS
rhoP_s_des1     =   GEN(PAR: 1,10,6,1,1000,0);      % desired speed
rhoP_s_des      =   INF(rhoP_s_des1 PAR:1,1,56);    % smoothed speed
mload           =   GEN(PAR: 0,10,5,1,481.24,0);    % desired load-torque
flux_k_des      =   PAR(0.8);                       % desired flux
k_reg           =   PAR(0.48);                      % gain PI-controller
tau_reg         =   PAR(56);                        % tau PI-controller
%*************************************************************************************
%VOLTAGE FREQUENCY CONTROL
sigma_s         =   PAR(l_sig_s/l);      %   relative leakage inductance of stator
sigma_k         =   PAR(l_sig_k/l);      %   relative leakage inductance of cage
alfaP_s_r_des1  =   PIC(rhoP_s_des-rhoP_s PAR:7.59051E-7,k_reg,tau_reg);
alfaP_s_r_des   =   LIM(alfaP_s_r_des1 PAR: -0.066,0.066,1);    % limited slip frequency
alfaP_s_s_des   =   alfaP_s_r_des + rhoP_s;                     % stator frequency
omega_1         =   r_s/l - (l/r_k)*((1+sigma_k)*(1+sigma_s)-1)
                    *alfaP_s_r_des*alfaP_s_s_des;
omega_2         =   (r_s/r_k)*(1+sigma_k)*alfaP_s_r_des + (1+sigma_s)*alfaP_s_s_des;
u_s_des1        =   flux_k_des*sqrt(omega_1*omega_1 + omega_2*omega_2);
u_s_des         =   LIM(u_s_des1 PAR: -1,1,1);                  % limited stator voltage
%*************************************************************************************
%             Link the induction machine model of appendix D1
%             below this line
%*************************************************************************************
```

D3: Non-linear control method using dc-link current

```
%*****************************************************************************************
%NON-LINEAR CONTROL METHOD USING THE DC-LINK CURRENT
%*****************************************************************************************
%CONTROL PARAMETERS
rhoP_s_des      =   GEN(PAR: 1,10,6,1,481.24,0);   % desired speed
mload           =   GEN(PAR: 0,10,5,1,481.24,0);   % desired load-torque
flux_k_des      =   PAR(0.8);                      % desired cage-flux
omega_u         =   PAR(1/8);                      % tau filter voltage loop
omega_a         =   PAR(1/96);                     % tau filter frequency loop
%*****************************************************************************************
%MODEL PARAMETERS
l_s             =   PAR(l+l_sig_s);          %   stator inductance
l_k             =   PAR(l+l_sig_k);          %   cage inductance
tau_s           =   PAR(l_s/r_s);            %   time constant of stator
tau_k           =   PAR(l_k/r_k);            %   time constant of rotor
sigma           =   PAR(1-l^2/(l_s*l_k));    %   leakage faktor
%*****************************************************************************************
%CONTROL RULES
i_s_b_des       =   flux_k_des/l;        %   flux component of statorcurrent
p_s             =   u_dc*i_dc;           %   input power
i_s_w_des1      =   -0.5*alfaP_s_s_des*i_s_b_des*tau_s*(1-sigma);     % torque component
i_s_w_des       =   i_s_w_des1+sqrt(i_s_w_des1^2+p_s/r_s-i_s_b_des^2);% of statorcurrent
alfaP_s_s_des1  =   rhoP_s_des+i_s_w_des/(i_s_b_des*tau_k);           % stator frequency
u_s_des2        =   sqrt(2*r_s*p_s +
                     (alfaP_s_s_des*l_s)^2*(i_s_b_des^2+sigma^2*i_s_w_des^2)-
                     r_s^2*(i_s_b_des^2+i_s_w_des^2));                % stator voltage
u_s_des1        =   LIM(u_s_des2 PAR:0,1,1);                  % limited stator voltage
%*****************************************************************************************
%FIRST ORDER LAG FILTER IN VOLTAGE LOOP
tau_u           =   PAR(1/omega_u);
u_s_des         =   INF(u_s_des1 PAR: .840084,1,tau_u);
%*****************************************************************************************
%FIRST ORDER LAG FILTER IN FREQUENCY LOOP
tau_a           =   PAR(1/omega_a);
alfaP_s_s_des   =   INF(alfaP_s_s_des1 PAR: 1.00002,1,tau_a);
%*****************************************************************************************
%              Link the induction machine model of appendix D1
%              below this line
%*****************************************************************************************
```

D4: Linearised control method using dc-link current

```
%*****************************************************************************************
%LINEARISED CONTROL USING THE DC-LINK CURRENT
%*****************************************************************************************
%CONTROL PARAMETERS
rhoP_s_des      =   GEN(PAR: 1,10,6,1,1000,0);          % desired speed
mload           =   GEN(PAR: 0,10,5,1,481.24,0);        % desired load-torque
Kr              =   PAR(0.84);          % v/f gain
Ku              =   PAR(0.04);          % voltage gain
Kf              =   PAR(0.02625);       % frequency gain
Iu              =   PAR(0);             % shift value voltage
If              =   PAR(0.034);         % shift value frequency
omega_W1        =   PAR(20);            % cut off frequency voltage loop filter
omega_W2        =   PAR(1/15);          % cut off frequency frequency loop filter
%*****************************************************************************************
%BUTTERWORTH FILTER IN VOLTAGE LOOP
a1              =   PAR(2*omega_W1);
a2              =   PAR(2*omega_W1^2);
a3              =   PAR(omega_W1^3);
in              =   i_dc_acc - a1*butt_out1 - a2*butt_out2 - a3*butt_out3;
butt_out1       =   INT(in PAR: 1.97783E-7);
butt_out2       =   INT(butt_out1 PAR: 7.01785E-8);
butt_out3       =   INT(butt_out2 PAR: 3.43256E-6);
i_dc_W1         =   a3*butt_out3;       % filtered dc-link current
%*****************************************************************************************
%FIRST ORDER LAG FILTER IN FREQUENCY LOOP
tau_W2          =   PAR(1/omega_W2);
i_dc_w2         =   INF(i_dc_acc PAR: 3.43224E-3,1,tau_W2);
%*****************************************************************************************
%CONTROL RULES
u_s_des1        =   Kr*alfaP_s_s_des +  Ku*(i_dc_W1 - Iu);   % desired stator voltage
u_s_des         =   LIM(u_s_des1 PAR: -1,1,1);               % limited stator voltage
alfaP_s_r_des   =   Kf*(i_dc_w2 -If);                        % desired slip frequency
alfaP_s_s_des   =   rhoP_s_des + alfaP_s_r_des;              % desired stator frequency
i_dc_acc        =   (u_dc*i_dc)/u_s_des;                     % adapted dc-link current
%*****************************************************************************************
%              Link the induction machine model of appendix D1
%              below this line
%*****************************************************************************************
```

APPENDIX E: Parameters of the test-machine

E1: Method of parameter calculation

The parameters of the test-machine can be calculated, with data of three measurements:

- a dc-measurement of the stator resistance
- an ac-measurement during no-load operation
- an ac-measurement during load-operation.

In no-load situation one can assume that the machine rotates almost at synchronous speed (slip ≈ 0), the equivalent per-phase circuit for an induction machine is then given in figure E-1.

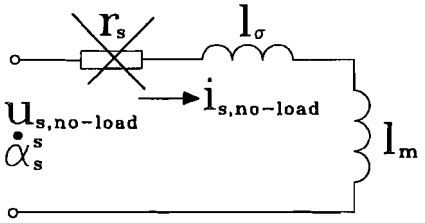

Figure E-1: No-load equivalent per-phase circuit

For most machines the stator resistance can be neglected (verifiable), resulting in the following equation:

$$\left|\frac{u_{s,no-load}}{i_{s,no-load}}\right| = \dot{\alpha}_s^s(l_\sigma + l_m), \tag{E1}$$

where the stator voltage magnitude during no-load, $|u_{s,no-load}|$, and the stator current magnitude during no-load, $|i_{s,no-load}|$ is known from a measurement in a no-load situation. During load conditions the equivalent per-phase circuit is given in figure E-2.

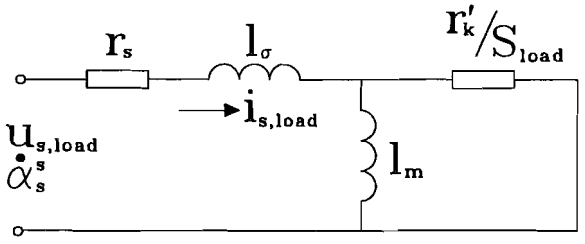

Figure E-2: Equivalent per-phase circuit during load operation

The stator input impedance of figure E-2 is defined as:

$$z_{in,load} = \left|\frac{u_{s,load}}{i_{s,load}}\right|\left\{\cos(\phi_{s,load}) + j\cdot\sin(\phi_{s,load})\right\}, \tag{E2}$$

where the stator voltage magnitude, $|u_{s,load}|$, the stator current magnitude, $|i_{s,load}|$ and the angle between them, $\phi_{s,load}$ is known from measurements in a loaded situation. The per phase stator input impedance of the circuit in figure E-2, can also be written as:

$$z_{in,load} = \left(r_s + \frac{(\dot{\alpha}_s^s l_m)^2 \cdot \frac{r_k'}{S_{load}}}{(\dot{\alpha}_s^s l_m)^2 + \left(\frac{r_k'}{S_{load}}\right)^2}\right) + j\cdot\left(\dot{\alpha}_s^s l_\sigma + \frac{\dot{\alpha}_s^s l_m \cdot \left(\frac{r_k'}{S_{load}}\right)^2}{(\dot{\alpha}_s^s l_m)^2 + \left(\frac{r_k'}{S_{load}}\right)^2}\right). \tag{E3}$$

The parameters can be calculated by equating (E2) and (E3)

$$\frac{(\dot{\alpha}_s^s l_m)^2 \cdot \frac{r_k'}{S_{load}}}{(\dot{\alpha}_s^s l_m)^2 + \left(\frac{r_k'}{S_{load}}\right)^2} = \left|\frac{u_{s,load}}{i_{s,load}}\right|\cos(\phi_{s,load}) - r_s = A, \tag{E4}$$

$$\dot{\alpha}_s^s l_\sigma + \frac{\dot{\alpha}_s^s l_m \cdot \left(\frac{r_k'}{S_{load}}\right)^2}{(\dot{\alpha}_s^s l_m)^2 + \left(\frac{r_k'}{S_{load}}\right)^2} = \left|\frac{u_{s,load}}{i_{s,load}}\right|\sin(\phi_{s,load}) = B, \tag{E5}$$

$$\dot{\alpha}_s^s (l_\sigma + l_m) = \left|\frac{u_{s,no-load}}{i_{s,no-load}}\right| = C. \tag{E6}$$

Because the constant values, A, B, C, are known from measurements, the induction machine parameters can be calculated, by solving the equation system, (E4), (E5) and (E6) :

$$l_m(3) = \frac{1}{\dot{\alpha}_s^s}\left((C-B) + \frac{A^2}{(C-B)}\right), \tag{E7}$$

$$r_k'(3) = S_{load}\cdot\left(A + \frac{A^3}{(C-B)^2}\right), \tag{E8}$$

$$l_\sigma(3) = \frac{1}{\dot{\alpha}_s^s}\left(B - \frac{A^2}{(C-B)}\right), \tag{E9}$$

The calculated parameters are parameters of 3 equivalent, three-phase, circuits (this is indicated with a '(3)' index in (E7), (E8) and (E9)). To transfer the parameters to a two-phase representation, all parameters must be multiplied with a factor $\frac{2}{3}$

$$l_m(2) = \tfrac{2}{3} l_m(3), \tag{E7}$$

$$r_k'(2) = \tfrac{2}{3} r_k'(3), \tag{E8}$$

$$l_\sigma(2) = \tfrac{2}{3} l_\sigma(3), \tag{E9}$$

E2: Calculation of the test-machine parameters

In this thesis, a three phase single-cage induction machine is used for testing purposes. Data of this machine is shown in table E1.

Table E1: Data of test-machine

Manufacturer	Brook Crompton
Frame/nr	UD90LN-2 S680584
Connection to grid	Star
Number of pole pairs	1
$[P_s]_N$	2.2kW
$[U_s]_N$	220V
$[I_s]_N$	4.5A
$[\dot{\alpha}_s^s]_N$	50Hz
$[\cos\phi_s]_N$	0.86
$[\dot{\rho}^s]_N$	2850rpm

The measurements are done with a 'cold' machine (motor temperature about 25°). The dc-measurement of the stator resistance resulted in a stator phase resistance of 2.6Ω. The results of the ac-measurements are given in table E2.

Table E2: Results of ac-measurements

Measured quantity	No-load test	Load test
$u_{s,eff}$ (per phase)	125 V	125 V
$i_{s,eff}$ (per phase)	0.67 A	3.0 A
ϕ_s	≈90°	≈24.1°
slip S	≈0	≈5.1%

To avoid saturation effects, the measurements are done with a low stator voltage (125V). Carry out the calculation method as described in appendix E1, results in parameters of the test-machine as shown in table E3.

Table E3: Two-phase parameters

Parameter	Value
$l_m(2)$	375.6 mH
$l_\sigma(2)$	20.3 mH
$r_k'(2)$	1.266 Ω
$r_s(2)$	1.733 Ω

Using equation (2-71)...(2-73) and assuming $\sigma_s = \sigma_k$, results in parameters as used in derivations in this thesis (second column of table E4). The parameters are given in per unit quantities (for reference quantities see appendix B2). To validate the calculated parameters, the results of a former executed identification[4] are shown in the third column of table E4.

Table E4: Parameters of test-machine

Parameter	Method as described in appendix E1	Method proposed by Blaschke
l_l	3.7169 pu	3.75 pu
$\sigma_s = \sigma_k$	0.0267 pu	0.0218 pu
r_k	0.0409 pu	0.0397 pu
r_s	0.0532 pu	0.053 pu

Comparing the results of both methods shows remarkable conformity. Therefore, it can be concluded that it is relatively simple to calculate the parameters of the test-machine by doing three measurements.

[4]The identification method is proposed by Dr. F. Blaschke and described in the prelimary paper: 'Vorläufiger Bericht über verschiedene Verbesserungen bei der Feldorientierten Regelung von Asynchronmachinen'. It is available on the section EMV, department E of the Technical University Eindhoven. The proposed method determines the machine parameters of an induction machine without saturation. The identification is done by J. van der Werf and the results are published in his thesis report [Werf, '94].

APPENDIX F: DSP PROGRAM

F1: Flow chart

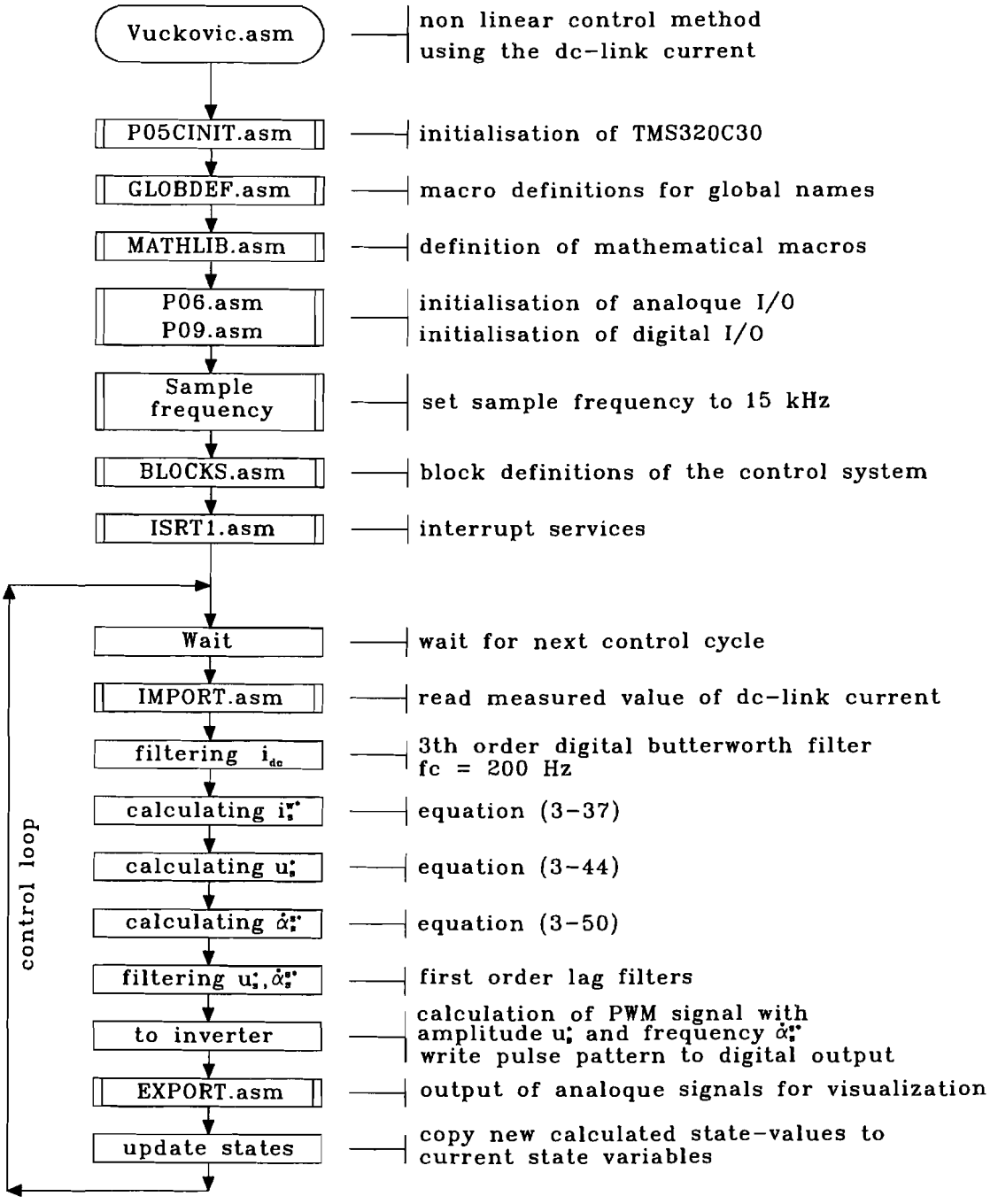

F2: Assembly program

```
*******************************************************************************
*  vuckovic.asm : scalar control method using dc-link current                 *
*                 proposed by Vuckovic/Vuckosavic                             *
*                                                                             *
*  TI320C30 code                                                              *
*                                                                             *
*  author       : E.L. van der Hooft                                          *
*  date         : december 1994                                               *
*******************************************************************************
;
*******************************************************************************
*  Main code automaticaly called after initialisation                         *
*******************************************************************************
;
*** application independent ***************************************************
;
;--- initialisation ----------------------------------------------------------
;
        .include "../c30/p05cinit.asm"  ; reset and interrupt vectors
;
;--- macro definitions for global names --------------------------------------
;
        .include "../c30/globdef.asm"
;
;--- include mathlib for testing purposes ------------------------------------
;
        .include "../c30/mathlib.asm"
;
;--- input-output data migration through ADCs --------------------------------
        .include "../c30/p06.asm"
;
;--- input-output data migration through fully digitized board ---------------
        .include "../c30/p09.asm"
;
*** application dependent ****************************************************
;
;--- auxiliary (global) variables for program flow
;
        .data
;
;--- set sample frequency ----------------------------------------------------
;
        definei sample,         268             ; timer period, 66.67us (15 kHz)
        define  sample_pu,      20.943951e-3    ; (timer period)*100pi
        define  _sample_pu,     47.7464829      ; 1pu time == 1/(2pi*50) sec
;
;--- block definitions and macros describing the drive system ----------------
;
        .include blocks.asm
;
;--- interrupt services ------------------------------------------------------
;
        .include "../c30/isr1.asm"
;
;*** beginning of code segment ************************************************
;
;   ***********************************************************
;   *  all program code should be inserted after this point   *
;   ***********************************************************
;
        .text                           ; start of program code
;
PROGRAM:  LDP   PROGRAM,DP              ; label PROGRAM defined at p05boot.asm
;
;--- set sample time ---------------------------------------------------------
;
        LDI     @T0PER,AR0              ; timer 0 period register
        LDI     @sample,R0              ; desired period
        STI     R0,*AR0                 ; AD and DA conv start at +flanc
        LDF     @sample_pu,R0           ; @sample_pu = integration step, dt
        STF     R0,@dt                  ;
        LDF     @_sample_pu,R0          ; @_sample_pu= 1/integration step, _dt
        STF     R0,@_dt                 ;
;
```

```
;--- loop from conv to conv ------------------------------------------------
;
lus:    LDI     EINT1,IE                ; enable ext int 1 only (from ADC)
        XOR     IF,IF                   ; reset int request occurence bits
        OR      GIE,ST                  ; enable execution interrupt
        IDLE                            ; wait interrupt 1, then execute ISR1
                                        ; (almost) nothing happens inside ISR1
                                        ;  at return IE() == 00H & GIE-bit == 0
        XOR IF,IF                       ; reset int bits, always do that!
;
;--- read inputs -----------------------------------------------------------
;
        .include import.asm
;       input variables and parameters:
;               i_link    : 0-5   A := 0-10V <--> 0-0.52pu
;
;--- filtering dc link current ---------------------------------------------
;
        filter  @i_link,@AFi_link,@aba200but,3,@i_link_fil ; 3th butterworth
;                                                          ; cut off freq=200Hz
;--- calculating the i_s_w_des current -------------------------------------
;
;       i_s_b_des = flux_k_des/L, magnetising stator current component
;
;       TERM = MPAR1*alfaD_fil*flux_k_des, temporarily variable
;
;       p_s = u_link*i_link_fil, (measured) motor input power
;
;                                 ____________________________
;                               \/                            \
;       i_s_w_des = TERM +     \  / TERM^2 + p_s/r_s - i_s_b_des^2
;                               \/
        LDF     @MPAR1,R4               ; 1/(2*r_s*(1+sigma_k)) --> R4
        MPYF    @SalfaD_fil,R4          ; alfaD_fil*MPAR1 --> R4
        MPYF    @flux_k_des,R4          ; TERM --> R4
        LDF     @u_link,R7              ; u_dc --> R7
        MPYF    @i_link_fil,R7          ; p_s = u_dc*i_dc_fil --> R7
        LDF     @flux_k_des,R6          ; flux_k_des --> R6
        MPYF    @_L,R6                  ; i_s_b_des --> R6
        MPYF    R6,R6                   ; (i_s_b_des)^2 --> R6
        MPYF3   R4,R4,R3                ; TERM^2 --> R3
        LDF     R7,R2                   ; p_s --> R2
        MPYF    @_Rs,R2                 ; p_s/r_s --> R2
        ADDF3   R3,R2,R0                ; TERM^2 + p_s/R-s --> R0
        SUBF    R6,R0                   ; TERM^2 + p_s/r_s - i_s_b_des^2 --> R0
        sqrt    R0                      ; sqrt(R0) --> R0
        ADDF3   R0,R4,R5                ; i_s_w_des --> R5
        STF     R5,@i_s_w_des           ; R5 --> i_s_w_des
;
;--- calculating the stator voltage amplitude, u_s_des ---------------------
;
;       TERM1 = 2*r_s*p_s
;
;       TERM2 = (alfaD_fil *l_s)^2 * (i_s_b_des^2 + (sigma*i_s_w_des)^2)
;
;       TERM3 = r_s^2 * (i_s_b_des^2 + i_s_w_des^2)
;
;                       ____________________________
;                     \/                            \
;       u_s_des =    \  / TERM1 + TERM2 - TERM3
;                     \/
;
        MPYF3   R5,R5,R3                ; (i_s_w_des)^2 --> R3
        LDF     @SQR_SIG,R2             ; sigma^2 --> R2
        MPYF    R3,R2                   ; (sigma*i_s_w_des)^2 --> R2
        ADDF    R6,R2                   ; (i_s_b_des^2 +(sigma*i_s_w_des)^2 ->R2
        LDF     @SalfaD_fil,R1          ; alfaD_fil --> R1
        MPYF    @Ls,R1                  ; alfaD_fil*l_s --> R1
        MPYF    R1,R1                   ; (alfaD_fil*l_s)^2
        MPYF    R1,R2                   ; TERM2 --> R2
        ADDF3   R3,R6,R1                ; i_s_b_des^2 + i_s_w_des^2 --> R1
        MPYF    @SQR_Rs,R1              ; TERM3 --> R1
        LDF     @TWO_Rs,R0              ; 2*r_s --> R0
        MPYF    R7,R0                   ; TERM1 --> R0
        ADDF    R2,R0                   ; TERM1 + TERM2 -->R0
        SUBF    R1,R0                   ; TERM1 + TERM2 - TERM3 --> R0
        sqrt    R0                      ; sqrt(TERM1 + TERM2 - TERM3) --> R0
        STF     R0,@u_s_des             ; R0 --> u_s_des
;
```

```
;--- calculating stator frequency ------------------------------------------
;
;       alfaD_des = rhoD_des + MPAR2*i_s_w_des/flux_k_des
;
        LDF     @rhoD_des,R3            ; R3 <-- rhoD_des
        LDF     @threshold,R0           ; R0 <-- threshold
        CMPF    @trigger,R0             ; step response?
        BP      no_step                 ; no!
        ADDF    @step,R3                ; yes!, increment rhoD_des
no_step STF     R3,@speed_des           ; save desired speed

        LDF     @MPAR2,R0               ; r_k/(1+sigma_k) --> R3
        MPYF    R5,R0                   ; MPAR2 * i_s_w_des --> R3
        MPYF    @_flux_k_des,R0         ; MPAR2 * i_s_w_des/flux_k_des --> R3

        ADDF    R0,R3                   ; rhoD_des+ slip_des --> alfaD_des

        STF     R3,@alfaD_des           ; R3 --> alfaD_des
;
;--- filtering u_s_des_top and alfaD_des -----------------------------------
;
        LDF         @u_s_des,R1         ; first order lag filter
        SUBF        @Su_s_fil, R1
        integrate   Su_s_fil,R1,_TAU_u  ; _TAU_u = cut off freq voltage-loop

        LDF         @alfaD_des,R1       ; first order lag filter
        SUBF        @SalfaD_fil, R1
        integrate   SalfaD_fil,R1,_TAU_f ; _TAU_f = cut off freq frequency-loop
;
;--- calculate PWM signal and put it to P09 --------------------------------
;
        to_inverter @Su_s_fil, @SalfaD_fil    ; desired amplitude = Su_s_fil
                                              ; desired frequency = SalfaD_fil
;
;--- write analog signals --------------------------------------------------
;
        .include export.asm
;       output variables and parameters:
;               u_sa_des  :    1 pu <--> 0-10 V
;               i_link_fil:    1 pu <--> 0-10 V
;
;--- the cycle is now finished ... -----------------------------------------
;
        update_states                   ; update states to new values
        BR   lus                        ; jump back
        .end                            ; END OF CODE
```

```
*******************************************************************************
*  blocks.asm : blocks of VUCKOVIC.asm                                        *
*******************************************************************************
;
*******************************************************************************
*  author       : E.L. van der Hooft                                          *
*                 J.L. Duarte                                                 *
*  date         : december 1994                                               *
*******************************************************************************
;
;*** math-macros and  precompiled C-routines ***********************************
;
;        .include mathlib.asm
;
; ************************************************************
; * declare all used variables                               *
; * reserve space and assign to initial value in data section *
; ************************************************************
;
        .data
;
;*** simulation step ************************************************************
;
        define dt,              3.1415927e-2 ; 100 us, initial
                                             ; 1pu = 1/100pi sec
        define _dt,             31.830989    ; don't forget to reassign  dt
;
;*** input/output signals *******************************************************
;
        define  _flux_k_des,    1.25    ; 1/flux_k_des
        define  rhoD_des,       0.0     ; desired speed in pu
        define  speed_des,      0.0     ; desired speed with excitation
        define  u_link,         1.61    ; rectified voltage in pu
        define  i_link,         0.0     ; dc link current inverter

        define trigger,         0.0     ; trigger signal
        define step,            0.1     ; increment in case of speed step
        define threshold,       0.5     ; if input higher than thresh then step
;
;*** internal signals ***********************************************************
;
;--- control variables ---------------------------------------------------------
;
        define  u_s_des,        0.0     ; top value of the des fund voltage
        define  alfaD_des,      0.0     ; desired stator frequency

        define  i_link_fil,     0.0     ; filtered dc-link current
        define  i_s_w_des,      0.0     ; torque component of stator current
;
;--- control parameters vuckovic -----------------------------------------------
;
;Measured by voltage/current method:

        define MPAR1,          -9.1541     ; -1/(2*r_s*(1+sigma_k))
        define MPAR2,           3.9836e-2  ; r_k/(1+sigma_k)
        define _Rs,             1.8797e1   ; 1/r_s
        define TWO_Rs,          1.0640e-1  ; 2*r_s
        define Ls,              3.8161     ; L*(1+sigma_s)
        define SQR_Rs,          2.8302e-3  ; (r_s)^2
        define SQR_SIG,         2.6353e-3  ;
        define _L,              2.6904e-1  ; 1/L

        define _TAU_u,          4.0        ; _TAU_u = (f_cutoff,u)/50
        define _TAU_f,          0.1        ; _TAU_u = (f_cutoff,f)/50
;
;--- 3rd harmonics -------------------------------------------------------------
;
        define injection,       0.12     ; percent of u_s_des_top
        define u_hom,           0.0
;
```

```
;--- carrier ------------------------------------------------------------
;
; triangle wave-form with boundary value : u_tri__top
;
; number of pulses                                  : Np = 15 (defaut)
; max stator frequency [pu]                         = 1.0 (at 50Hz)
; min period stator freq [pu]                       = 2pi (at 50Hz)
; carrier frequency [pu]                            = Np*(max stator freq)
; carrier period [pu]                               = 2pi/Np
; time step [pu]                                    : dt = 31.41592654e-3 {100us}
; number of time steps in one carrier period        : s = (2pi/Np)/dt
; amplitude range variation in one carrier per      : r = 4*u_tri__top
; carrier increment at each time step :             = r/s
;--------------------------------------------------------------------------
;
        define  u_tri__top,     0.8       ; u_s_des_top_max
        define  u_tri,          0.0       ;
        define  inc_tri,        0.16      ; 0.16 dt=66.67us,Np=15,u_tri__top=0.8
;
;--- reference voltages for each phase ----------------------------------
;
        define  u_sa_des,       0.0
        define  u_sb_des,       0.0
        define  u_sc_des,       0.0
;
;--- phase voltages -----------------------------------------------------
;
        define  u_sa,           0.0
        define  u_sb,           0.0
        define  u_sc,           0.0

        define  u_ka,           0.0
;
;*** state-variables *************************************************
;
; don't forget to assign good initial values to get a stable start
;
;--- scalar states ------------------------------------------------------
;
Astates         .word states
Anew_states     .word new_states
;
states
;
        define  Su_s_fil,    0.0
        define  SalfaD_fil,  0.0

        .asg    2,NUMBER_SCALAR         ; Used in update_states macro
                                        ; Dont forget to change it when the
                                        ; number of scalar-states changes
;
;--- angle-states (states are always between -2 PI and 2 PI) ------------
;
        define Salfa,           0.0
;
        .asg    3,NUMBER_STATES         ; Used in update_states macro
                                        ; Dont forget to change when the total
                                        ; number of states changes
;
;--- reserve space for new calculated states ----------------------------
;
new_states .space   NUMBER_STATES
;
bak_states define Bu_s_fil,     0.0
           define BalfaD_fil,   0.0
           define Balfa,        0.0
;
```

```
*******************************************************************************
*  macro          :    to_inverter                                             *
*  calling syntax:     to_inverter u_s_des_top, alphaD_des                     *
*  description    :    Calculate a pulse width modulated signal with amplitude *
*                      u_s_des_top and frequency alfaD_des and put it to P09   *
*                      The sinusoidal reference signals contain 3_rd harmonics *
*  input          :    RD_input1, RD_input2                                    *
*  output         :    -                                                       *
*  uses           :    R0,R1,R2,R5,R7                                          *
*  cycles         :    380                                                     *
*******************************************************************************
;
to_inverter     .macro RD_input1, RD_input2
;
;--- carrier generation: triangular wave-form ---------------------------------
;
        LDF  @u_tri,R0                  ; increment wave
        ADDF @inc_tri,R0                ;
        STF  R0,@u_tri                  ;
        ABSF R0,R1                      ;
        CMPF @u_tri__top,R1             ; test boundaries
        BLT  out_tri                    ; if necessary perform then
                                        ; overflow correction:
        SUBF @u_tri__top,R1             ; R1() = fabs(u_tri) - u_tri__top
        MPYF @TWO,R1                    ;
        LDF  @u_tri,R0                  ;
        BN   correct                    ; if u_tri<0 then add R1 to   R0
        NEGF R1                         ; else       subtract R1 from R0
correct ADDF R0,R1,R0                   ;
        STF  R0,@u_tri                  ;
        NEGF @inc_tri,R0                ;
        STF  R0,@inc_tri                ;
out_tri NOP                             ;
;
;--- internal oscillator generating fundamental sinusoidal wave-forms ---------
;----------------- containing a 3rd harmonic component ----------------------
;
        LDF  RD_input2,R1
        integrate Salfa,R1,ONE          ; update fundamental basis angle

        LDF  @Salfa,R7                  ; update 3rd harm component
        MPYF @THREE,R7                  ; since -2pi  < Salpha < 2pi
                                        ; make -4.5pi < R7 < 4.5pi
        LDF   @TWO_PI,R0                ; (max input for function SIN)
        CMPF  R0,R7                     ; R7 > 2pi ??
        BLE   l_                        ;
        SUBF  R0,R7                     ; R7 = R7 - 2pi
        B m_                            ;
l_      NEGF R0                         ;
        CMPF R0,R7                      ; R7 < -2pi ??
        BGE  m_                         ;
        SUBF R0,R7                      ; R7 = R7 + 2pi
m_      sin  R7                         ; output in R0

        MPYF RD_input1,R0               ; R0 = u_top*sin(3wt)
        MPYF @injection,R0              ; correct 3rd harm injection
        STF  R0,@u_hom                  ;

        LDF  @Salfa,R5                  ; desired voltage for phase A
        sin  R5                         ;
        MPYF RD_input1,R0               ;
        ADDF @u_hom,R0                  ;
        STF  R0,@u_sa_des               ;

        LDF  @Salfa,R5                  ; desired voltage for phase B
        ADDF @TWOTHIRD_PI,R5            ; add 120 degrees
        sin  R5                         ;
        MPYF RD_input1,R0               ;
        ADDF @u_hom,R0                  ;
        STF  R0,@u_sb_des               ;

        LDF  @Salfa,R5                  ; desired voltage for phase C
        ADDF @FOURTHIRD_PI,R5           ; add 240 degrees
        sin  R5                         ;
        MPYF RD_input1,R0               ;
        ADDF @u_hom,R0                  ;
        STF  R0,@u_sc_des               ;
```

```
;--- switch pattern construction yielding PWM -------------------------------
;
        XOR  R1,R1                          ; R1() = 000000, all switches off

        LDF  @u_tri,R0                      ; switches A+ and A-
switchA CMPF @u_sa_des,R0                   ; A- off, A+  on : xxxx01 : 01H
        BLE  Ap_on                          ; A-  on, A+ off : xxxx10 : 02H
Ap_off  OR   02H,R1                         ;
        B    switchB                        ;
Ap_on   OR   01H,R1                         ;
                                            ; switches B+ and B-
switchB CMPF @u_sb_des,R0                   ; B- off, B+  on : xx01xx : 04H
        BLE  Bp_on                          ; B-  on, B+ off : xx10xx : 08H
Bp_off  OR   08H,R1                         ;
        B    switchC                        ;
Bp_on   OR   04H,R1                         ;
                                            ; switches C+ and C-
switchC CMPF @u_sc_des,R0                   ; C- off, C+  on : 01xxxx : 10H
        BLE  Cp_on                          ; C-  on, C+ off : 10xxxx : 20H
Cp_off  OR   20H,R1                         ;
        B    signal                         ;
Cp_on   OR   10H,R1                         ;

signal  STI  R1,@pattern_now
;
;--- write pattern to optical communication ---------------------------------
;
        point_to p09
        out_switch_state @pattern_now
;
;--- converte state switch for analog visualisation -------------------------
;
         LDF    0.0,R1
         LDI    @pattern_now,R0
         TSTB   01H,R0                  ; switch A+
         BZ     p_to_a
         LDF    @u_link,R1
p_to_a   STF    R1,@u_ka
;
        .endm
;
*******************************************************************************
*  macro     : update_states                                                  *
*  calling syntax:    update_states                                           *
*  description:       Copy new calculated state-values to current state var   *
*                     Keeps angle type state between -2PI and 2PI             *
*  inputs:    -                                                               *
*  output:    -                                                               *
*  uses:      R0, AR0, AR1                                                    *
*  cycles:    18                                                              *
*******************************************************************************
;
update_states   .macro
        .asg 0,x
        LDI @Astates,AR1                    ; copy to states
        LDI @Anew_states,AR0                ; copy from new_states
        LDF *AR0++,R0                       ; load R0 with first state
        .loop
               .break (x==NUMBER_STATES-1)  ; loop until all states are copied
               LDF *AR0++,R0                ; store st and load next st in R0
               || STF R0,*AR1++
               .eval x+1,x
        .endloop
        STF R0,*AR1                         ; store last state
        .endm
```